EXPERIMENTAL AND NUMERICAL INVESTIGATIONS ON FRICTION STIR WELDED AND FRICTION WELDED JOINTS OF ALUMINIUM ALLOYS AND STEEL ALLOYS

A THESIS

submitted by

BAIJU SASIDHARAN

for the award of the Degree

of

DOCTOR OF PHILOSOPHY

Department of Ship Technology
Cochin University of Science and Technology
Kochi-22, Kerala, India

January 2017

Dedicated to

My Late Parents
My Guru Dr.C.G.Nandakumar
My Respected Teachers
and
The God Almighty

Acknowledgements

I am very much indebted to my guide Prof.Dr.K.P. Narayanan , Professor (Retd.), Department of Ship Technology) for all the guidance, critical suggestions, encouragements through out my work.

God reaches to all in various version in various occasion if he is deserving genuine uplifting. The same feeling I am getting from my Guru, Dr.C.G. Nandakumar, Professor and Head, Department of Ship Technology in every moment of my life. This thesis is one of his great blessings to me.

I am very much thankful to Dr.J.Letha (Vice Chancellor of CUSAT and former DTE-Kerala), Dr. Kuncheria P Isaac (Vice Chancellor of APJ Abdul Kalam Technological University and former DTE-Kerala), Dr.K. Vijayakumar (DTE-Kerala) and Prof.S.K. Mohan (former DTE-Kerala) who gave their timely support to get the administrative sanctions to pursue my PhD program at CUSAT. I also extend the same.

I extend my sincere gratitude to Dr.K. Sivaprasad, Dr.A. Mathiazhakan, Dr.-Ing C.B. Sudheer and Dr. Mariamma Chacko of Dept. of Ship Technology, for their suggestions at the time of research progress evaluation.

Prof.T.G.Vijayakumar, Prof. J Meerakumari and Dr. B. Anil (former Professors), Heads in Department of Mechanical Engineering, The Principals and Principal in charges, of College of Engineering Trivandrum from 2007 to 2017 have given me all the supports for my thesis. Dr. Bijulal and Dr. Dileep Lal need a special mentions as they have taught me Latex documentation and DOE tools. STTPs by Dr.S.Jayakumar, Dr.S. Sreekumar, Dr.G. Venugopal, Dr. V R. Rajeev, Dr.JagetBabu, Prof. N. Sasi, Dr.V. Regikumar, Dr.Sunil Kumar.K and Sri. Renju Mohan are also helped me to study software packages suit to my research work. The technical assistance given by Sri. Madhavan Kutty, Sri. Manoharan, Sri.Ganesh and staff in SM Lab of CET, material science lab of IISTK and metallurgy lab of NIISTK are really appreciable.

I also express my thanks to all the administrative staff in Dept. of Ship Technology and research related sections in administrative block of CUSAT.

Thanks to my beloved students Er. Darwin-VSSC, Er. Arivazhakan-Brahmos, Er. Prakash-IISTK, Athira, Aneesh.S, Thanoj Surendran,Nick Franklin and Sreejith for their supports. Also, the inspiration given by the team of OPES/STEP4U in CET, especially, Prof. Thara Mohanan, Er.Jithin Mohan, Er.Sikha Abraham, Aswathy, Asif, Helen M Jacob, Viji, Renjith Kumar,Veena Senan,Akhila,Reshma, Anupama and Bimna Raveendran is worth remember always.

Thanks to the help by my close relatives -Subhashini N, Suresan K,Leena Dhanda, Gayathri B S, Lekshmy, Jithin, Anjali, Lizy Darling, Dr.Jyothi, Dr.Mukundan and Dr.Kalakumari at the time of thesis submission.

Last but not the least I would like to thank my wife Deepa S Sekhar for her patience, support and the care given for the completion of my thesis.

Baiju Sasidharan

Abstract

Friction Stir Welding (FSW) and Friction Welding (FW) are the most popular emerging solid welding techniques in aircraft and shipbuilding industries. FSW is mainly used for the joining of metal plates and FW is mainly used for the joining of rods. Both techniques are suitable for high strength material having less weight. These techniques are environmentally friendly and easy to execute. Hence, study on these techniques can contribute much in the field of green technology. This research work is dealt with the experimental and numerical investigations on FSW and FW of aluminium alloys and steel alloys.

This research is started with a detailed literature survey on both techniques. Latest trends in research and their industrial applications have been reviewed. Objectives have been fixed according to that. Thus FSW setup has been developed from a vertical milling machine and FW setup from a medium duty lathe. The material considered for the experimental investigation on FSW is AA2219 and for FW is Al6061. AA2219 is an alloy of aluminium and copper. It is a heat treatable wrought alloy. It possesses good combination of strength and toughness. It's good weldability at cryo temperature made it a better choice for the fabrication of cryo tanks for space applications. Al 6061 is a precipitation hardening aluminium alloy, containing magnesium and silicon as its major alloying elements. It possesses good mechanical properties and exhibits good weldability. It is one of the most common alloys of aluminium for general purpose use.

Experimental investigation on FSW mainly includes the comparative study of tensile and micro structure characteristics of friction stir welded joints with the conventional welded joints from AC square wave (ACSQW) TIG welding and Direct current straight polarity (DCSP) TIG welding. Taguchi analysis has been used to fix and optimize FSW process parameters. The tensile characteristics of friction stir welded joints are found to be higher than conventional welded joints. It is also seen that FSW joints possessed 67% of Ultimate tensile strength, 48% of Yield strength and almost 1.4 times percentage elongation, compared to the parent metal. The micro structure photographs of friction stir welded joints have not indicated any phase change at weld zone and heat affected zone compared to conventional welded joints. These studies clearly proved the effectiveness of FSW technique for the joining of light weight and higher strength material like aluminium alloys.

Numerical investigations on FSW included the thermal modelling of FSW process. The material considered for the study is Al6061-T6. Comsol Mutiphysics software package has been utilized for the numerical study. The temperature distribution in the workpiece during FSW process has been predicted by the thermal model created. The predicted temperature has been validated with the numerical and experimental results forwarded by other researchers like Hamilton et al. An effective thermal model has been established for FSW.

Experimental investigation on FW started with preliminary studies to assess the tensile characteristics of friction welded joints. From the preliminary studies it is inferred that friction welded joints are possessing comparable tensile characteristics with the parent metal.

The effect of interface surface geometry in the strength characteristics of friction welded joints has not been studied and not much popularized. Hence next stages of experiments have been focussed to find the influence of interface surface geometries in the mechanical characteristics of friction welded joints. Various interface geometries considered for the study are Flat - Flat, Taper - Taper, Convex - Convex and Concave - Convex. Taguchi orthogonal arrays has been used to fix the number of experiments. Grey Relational Analysis has been carried out to find the optimum process parameters. ANOVA has been carried out to find out the percentage contribution of each process parameters in the mechanical characteristics of FW joints.

From the experimental investigations on FW, it is found that interface surface geometries influence almost equally with other process parameters like tool rotation and axial loading on the strength characteristics of friction welded joints. It is also found that friction welded joints formed with Taper-Taper interface geometry holds good strength characteristics than joints obtained with other interface geometries. The suitable taper angles found in this regard are in the order of 30°, 60°and 45° and 15°along with other process parameters (speed of rotating specimen -775 rpm , Axial load-3 MPa and Forge pressure- 5 MPa) to obtain friction welded joints having comparable desired mechanical characteristics with the parent metal.

FW joints obtained with 30° Taper-Taper interface geometry possessed higher tensile strength. FW joints obtained with 45° Taper - Taper interface geometry possessed higher hardness value and those obtained with 60° possessed higher impact toughness characteristics than others. Microhardness values are also found high for friction welded joints with 60° tapered angle. It is noticed that even with lower speed for the rotating specimen, strong joints can be obtained with adequate interface geometry change according to the desired characteristics.

Numerical modelling of FW process has been initiated with its thermal modelling. ANSYS software package has been used to make the thermostructural model. The material considered for the thermal modelling is AISI 316 Alloy. The FE model has predicted the temperature distribution, stress, strain, contact friction stress and displacements. The predicted effects are seen matching with a real FW process.

Followed with the preliminary studies numerical modelling of dissimilar friction welding process has been carried out to assess the residual stress developed in friction welded joints. The materials considered for the same are AISI 304 and AISI 430. The predicted residual stresses are found matching with the experimental results available in literature.

From all these studies, it is inferred that, the investigations considered for the present study can lights on the effective joining techniques like FSW and FW, for the joining of aluminium alloys and steel alloys. It also give the idea on enhancing strength characteristics of friction welded joints, by making use of various interface geometries for the weld specimens, while welding.

Contents

List of Figures

List of Tables

Chapter 1

INTRODUCTION

Welding is one of the most important joining processes in any manufacturing industry. It is widespread and versatile technique for joining two pieces of the same kind of metal. It is done by melting the joining faces of workpieces and adding filler material to form a pool of molten material at that region which cools to become strong joint. Many different energy sources like gas flame, electric arc, laser, electron beam and ultra sound etc. are used as the energy sources for welding.

The criticality of joining processes is both due to development of new materials as well as improvement of design techniques which requires a higher load capacity. In this way a high responsibility is attributed to welding process which has to guarantee a suitable strength together with a high degree of reliability. Traditional processes are inadequate for this aim because of the expensive surface preparation that must be carried out to reduce the presence of oxides in the melted metal. Furthermore pores, inclusions and metallurgical defects may occur in the solidification stage of the material after welding. For this reason new processes are emerging in the industrial scenario based on new approaches. Among them solid state welding processes such as Friction Stir Welding (FSW) and Friction Welding (FW) are having significant role. From the literature it is seen that solid welding techniques keep the properties of welded joint comparatively similar to that of parent metal. This research work explores the capability of two major solid welding techniques namely friction stir welding and friction welding processes for the joining of aluminium alloys and steel alloys. The study has also focussed on the influence of process parameters on the physical mechanical and micro structural characteristics of friction stir welded and friction welded joints by experimental and numerical investigations.

1.1 Conventional Welding Techniques

The common conventional welding techniques used for the joining of aluminium alloys are Gas welding and Arc welding. But too much control over the process parameters are required while using these welding techniques. Hence, weld defects are common in conventional welded joints. In CW techniques, fusion of materials are taking place while welding. Phase change at joints are seen in conventional welded joints. CW techniques used for the present study are DCSP TIG and ACSQ TIG.

1.2 Solid Welding Techniques

In solid welding techniques, the joining of surfaces are occurring at a thermoplastic state developed by the heat energy due to friction between joining surfaces or with any external tool. FSW and FW are the two important type of solid welding techniques. Both are now used extensively in aerospace and shipbuilding industries, where high strength and light weight material like aluminium and steel alloys are commonly used for structural fabrication.

FSW utilizes a rotating tool progressing along a joint to heat and forge metals. After the non-consumable rotating tool is applied to the base metals, a central pin, or probe, makes contact with the parts to be joined, followed by the shoulder. As the tool rotates and progresses down the joint, it heats and plasticizes the materials where it makes contact, sweeping them behind it and eliminating the interface. The process is shown in Figure 1.1. Various process parameters which determine the strength characteristics of friction welded joints are geometry of the tool, tool material, tool traversing speed, rotation of the spindle, orientation of spindle, axial load on the tool, tool tilt angle, position of the tool, tool heat input, cooling rate, plates thickness and material of the specimen. (E.Massoni et al., 2002). Many research publications are available on almost all these aspects. Major publications include design of experiment based optimization of process parameters, numerical study on heat generation while FSW process, dissimilar metal joining (Elatharasan and Kumar, 2012; Galvao et al., 2013), influence of tool geometry etc. For the present study mechanical and microstructural characteristics of FSW joint from AA2219 material compared to conventional welded joints from Direct Current Straight Polarity (DCSP) TIG welding and AC Square Wave (ACSQW) TIG welding have been investigated.

Friction welding (FW) is a class of solid-state process that generates heat through mechanical friction between a moving work piece and a stationary component, with the addition of

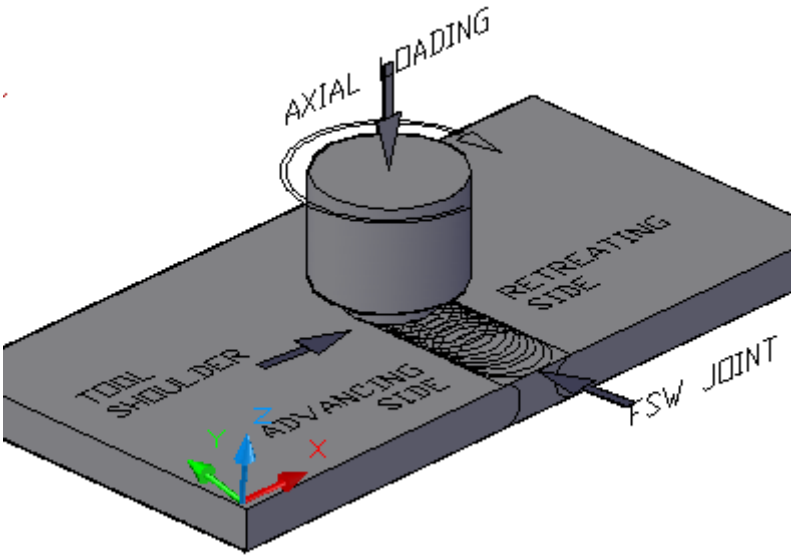

Figure 1.1: Friction Stir Welding

lateral force called upset to plastically displace and fuse materials. As per AWS, it is a solid state joining process in which bonding is produced at temperature lower than the melting point of the base materials. There are different types of friction welding techniques. Some of them

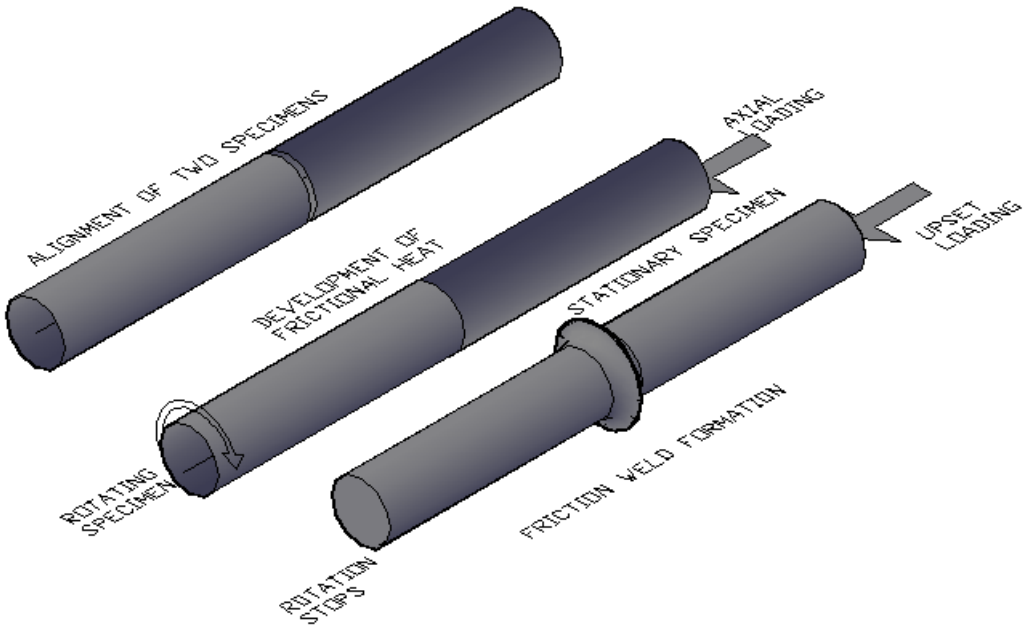

Figure 1.2: Rotary Friction Welding

are linear friction welding, inertia friction welding and rotary friction welding. Most common technique which is used to join specimen with circular cross section are rotary friction welding. In all these cases, heat is generated by conversion of mechanical energy both into heat energy

and visco-plastic deformation work (energy), at the interface of the work piece, during rotation under pressure. Thus metallic bonding is produced at temperatures lower than the melting point of base metals. Figure 1.2 represents the various stages in a rotary friction welding process. Initially, the two specimen are aligned. Frome these, one specimen rotated and the other is subjected to axial load. Due to both of its relative motion and axial loading, the interface get heated due to friction. As a result, the interfaces turninto a plasticized stage. At that time, the rotating specimen is stopped and a sudden upsetting axial pressure will be applied on the stationary specimen. On cooling a strong bond between mating surfaces will be resulted.

1.3 Welding Techniques for Aluminium Alloys

Common conventional welding techniques for aluminium alloys existing in aerospace and ship building industries are gas tungsten arc welding, sheet metal arc welding, oxyfuel gas welding,electron beam gas welding and Laser beam welding etc. Each process is having its own advantages and disadvantages. Oxide layer formation is the major problems in arc welding. All these welding techniques need much more attention for the control of process parameters to avaoid the failure of welded joints. In addition, intermittent intervals are also needed in these cases to control the temperature developed during the welding processes. In such scenario FSW and FW has got much importance as they are doing within the liquidus temperature of the weld specimen.

1.4 Scope of FSW and FW

Friction stir Welding finds application in shipbuilding and marine industries (panels for decks, sides, bulkheads and floors, aluminium extrusions, hulls and superstructures, helicopter landing platforms etc), aerospace industry (wings, fuselages, empennages, cryogenic fuel tanks for space vehicles, aviation fuel tanks etc), railway industry (high speed trains, rolling stock of railways, underground carriages, trams, railway tankers and goods wagons, container bodies etc. Figure 1.3 represents examples for industrial products made by FSW techniques for marine applications. Friction welding processes are mainly used to join circular shafts and pipes. Hence it has got wide application in the area of joining carbon-steel vehicle axles and sub-axles. It is also used to fabricate suspension rods, steering columns, gear box forks and engine valves. Thus it finds wide applications in automotive industries. Figure 1.4 represents various industrial products made by FW techniques. Friction welding process are very economical

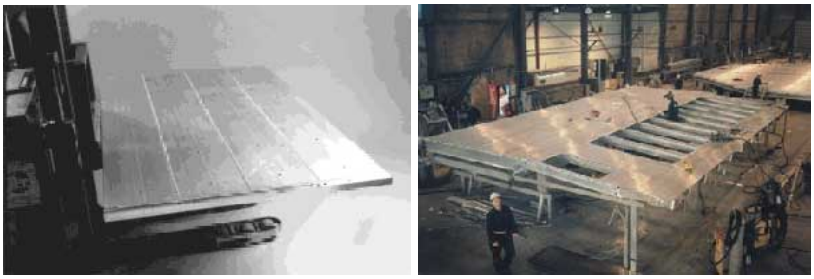

Figure 1.3: A panel and a catamaran side wall made by FSW (Source: Stephan Kallee (2000))

Figure 1.4: Components made of FW techniques (Source: Inc (2016))

and can have high production rate. Not require highly skilled labours. Various ferrous and non ferrous alloys having any cross sectional geometry, with various mechanical and thermal properties can easily be joined by the friction welding technique. Nowadays, this method also have large scope for the joining of dissimilar metals.

1.5 Objectives

The objectives set for the present research work are as follows.

- To develop FSW and FW setups using conventional vertical milling machine and Medium duty lathe respectively. Apply Design of Experiment procedures such as Taguchi orthogonal array, Grey Relational Analysis and ANOVA to set the number of experiments, to fix the best combination of process parameters.
- To conduct experiments to compare tensile and microstructural characteristics of FSW joints of AA2219 Aluminium Alloys with the conventional welded joints. Also to conduct experiments to study the influence and percentage contribution of interface geometry for FW specimen in the strength characteristics.
- To carry out thermal modelling of FSW using Finite Element Method and to predict the temperature distribution in the Al6061-T6 workpieces during FSW processes. Also

to conduct numerical modelling of FW process to predict the displacement, stress and strain in the joining specimen during FW process. Besides, the capabilities of numerical modelling have to be extended to predict residual stress development in dissimilar FW joint.

1.6 Content of the Thesis

There are five chapters for this thesis. The first chapter gives a general description of various welding processes and types of welded joints. It also gives the objectives and scope of thesis. Second chapter narrates the literature review and the third chapter gives the details of experimental studies. Fourth chapter deals with the numerical studies carried out on FSW and FW process. Conclusions are given in fifth chapter. Appendix. A deals with the comparison of FW joints with conventional welded joints. Detailed steps involved in the numerical modelling of FSW and FW are given in Appendix B. Followed with the appendices list of references are given.

Chapter 2

LITERATURE REVIEW

This research work deals with the experimental and numerical investigations on friction stir welding and friction welding of aluminium alloys and steel alloys. Literature review on basic principles of both, study on related solid welding techniques, materials and methods adopted by various researchers on both process have been discussed in this chapter.

2.1 Various Solid Welding Techniques

In solid welding techniques, there occurs no fusion or phase changes of metals to be joined. In these cases, the surface of joining metals are made in a plasticized stage which is created due to the development of frictional heat. Different types of solid welding techniques are friction stir welding, rotary friction welding, continuous drive rotary friction welding, inertia friction welding, stored energy rotary friction welding, linear friction welding and orbital friction welding etc. The theory and working principle behind two major friction welding are as follows.

2.1.1 Friction Stir Welding

As explained in section1.2, FSW utilizes a rotating tool progressing along a joint to heat and forge metals. After the non-consumable rotating tool is applied to the base metals, a central pin or probe makes contact with the parts to be joined followed by the shoulder. As the tool rotates and progresses down the joint, it heats and plasticizes the materials where it makes contact, sweeping them behind it and eliminating the interface. The main advantages of the FSW process are excellent weld quality, mechanical properties equal to or better than fusion

welding. In addition to that, this process is environmental friendly (no fumes or spatter are generated). It also involves no arc glare or reflection of laser beams. Minimal distortion$\not\leq$ $and residual stress and ability for welding dissimilar metals are other special features of this process.$

2.1.2 Friction Welding

Rotary friction welding (generally speaking "friction welding") was introduced around 50 years ago as a mass production process for the automotive, electrical and domestic appliance sectors. It was the first of the friction processes to be developed and used commercially. The first patent on rotary friction welding, issued in USA, was published in 1891. It describes the use of frictional heat for joining the ends of wire cable. It was not until the 1950s that the friction welding process was used significantly in the USSR. Friction welding then spread throughout industrially developed European countries (including the former USSR), Japan and the USA. Three major variables in rotary friction welding process are rotational speed, axial pressure and heating time. Rotational speed provides necessary relative velocity for the faying surfaces. High rotational speed is useful for welding but axial pressure and heating time are to be carefully considered to avoid overheating of the weld zone. In dissimilar metal, lower rotational speeds can minimize brittle inter-metallic compounds (GohariKia and Akbarimousavi, 2011).

A continuous-drive rotary friction welding involves two cylindrical bars held in axial alignment. One of the bars is rotated while the other is advanced into contact under a pre-selected axial pressure. Rotation continues for a specific time, sufficient for achieving the temperature at which metal in the joint zone is in the plastic state. Having achieved this condition, the rotating bar is stopped while the pressure is either maintained or increased to consolidate the joint.

Stored energy friction welding or spin welding systems consist of two chucks for holding the materials to be welded, one of which is fixed and the other rotating. Before welding one of the work pieces is attached to the rotating chuck along with a flywheel of a given weight. The piece is then spun up to a high rate of rotation to store the required energy in the flywheel. Once achieving the spinning at the proper speed, the motor is removed and the pieces are forced together under pressure. The force is kept on the pieces after the spinning stops to allow the weld to "set". This technique is also known as inertia welding, rotational welding or inertial friction welding.

Orbital friction welding is similar to rotary friction welding. But both parts to be welded are rotated in the same direction and at the same speed, but with their axes offset by up to 3 mm. At the end of a weld the relative movement is ended by returning both parts to the common

axis of the machine and the welding force is maintained or increased.

Linear friction welding (LFW) is a form of friction welding in which components to be welded are moved against each other linearly, as opposed to in a rotary fashion. It involves rubbing one component across the face of a second rigidly clamped component, using a linear reciprocating motion. This motion is produced using a small amplitude of 1-3mm, at a frequency of 25-125 Hz and a maximum axial welding force of 150kN. Linear friction welding is commonly used in the aero engine industry to join blades and discs.

2.2 Investigations on FSW

Literature review on FSW has been carried out as two sections, experimental and numerical. About twenty two papers on experimental investigation and nineteen papers on numerical investigations have been reviewed. In almost all the papers, the influence of process parameters, mechanical and micro structural characteristics studies and FSW process simulations are discussed.

2.2.1 Experimental Investigations

Most of the papers are related to comparative study on mechanical and microstructural characteristics of friction stir welded joints with conventionally welded joints. In all those cases friction stir welded joints found good mechanical and microstructural characteristics compared to conventionally welded joints. Almost all the mechanical characteristics studies included tensile test, fatigue and fracture characteristics studies, hardness and microhardness studies etc. Some papers have focussed on the measurement of process parameters like tool rotation, tool torque and temperature distribution along longitudinal and transverse direction of friction stir welding specimen while welding. Some experiments are related to residual stress measurement and its comparison with numerical predictions. Both similar and dissimilar materials have been considered by various researchers for experimental investigations.

Ericsson.M and Sandstorm.R (2003) have done experiments to evaluate the influences of welding speed on the fatigue of friction stir welded joints and compare the same with the joints from MIG and TIG welding. For the experiment two materials have been considered. They have found that welding speed had no major influence on mechanical and fatigue properties of the friction stir welded joints except some areas. MIG Pulse and TIG weld have showed lower static and dynamic strength than FS Welds. It is also found that TIG has better fatigue

performance than MIG. They have also presented the hardness profile across the weld as a function of welding speed.

Minton.T and Mynors.D.J (2006) have made attempt to develop friction welding set up in a conventional milling machine. Trials have been made to produce friction stir welded joints from Aluminium 6082-T6 sheets of thicknesses 6.3 mm and 6.4 mm. Silver steel tool of 19 mm diameter have been used for the welding. The friction stir welded joints have been subjected to tensile and hardness tests.

Cavaliere.P et al. (2006a) have conducted experiments to study the effect of welding parameters on mechanical and microstructural properties of AA6056 joints produced by FSW. Friction welded joints with different combinations of process parameters have been produced in this study. The various speeds used in this study are 500,800 and 1000 rpm and the different welding speeds used are 40,56 and 80 mm/min respectively. Mechanical properties of the specimen have been evaluated by conducting micro hardness and tensile tests. Fatigue test has also been carried out by using resonant electro-mechanical testing machine under constant loading control up to 250 Hz sine wave loading. It is observed that highest tensile strength is reached corresponding to high value of rotating speeds and welding speed. The fatigue endurance curve showed very different response of the material as a function of the different processing parameters. It is also observed that hardness at the weld region has been increased for higher values of tool rotation as well as the welding speeds.

Barcellona et al. (2006) have conducted experiments to study micro structure characteristics of FS welded joints from AA2024-T4 and AA7075-T6 materials. Grain dimensions and insoluble particle densities have been investigated by them both in the parent metal and in the joints. They have also studied the effect of post welding heat treatment on the joint strength.

Cavaliere.P et al. (2006b) have done experiment to study the mechanical and microstructural behaviour of 2024-7075 Aluminium alloy sheets joined by FSW. The joints have been subjected to tensile and fatigue characteristic studies. Scanning electron microscopy has been used for the microstructure studies. The specimens fracture surface after testing have been deeply analysed using FEGSEM microscope. The defect topology, the microscopic mechanisms occurred during high stress deformations and the final failure have been studied by them.

Marzoli et al. (2006) have done FSW of AA6061/Al2O3/20p reinforced alloy. The joints produced have been subjected to mechanical and micro structure characteristic studies. Micro structure has been observed with optical microscope and the images have been analysed with an image analysis software. It is seen that tool's stirring effect has significant effect on the reinforcement particle distribution and shape. Tensile test revealed that joints have 70% strength

compared to the parent metal.

Watanabe et al. (2006) have done attempt to weld aluminium alloy to steel by FSW. They have investigated the effect of pin rotation speed, the position for the pin axis to be inserted on the tensile strength and micro-structure of the joint. The behaviour of the oxide film on the faying surface of the steel during welding has also been examined. Successful butt weld formation of aluminium and steel alloys is the major reported result by them. In addition they have also reported that the maximum tensile strength of the joint has been found about 86% of the aluminium alloy base metal. Another observation they have made in the study that a small amount of inter-metallic compound has been found at the upper part of the steel/aluminium interface while no inter-metallic compound has been found in the middle and bottom part of the interface.

Ceschini et al. (2007) have conducted experiments to find the effect of FSW on micro-structure, tensile and fatigue properties of the AA7005/10 vol. Al2O3p composite. Friction stir welded joints have exhibited high tensile values. The low-cycle fatigue tests evidenced a fatigue life reduction for the friction stir welded material with respect to the base composite.

Cavaliere et al. (2008) have conducted experiments to evaluate the effect of welding parameters on mechanical and micro structural characteristics of AA6082 FSW joints. Different welded joints have been produced by them with fixed tool rotation of 1600 rpm and varying welding speed from 40 to 460 m/s. Tensile, Fatigue and micro-structure characteristics of the FSW joints have also been evaluated.

Hwang et al. (2008) have conducted experimental study on temperature distributions within the workpiece during FSW of aluminium alloys. Various types of thermocouple layout are devised to measure the temperature histories during the process. Successful welding processes have been achieved by appropriately controlling the maximum temperature during the welding process. Regression analyses by the least square method have been used for the prediction of temperature at the joint line. The appropriate temperature range for the successful FSW has been found between 3 65 and 390 °C. The temperature at the advancing side has been seen slightly higher than that in the retreating side. They have also evaluated hardness and tensile strength of welded joints.

Elangovan and Balasubramanian (2008) have conducted experiments to evaluate the influence of welding speed and tool pin profile in the formation of FSW joints in AA2219 Aluminium Alloys. Five different tool pin profiles with three different speed have been considered for the study. Micro-structural and tensile characteristics of each set has also been carried out. From the investigation they have found that the square pin profile tool produced mechanically

sound and metallurgically defect free welds compared to other tool pin profiles.

Cavaliere et al. (2009) have done experiment to study the effect of anisotropy on fatigue properties of 2198 Al-Li plates joined by FSW. Al-Li alloys are characterised by a strong anisotropy in mechanical and micro-structural properties with respect the rolling direction. This work explain the effect of FSW process along parallel and orthogonal direction of the rolling direction. The joints obtained by this two options have been subjected to tensile and fatigue characteristic studies.

Hwang et al. (2010) have conducted experiments to weld copper metals (C11000) using FSW. The study mainly aimed to explore the thermal history of work piece during FSW. K-type thermocouples have been used by them to record the temperature history at various locations of the work pieces. The temperature data combined with preheat temperature records helped them for obtaining effective friction stir welded joints. Vickers hardness test has been conducted on the weld to evaluate the hardness distribution in thermal-mechanical affected zones, heat affected zones and the base metal. Additionally tensile test has been conducted by them. They have found that the approximate temperature for the FSW of C11000 are between 460°C and 530 °C.

Elatharasan and Kumar (2012) have conducted experiments to find out optimum welding process parameters for the dissimilar metal joining of Aluminium Alloys (AA6061-T6 and AA7075-T6). Response surface methodology has been used to predict the ultimate tensile strength and yield strength based on the main FSW process parameters like rotational speed, welding speed and axial force.

Trimble.D et al. (2012) have done experiments to monitor the force generation during FSW of AA 2024-T3 plates. A rotating component dynamometer has been utilized for the same. An FE model based on the experimental results utilized to predict the tool force developed during the FSW process.

Cavaliere (2013) have conducted experiments to evaluate the fatigue life and crack behaviour of several friction stir welded aluminium alloys. Based on their studies a multi objective optimization tool capable of correlating all the material properties and processing parameters to the final mechanical performance of weld, have been developed. The tool has been developed using the software FRONTIER (ESTECO).

Su.H et al. (2013) have done experiment on FSW to facilitate simultaneous measurement of tool torque, tool traverse force and axial forces. Different from traditional measurements methods using load cell rotating compound dynamo meter has been utilised for the work. Observation of the surface structure at different experimental condition have also been carried out

using an X- Ray diffractometer.

Yu-E-Ma et al. (2013) have done experiments to study the effect of welding process parameters on mechanical and fatigue properties of friction welded 2198-T8 Aluminium Lithium Alloy joints. The objective of the experiment is to find out the effect of the ratio -"ω/v" on the micro structure and tensile properties of the friction stir weld. Fatigue test have also been conducted by them to assess the crack growth rates, based on the procedure in ASTE647 standards. It is seen that micro hardness and tensile strength of the joints have decreased with increasing "ω/v" ratio. From the microstructure photographs it is seen that there is an abrupt transition to the nugget at the advancing side. While on the retreating side there has been found a wide transition region between the thermo-mechanically affected zone (TMAZ) and weld zone (WZ)

Jau-WenLin et al. (2013) have done experiments on FSW process to compare the mechanical and micro structure properties of pure copper welded using FSW and TIGW. Mechanical characteristic studies included tensile strength, impact resistance and hardness tests. They have found that notch tensile strength, notch strength ratio for the friction welded joints are higher. XRD tests have also been performed to determine components of copper before and after TIG and FSW processes.

Paulo.R.M.F et al. (2014) have done experiment to study the influence of friction welding residual stress on compressive strength of aluminium plates. Longitudinal residual stress distribution has been measured by means of contour method.

DUrso.G et al. (2014) have done experiment to study the fatigue crack growth in the welding nugget of FSW joints of 6060 aluminium alloy. Tensile tests, metallographic analyses and micro Vickers tests have also been carried out to evaluate the mechanical properties of the joints as a function of process parameters. The fatigue behaviour has been studied by means of crack growth tests performed according to ASME647 standard on CT specimens with propagation in the middle of joint along the weld nugget.

Prater (2014) has done experiments on FSW of composites for use in Aerospace structures. According to him FSW has been used to join structural components of the Delta IV, Atlas V, and Falcon IX rockets as well as the Orion crew exploration vehicles. Also he has described that current research on FSW is the joining of newly developed composite material to be used in Aerospace structures, which are very difficult to weld by conventional methods. Melting of such material results in the formation of an undesirable phase which leaves a strength depleted region along the joint line. Since FSW occurs below the melting point of work piece material this deleterious phase is absent in FS welded MMC joints.

2.2.2 Analytical Investigations

Most of the investigators have done thermal and thermo-mechanical modelling of FSW process. Both 2D and 3D modelling have been done by them. By the numerical modelling, the researchers have simulated FSW process in which attention has been made to exhibit the material flow during welding. By the numerical modelling some researchers have also predicted the residual stresses developed in FSW joints.

Thermal modelling of FSW using a moving coordinate system has been done by Song and Kovacevic (2003). The moving coordinate system has reduced the difficulty in modelling the moving tool. The finite difference method has been used to solve the control equation. A non uniform grid has been used for the calculation. The result from the numerical studies has been compared with the experimental results. The mathematical model of FSW process has included the tool penetration period, welding period and the tool pulling out period etc. Important assumptions considered for the modelling are (a) the heat generated at the tool shoulder/workpiece interface , is frictional heat. (b). Tool pin is cylindrical without any effects of threads and (c). No heat flow in to the workpiece when the local temperature reaches the material melting temperature. Three main boundary conditions have been considered for the thermal modelling. They are "(1) heat flux boundary condition (2) convection boundary condition and (3) symmetric boundary condition." To validate numerical results with the experiments, temperature histories have been noted by making use of type-K NiAl/ NiCr thermocouples. An infra-red camera has been used to take surface temperature of the work piece in front of the tool. The various micro structure morphology found under this investigations are (a) the nugget zone (b) TMAZ (c) the HAZ and (d) the base material.

A numerical simulation of transient temperature and residual stresses in FSW of 304L stainless steel has been done by Lee et al. (2004). 3D non linear thermal and thermo-mechanical numerical simulations have been conducted by them. The FE analysis code WEKLDSIM has been developed for the study. Two welding cases with tool rotational speed of 300 and 500 rpm have been analysed. The effect of fixture release after the welding on residual stresses has also been studied by them. An agreement between experimentally found residual stresses by neutron diffraction techniques and the corresponding numerical results has been formed in this study.

Heurtier et al. (2006) has done the numerical study for the mechanical and thermal modelling of FSW using AA2024-351 alloy. The model is based on the velocity fields classically used in fluid mechanics. It is also incorporated the heat input from the tool shoulder and the plastic strain of the bulk material. The model has predicted the strain rates, temperature dis-

tribution and micro hardness at various zones. The calculated results based on the numerical study has made a close agreement with the experimental studies.

Williamson and Abdel-Salam (2006) have done a moving boundary formulation for recursive plastic heat release during FSW. Under this model the growth of the third region during the process has been identified. The domain of interest in this study is the heat and deformation affected zone under tool shoulder.

Mandal and Williamson (2006) have developed a thermo-mechanical hot channel approach for the numerical modelling of FSW. The model follows the Rosenthal solution for moving point source where heat input from the tool shoulder act as a warm source while plasma or laser heat source provide higher energy input. The THC approach aims at decreasing tool wear by reducing the demand for frictional heat from the tool shoulder and pin. In the proposed model the processing temperature is approximately 1000°C, which is close to the temperature required for the welding of steel. The result has indicated that the presence of preheating source ahead of the stir tool has significantly reduced the temperature gradient, as compared to conventional FSW.

Soundararajan et al. (2005) have developed a thermo-mechanical model with adaptive boundary conditions to simulate and predict transient temperature field, active stress developed and residual stresses in friction stir welded joints of Al6061. Newton's law of cooling has been used to determine the convection heat transfer coefficient of the surface exposed to air.

Numerical studies based on 3D modelling of FSW under different process parameters has been conducted by H.W.Zhang et al. (2007). They have used non-linear continuum mechanics for the FEM based simulations to show the influence of process parameters. They have correlated the distribution of equivalent plastic strain with the microstructure zone in the weld. They have also found that the material flow has been accelerated with the increase in translational velocity and angular velocity of the pin.

Hamilton et al. (2009) have developed a thermal model of FSW in aluminium alloys. The model utilized a new slip factor based on the energy per unit length of the weld. The slip factor has been derived from an empirical linear relationship observed between the ratio of maximum welding temperature to the solid temperature and welding energy. The authors have also extended this study in the friction stir welded joints from Al-Mg-Cu alloy extrusions. In an another study conducted by the same authors, a thermal model for FSW of Sc-modified Al-Zn-Mg-Cu alloy extrusions have been developed. The said model is based on Johnson-Cook plasticity approach in which heat generation due to plastic deformation have been accounted. With the incorporation of heat generation due to plastic deformation, the thermal model has ac-

curately predicted the maximum weld temperature and temperature profile at the higher energy weld conditions.

Zhang and Zhang (2009) have conducted numerical studies on controlling process parameters in FSW. A thermo-mechanical model has been developed by them to predict the material deformation and temperature histories in FSW. It is found that welding temperature has been increased with the increase in tool rotation. It is also noticed that the input power has been increased with the increase in welding speed.

Kim et al. (2010) have done the numerical simulation of FSW butt welding process for AA5083-H18 steel. A thermo mechanical model and its simulation has been performed by them. The commercial FEM code STAR-CCM+ based on Eulerian formulation has been used for the study. Distribution of temperature and strain rate histories have been calculated under steady state condition. It has been found that inclusion of thermal boundary condition for back plate will enhance the accuracy of prediction.

Assidi et al. (2010) have developed numerical model based on the FSW experiment conducted. Material used for the study is Al6061. The model is based on an arbitrary Legrangian Eulerian formulation implemented in the Forge 3 FE software. The main feature of the numerical approach is the accurate computation of contact and frictional surface between the plate and the tool.

Jackuin et al. (2011) has developed a simple Eulerian thermo mechanical model of FSW. The study is based on the model proposed by Heurtier et al. (2006) based on a combination of fluid mechanics, numerical and analytical computations. They have allowed a partial sliding between shoulder and the workpiece, the amount of which has provided as an additional result of the model. The thermal calculation accounts for the conduction and convection effects by means of the particular derivative. It is reported that the complete thermo-mechanical history of the material during the process can be accessed by temperature and strain rate contours.

Buffa.G et al. (2011) have developed numerical procedure for residual stress prediction in FSW. The commercial FEA software DEFORM-3D TM has been utilized for the prediction.

Chen and Kovacevic (2013) have done FE Analysis of FSW. Both thermal and thermo mechanical analysis have been carried out by them. The model has incorporated the mechanical reaction of the tool and thermo-mechanical process of the welded material. The heat source incorporated in the model includes the friction between the material, probe and the shoulder. Using the numerical model, the prediction of thermal history, evolution of longitudinal, lateral and through thickness stresses have been carried out. The residual stresses evaluated based on the X Ray diffraction techniques has been found matching with the numerical predictions.

They have also formulated the relationship between the calculated residual stresses and the tool traverse speed.

Al-Badour et al. (2013) have done analytical investigation on FSW. They have developed a coupled Eulearian Legrangean FE model for FSW process. The model can predict the likely conditions that results for the defect generation in FSW joint formation. The workpiece has been modelled using Eulearian formulation while the tool has been modeled using Lagrangean approach. Coulumb friction at contact model has been adopted to define the tool workpiece interaction. Welding speed has been defined by material inflow and outflow velocities. It is found that μ has major effect on the weld formation.

2.2.3 Materials

Almost all the investigators have used aluminium alloys for the experimental investigation on FSW. Table 2.1 indicates most common materials used by various researchers.

Table 2.1: Material used for the research in FSW

Sl No	Name of Material	Name of Researchers
1	304L stainless steel	Lee et al. (2004)
2	Al 6061	Soundararajan et al. (2005) and Assidi et al. (2010)
3	AA2024-351 Alloy	Heurtier et al. (2006)
4	AA2024-T4 and AA7075-T6 sheets	Barcellona et al. (2006)
5	AA6061/Al2O3/20p reinforced alloy	(Marzoli et al., 2006)
6	AA7005/10vol Al2O3 p composites	Ceschini et al. (2007)
7	AA6082	Cavaliere et al. (2008)
8	AA2219	Elangovan and Balasubramanian (2008)
9	2198Al Li -plates	Cavaliere et al. (2009)
10	Sc modified Al-Zn-Mg-Cu	Hamilton et al. (2009)
11	copper metals (C11000)	Hwang et al. (2010)
12	AA5083-H18 steel	Kim et al. (2010)
13	Copper and its related Alloys	Hwang et al. (2010)
14	6060 Aluminium Alloy	Elatharasan and Kumar (2012)
15	AA 2024-T3 plates.	Trimble.D et al. (2012)
16	2198-T8 Aluminium Lithium Alloy	Yu-E-Ma et al. (2013)
17	Metal matrix composites	Prater (2014)

2.3 Investigations on FW

Literature review on FW has been carried out as two sections, experimental and numerical. About fifteen research papers have been reviewed. In almost all the papers, the influence of process parameters, mechanical and microstructureal characteristics and numerical simulations of friction welding process have been discussed.

2.3.1 Experimental Investigations

Nearly ten papers on experimental investigations on FW relevant to this research are available. In these papers, the investigations on the feasibility of FW on dissimilar metal joining have been discussed. The main material utilized by researchers are alloys of steel and copper. Major studies have been focussed on the optimization of FW process parameters, mechanical and micro structural characteristics of friction welded joints. A few papers have also discussed on the residual stress prediction in friction welded joints.

Sahin (2004) and Deng and Xu (2004) have done experiments on joining plastically deformed steel with friction welding. As per them the most interesting parameters which governs the friction welding process are friction time, friction pressure, forging time, forging pressure and rotation speed.

Reddy et al. (2005) have done dissimilar friction welding of austenitic and ferritic stainless steel. They have performed the welding parameter optimization. They have also done the microstructure studies and mechanical characteristic studies. The results from both studies have been correlated. They have also studied the fracture behaviour of dissimilar friction welded joints. A continuous drive friction welding machine has been used by them for the experiment. 23 factorial design of experiments has been adopted for the process parameter optimization. Vickers hardness test, notch tensile test, charpy V notch impact testing etc have been done under mechanical characteristic studies. They have also performed residual stress measurement across the interface using X-Ray stress measurement technique.

Mumin-Sahin (2005) have done experiments for the joining of high speed steel and medium carbon steel using FW. They have also performed mechanical characteristics studies of FW joints by conducting tension tests, fatigue tests, notch impact test and hardness tests. The parameters have been optimized using factorial design. The two key factors considered for the study are friction time and friction pressure. The other parameters which maintained as constants are upset time, upset pressure and rotational speed. tensile strength verses friction

time, tensile strength verses friction pressure and Vickers hardness verses distance from the centre of welded joint have been plotted based on the studies.

Mohandas.T et al. (2007) have done friction welding of dissimilar pure metals. Different joints considered are Fe-Ti, Cu-Ti, Fe-Cu, Fe-Ni and Cu-Ni. All the joints have been subjected to tensile and micro structure studies. Continuous drive friction welding machine has been utilized for the studies. Different testing methods utilized are scanning electron microscopy, Electron Probe Micro Analysis (EPMA), X Ray Diffraction and Tension test.

Ambroziak et al. (2007) has done friction welding of In-coloy MA956 Alloys. One of the specimens is work hardened and the other is thermally treated. Micro structure, micro hardness and tensile strength of the joints have been determined. They have also found out the optimum friction welding process parameters.

Madhusudhan.G and Ramana.P (2012) have conducted experiments to assess the role of nickel as an interlayer in dissimilar metal friction welding of maraging steel to low alloy steel. They have used continuous drive friction welding machine for the study. To incorporate nickel as an inter layer, maraging steel and nickel have been welded first.

Budau et al. (2012) have done experiment on dissimilar friction welding of induction surface hardened steel and thermo-mechanically treated steels. For this case a high axial pressure of 200 N/mm^2 has been used for the effective joining of C55 steel with C45 nitried steel. The chemical composition of each steel has been determined by optical emission spectrometry in an ARL Quantorac 3460 metal analyzer. A direct drive custom made friction welding machine capable of performing up to 120 welds per hour has been used for the experiment. The macroscopic observation has been made using an Olymbus SZH-10 stereo microscope and the micro structure has been analysed using an Olymbus BH-2 metallographic microscope with focus on the interface, HAZ and TMAZ. Welded joints have also been subjected to mechanical characteristic studies by conducting bending test, torsion test, impact test and hardness tests etc.

Udayakumar et al. (2013) have performed experiments on super duplex stainless steel joints using FSW. Design of experiments has been done using central composite design of response surface methodology. Phase analyser software has been used to assess the ferrite contents. It is seen that FSW joints have possessed mechanical characteristics higher than the base metal

Radoslaw-Winiczenko and Mieczyslaw-kaczorowski (2013) have conducted friction welding of ductile iron with stainless steel. Scanning electron microscopy has been used for the investigation of the fracture morphology and phase transformation. The distribution of selected elements on both sides of the joining interface has been studied using EDS line and maps

spectrometry.

Shanjeevi.C et al. (2013) have conducted experiment to evaluate the mechanical and metallurgical characteristics of dissimilar friction welded joints. The materials used are austenitic stainless steel 3042 and Copper. Tensile tests, hardness tests and micro structure studies and EDX line tests have been performed. Taguchi analysis has been used to assess the effect of friction pressure, upset pressure and rotational speed. They have found that the highest tensile strength is 2.52 higher than the parent metal-copper.

2.3.2 Analytical Investigations

Izani et al. (2010) have carried out thermal modelling of the FW in mild steel and aluminium. Numerical modelling has been performed using an explicit one dimensional finite difference method, to approximate the heating and cooling temperature distribution of the joint. In addition to that they have also performed mechanical characteristic studies. It is found that the thermal effects of the FW has lowered the welded materials hardness compared to the parent materials. The tensile strength of the welded rods was found lower than the parent rods due to incomplete welding.

Ceretti.E et al. (2010) have done the numerical modelling of the LFW of AISI 1045 parts. The numerical model has highlighted the process mechanics and the physical conditions which must be reached in order to obtain a correct and effective bonding between the specimens. In this way, the distribution and the history evolution of the most relevant field variables, namely temperature, strain, strain rate and pressure reached at the interface between the two specimens have been investigated. The numerical simulation of the LFW has been carried out using E Deform2DTM commercial code. The study has proved the ability of a two dimensional model, in plane strain conditions to simulate the actual LFW process conditions.

Wladyslaw-Wlosinski et al. (2009) have performed investigations on thermo-mechanical and diffusion modelling in the process of ceramic-metal friction welding. The model has been practically verified in the process of friction welding by corundum ceramic of 97.5 Al2 O3 content and Al6061-T6, ceramic and electrolytic copper of 99 Cu content. A simulation of the process has been performed by means of FEM based systems like ADINA T and ADINA. The temperature distribution and thermo mechanical effects during the FW process has been simulated in this study. The results showed that the temperature, pressure and deformation distribution near contact surfaces are non-homogeneous. Thus, the numerical simulation of the friction welding process has helped for the better understanding of the whole process and final product shape prediction.

Skalski et al. (2006) have done the FE modelling of thermo-mechanical effects in the FW process. The material considered are corundum ceramics which contains 97% of Al2O3 and aluminium. The mechanical and temperature fields have been considered as coupled fields. The model has simulated the loading of the elements bonded with the heat flux from the friction heat on the contact surfaces. Along with the numerical modelling experiments have also been done to note the temperature distribution on the periphery of the cylindrical surfaces using thermovision camera. It is found that pressure distribution on the contact surface during friction heating-up is highly non-uniform.

Sahin (2004) have made studies on the simulation of friction welding using a developed computer program which simulated weld flashes in friction welded joints having equal and different diameters of AISI 1040 (medium carbon steel). The program is coded with Microsoft Visual BasicTM 6.0. The 3D models has been created with 3D Studio Max R3. The simulated results has been compared with those of the experiments. The simulation has been found quite properly similar to the macro-photos of the joints. This study has helped the experimenters to examine occurrence of the welding flashes at various time and pressures. The simulation has also helped to understand the location of maximum upsetting in joints.

citetkubiszyn2003 have carried out a 3D numerical analysis of FW. Material considered are general purpose 45-grade constructional steel rods and 34 HNM-constructional alloy steel used in hardening and tempering. Rods are assumed with 60 mm long. It is also assumed that heating at contact surfaces with an unidentified flow of thermal energy has been occurred under the pressure of 100 MPa. The distribution of the intensity of heat flow within the rod, the generation of the thermal field during the FW operation and the effects in stresses with changes in the thermal field have been investigated. It is found that frictional radial heating has been varied with the rotational speed.

2.3.3 Materials

Almost all the researchers have used alloys of steel for FW studies. Some of the combinations of steel alloys used are shown in Table 2.2

Table 2.2: Material used for the research in FW

Sl No	Name of Material	Name of Researchers
1	General purpose 45-grade constructional steel	Kubiszyn and Pietras (2003)
2	AISI 1040 (medium carbon steel)	Sahin (2004)
3	Austenitic and Ferritic stainless steel	Reddy et al. (2005)
4	High speed steel and medium carbon steel	Mumin-Sahin (2005)
5	In coloy MA956 Alloy	Ambroziak et al. (2007)
6	(Fe-Ti, Cu-Ti, Fe-Cu,Fe-Ni and Cu-Ni)	(Mohandas.T et al., 2007)
7	mild steel and aluminium	Izani et al. (2010)
8	nickel, marraging steel and low alloy steel	Madhusudhan.G and Ramana.P (2012)
9	super duplex stainless steel	Udayakumar et al. (2013)

2.4 Critique of the Literature Review

Literature review on more than twenty research papers in experimental investigations and fifteen research papers on numerical investigations has been carried out. In the case of FW, ten papers on experimental investigations and five papers on numerical investigations have been reviewed.

Experimental investigations on FSW mainly includes mechanical and micro-structure studies of friction stir welded joints (5 Nos), influence of process parameters (4 Nos), dissimilar friction stir welding (3 Nos) and methods on simultaneous measurement of process parameters like tool rotation and tool traverse (2 Nos). Discussion on temperature measurement techniques during FSW process, FSW of metal matrix composites and methods on residual stress measurement have been discussed in some papers. In addition to that, fatigue and Fracture behaviour studies of friction stir welded joints and its comparison with conventionally welded joints have been presented in few papers.

In the case of numerical investigations on FSW, six papers are dealt with the thermal modelling of FSW. Discussion on the material flow simulation in FSW, numerical modelling to predict residual stresses in FSW joints, numerical modelling to study influence of process parameters of FSW have also been discussed in few papers.

Experimental investigations on friction welding includes joining of steel and related alloys using FW (7Nos). In all these studies, mechanical and micro structure characteristics have been discussed. Friction welding of similar pure metals and its dissimilar combinations have also been discussed in some papers.

In the case of numerical investigations on Friction Welding, 11 research papers have been reviewed. All the papers are dealt with the thermo mechanical or thermostructural modelling

using FE software packages like ANSYS, Abaqus etc. All these models have predicted stress, strain during FW processes.

2.5 Scope of Experimental Study

Experimental studies give opportunities to familiarize real processes, process parameters, materials for specimen, materials for tools, various forces and its measuring techniques, constraints in the joining techniques, comparison with existing techniques etc. Hence considering the huge applications in aerospace, shipbuilding and automotive industries experimental studies on FSW and FW have huge scope to provide contributions to the benefits of society.

2.5.1 Friction Stir Welding

A good FSW joint is an outcome from the setting up of optimum process parameters, selection of suitable materials, usage of properly designed FSW tool etc. considering this aspects, experimental investigations on FSW joints is having much scope which enhance the developments in automotive, aerospace and shipbuilding industry. Hence, the studies give the scope for conducting experimental study on FSW of Al2219 alloy. It also give the opportunity to use statistical tool based software package like Minitab to optimize the process parameters. In addition, it give the scope for comparing the FSW joint of Al2219 alloy with conventional welded joints of the same especially by DCSP TIG and ACSQW TIG welding techniques.

2.5.2 Friction Welding

A good friction welded joint is an outcome from the setting up of optimum process parameters, selection of suitable materials, usage of properly designed setup to provide adequate speed for the rotating specimen, adequate loading system etc. In addition, study on friction welding methods has got much importance for the joining of various materials. Considering this aspects, experimental investigations on FW is having much scope in automotive, aerospace and shipbuilding industry. Hence, the studies give the scope for conducting experimental investigation on FW of Al6061 alloy. It also give the scope for comparing the FW joint of Al6061 alloy with conventional welded joints of the same especially by Arc and Gas welding techniques. In addition to that, it give the scope for studying optimization techniques of process parameters. Besides that it give the scope for doing experiments to understand the effect of interface

geometry in the FW of aluminium alloys.

2.6 Scope of Numerical study

A large amount of money has been spent by Government to carry out experimental studies as part of R & D works in joining techniques, in aerospace and shipbuilding industry. All the experiments are time consuming also. Numerical modelling of those problems by incorporating governing equations can contribute much for the understanding of the processes and prediction of response characteristics. Hence numerical modelling of FSW and FW process have got much scope for the development Aerospace and Shipbuilding industry.

2.6.1 Friction Stir Welding

Measurement of process parameters in an FSW process by experimental methods need proper attention and care. In addition, it is seen that all the measuring instruments are making use of complicated micro electronic circuits which may get spoiled with the temperature developed. It is also observed that tool rotation measuring device may subject to high vibration. In addition, tool wear, friction etc may affect the value of process parameters. In such situation development of numerical model on FSW has got much scope in the understanding FSW characteristics. Hence, the literature review gave the scope for conducting numerical study of FSW process to assess the temperature distribution in FSW joints.

2.6.2 Friction Welding

Measurement of process parameters in FW process by experimental methods also need proper attention and care. Slight variations may be occurred while noticing friction pressure and up-setting pressure. In such situation, development of numerical model on FW has got much scope in the understanding of friction welding characteristics. Hence, the literature review give the scope for conducting numerical study of FW to assess the temperature distribution, stress, strain and residual stress developed in similar and dissimilar friction welded joints.

Chapter 3

EXPERIMENTAL INVESTIGATIONS

This chapter explains the experiments conducted for the present research work. The main work includes the development of FSW as well as FW setups. As per the various researchers followed, FSW setup has been made in a conventional vertical milling machine. For the FW setup a conventional lathe attached with a hydraulic loading cum work holding arrangement has been used. The welded joints obtained from both the cases have been subjected to mechanical and microstructure studies.

3.1 Friction Stir Welding

The very first stage under this section is the development of a FSW setup from a vertical milling machine attached with a suitable friction stir welding tool. In addition a suitable fixture is also required to fix the specimen suitably for the FSW operation. A friction stir welding tool is always subjected to static and dynamic loading due to tool axial forces, its stirring effect at the joining faces of workpiece, frictional effect due to the initial piercing into the work pieces, frictional force due to its own rotation and traversing along the joining line of workpieces and the high thermal loading occurred at the time of FSW process. To withstand all this static, dynamic and thermal loading the tool material should be sufficiently strong, tough and hard. Further it should have a good oxidation resistance and a low thermal conductivity to minimize heat loss and thermal damage to the machinery. Hence for the present work, a friction stir welding tool has been made from hot-worked tool steel named AISI H13. Figure 3.1 represents the geometrical requirements of the tool made as per the ASTM standards. The main purpose of a fixture is to hold the workpiece during machining operation. In FSW process, the type of forces which act on workpiece are lateral forces, traverse force, downward force and their

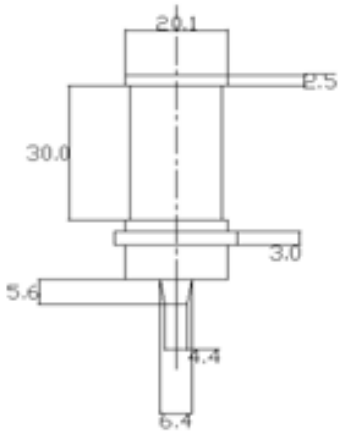

Figure 3.1: Geometrical details of FSW tool

reactive forces. To withstand all the above said forces adequate fixture has been made by special purpose C-clamps, nut and bolt arrangements and additional plates. Fixture is strong enough to protect the specimen motion from all the loadings. Figure 3.2 represents the fixture prepared for the FSW unit. Trial welding procedures have been made and using design of experiment,

Figure 3.2: Fixture prepared for the FSW process

the various process parameters for the setup has been fixed.

The material used for obtaining friction stir welded joints is AA2219 Aluminium alloy with T87 tempering condition. It is an Aluminium copper alloy developed by ALCOA in 1954 for applications at temperatures up to 315 °C. It is heat treatable wrought alloy with excellent cryogenic properties and is nick named as wonder alloy. It is basically Al-Cu-Mn turnery alloy with minor additions of Ti, V and Zr. It is the most widely and successfully used cryo aluminium alloy that flown in various launch vehicles including ARIAN V, Space Shuttle, Buran etc, it is the material obviously selected for Indian cryostage of GSLV. It possess good combination of strength and toughness. It's good weldability at cryo temperatures made it a better choice for the fabrication of cryo tanks. Its excellent weldability has been attributed to

its high copper content (5.8 to 6.8 %) and in turn related to the presence of an increased volume fraction of liquid during critical stage of solidification. Hence the solidification weld cracks if any that form during welding get healed. AA2219 can withstand weld shrinkage strains up to 12% compared to normally encountered weld strains of the order of 4%. This implies that the probability of occurrence of cracks in this material during welding is minimal compared to other aluminium alloys. The chemical composition of AA2219 is given in Table 3.1. The mechanical characteristics of the same is given in Table 3.2.

Table 3.1: Chemical composition of AA2219

Element	Cu	Si	Mn	Zn	Zr	Mg	Va	Other impurites	Ti	Al	Iron
Minimum (%)	5.8	-	0.2	-	0.25	-	0.15	-	0.2		
Maximum(%)	6.8	0.2	0.4	0.1	1	0.1	0.5	0.15	0.1	Remainder	0.3

Table 3.2: Mechanical characteristics of AA2219

Density ($\times 10^3 Kg/m^3$)	$0.6 - 2.8$	Poisson's ratio	0.33
Elastic Modulus (GPa)	$70 - 80$	Ultimate tensile strength (MPa)	440
0.2%Yield strength (MPa)	350	Percentage elongation	6
Fatigue strength (MPa)	105	Thermal conductivity (Wm-K)	170

Testing of the FSW setup has been carried out by performing friction welding process. At the very beginning of the FSW process, the rotating tool has been allowed to pierce the joining interface till the shoulder just rub the plates to create frictional heat as shown in Figure 3.3. When the joining point reached in a plastic state (it can be identified by feeling the smell) the table holding the fixtures and plates are allowed to move by auto travel mode. The milling spindle has been drawn upward and stopped after the entire joining has been over. Figure 3.4 shows the initial trial of friction stir weld formed. Very good friction stir welded joints have been obtained. Figure 3.5 shows the dimension for the same as per ASTM standards. Details of the FSW setup made for the present study is presented in the Table 3.3. Sample of surface finished friction stir welded joint obtained is shown in Figure 3.6. The joints obtained are then subjected to mechanical and microstructural studies. These characteristics have been compared with the characteristics of joints obtained from the conventional welding techniques.

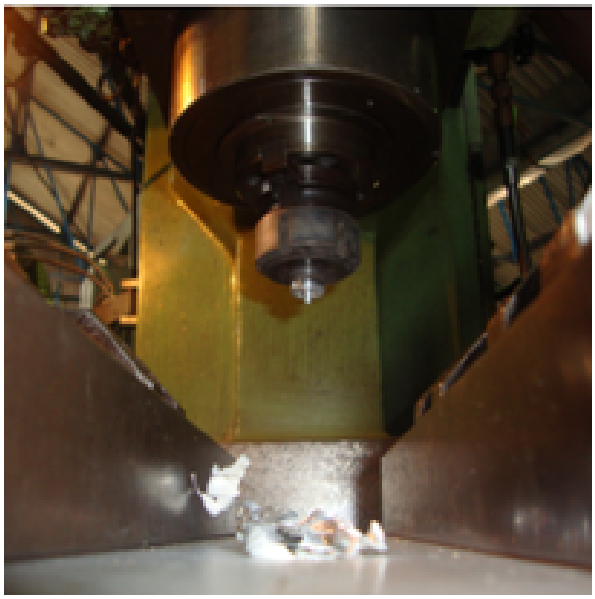

Figure 3.3: Trial of initial piercing for FSW process

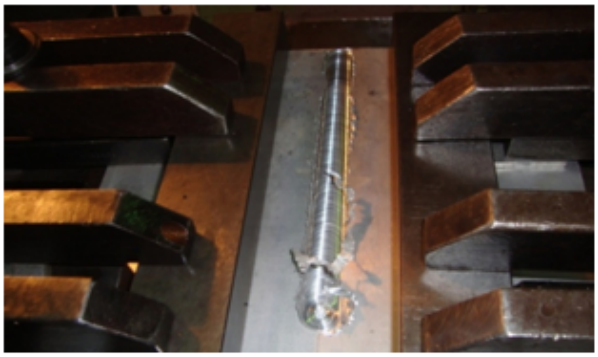

Figure 3.4: Friction stir weld formed from the initial trial

Table 3.3: Features of the FSW setup

Sl No	Features	Specification
1	Milling machine used	Vertical, with digital readout
2	Tool material	High Carbon High Chromium (D13)
3	Tool rotation speed	1500-2000 RPM
4	Speed of tool traverse	70-120 mm/min
5	Shoulder Diameter	20 mm
6	Pin diameter	6.35mm
7	Pin Minor Diameter	4.5 mm
8	Included angle	22^o

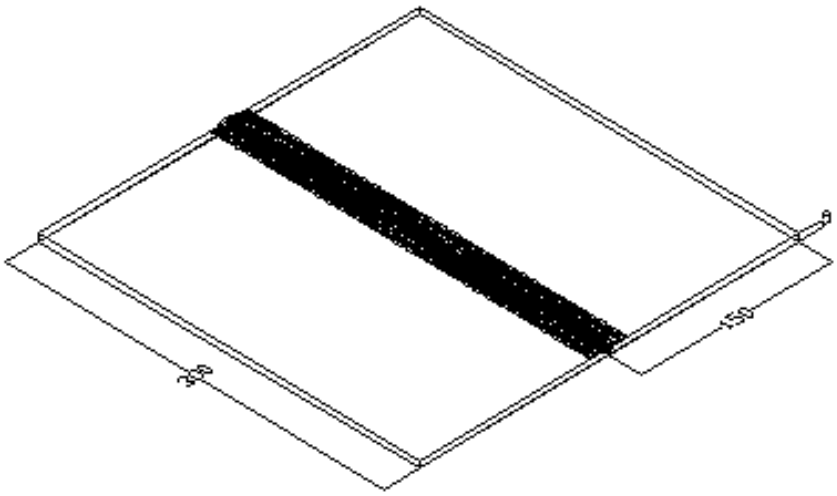

Figure 3.5: Dimensions of friction stir welded joint in mm

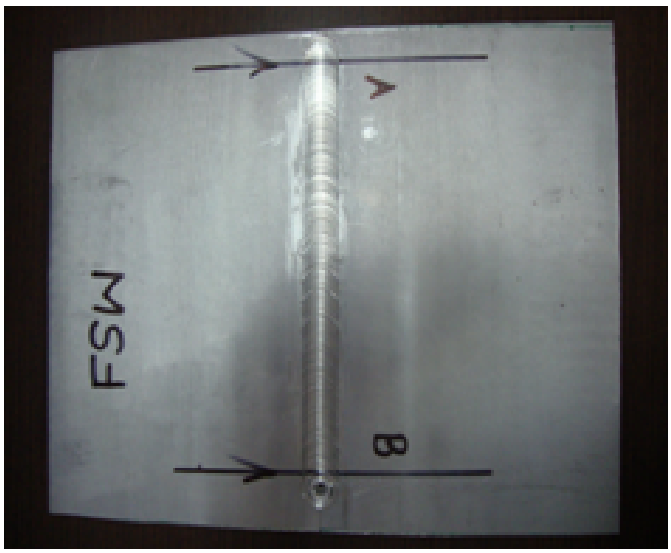

Figure 3.6: Friction stir welded joint of AA2219 Alloy

3.1.1 Mechanical Characteristics Study

It is seen that the majority of researchers have focused on the tensile characteristics study of friction stir welded joints under mechanical characteristic study. According to that, present study have also been given emphasize on the tensile characteristics of the friction stir welded joints. Tensile test specimens have been prepared as per ASTM E8 standard (See Figure 3.7) The specimens have been prepared by wire cut EDM machine and milling machine. Universal testing machine has been used for the tensile test.

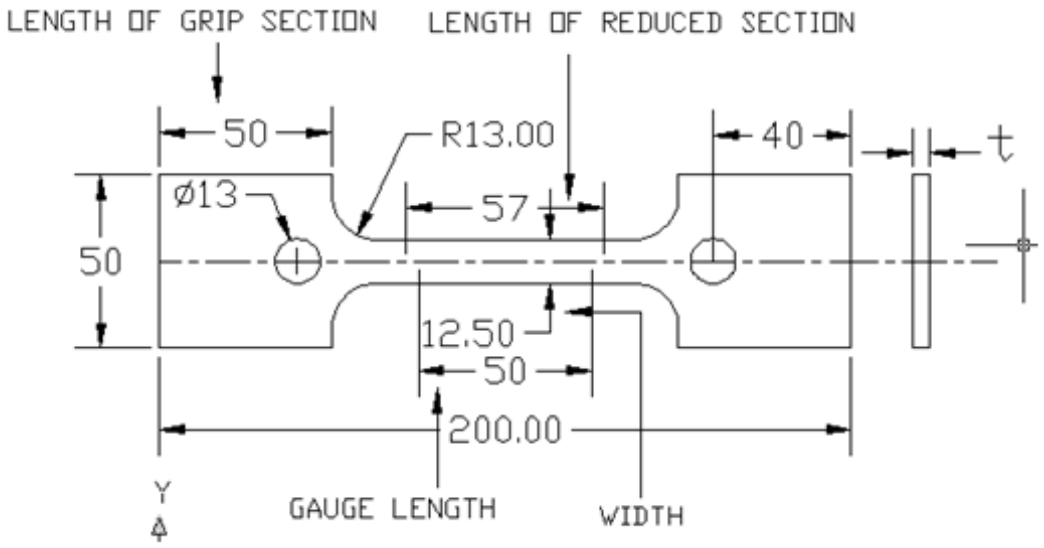

Figure 3.7: Tensile test specimen as per ASTM standards

3.1.2 Microstructural Characteristic Study

The micro structure specimen of 20 x 10 x 5 mm has been cut from each test coupon. The procedure carried out for the microstructure studies are as follows.

- Samples for metallography examination have been cut transversely to the welding direction from length of the joints.
- The samples have been cold mounted and then wet grounded using successively finer grades of SiC impregnated emery papers.
- The samples have been mechanically polished using 6, 3 and finally 1 μ diamond paste as the lubricant on polishing cloths.
- Macroscopic examination has been carried out by etching the specimen using a caustic etch, i.e.10g NaOH in 90 ml H_2O with 50% HNO_3 solution and a final rinse in water. Kellers reagent has also been used for the microscopic examination.
- The microstructure has been observed under Olympus optical microscope.

3.1.3 Comparison of Friction Stir Welded and CW Joints

DCSP TIG, DCRP (Direct Current Reverse Polarity) TIG and ACSQW TIG welding are the different versions of TIG welding techniques, conventionally used to join aluminium alloys.

DCSP TIG welding is mainly used for the aluminium alloys with thickness equal or greater than 5 mm. DCRP TIG welding is usually used to join aluminium alloy plates with thickness less than 5 mm.

In DCSP TIG welding, the job (weld plate) is connected to positive lead of weld transformer and electrode is connected to negative terminal. The current is steady and the electron flow is from electrode to job. As more electrons are hitting the job, more heat will be produced at job rather than at electrode. This results in melting of job with less heat input and better weld strength. Even though the refractive oxide layer is a major problem for this, it can be eliminated by scrapping the weld joint well before welding. In the case of DCRP TIG welding more heat is generated at electrode than job. Figure 3.8 represents DCSP TIG and DCRP TIG weld formation. In ACSQW TIG welding the job and electrode are getting connected alternately

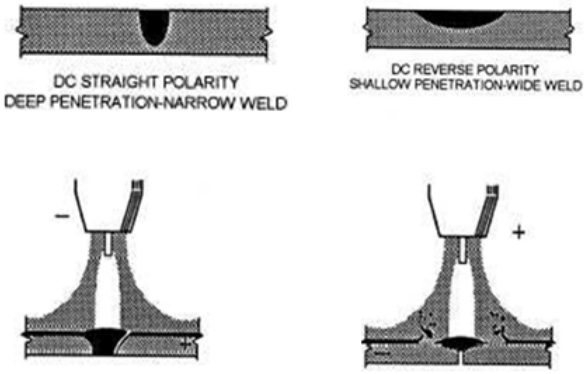

Figure 3.8: DCSP TIG and DCRP TIG weld formation (Source:tpub (2016))

with positive and negative leads of welding transformer. Hence it offers less heat input in one cycle and in another cycle good cleaning of refractive aluminium oxide can be made. Same welding machine has been used for executing DCSP TIG and ACSQW TIG welding for

Figure 3.9: TIG welding machine and the fixture

the present study. Figure3.9 represents the TIG welding machine and the fabricated fixture used for the welding processes. Welding fixture consists of back up plate made up of SS304 material and clamping plates. The base plate is having groove of 4 mm width and 2 mm depth to support the penetration part of weld. Table3.4 shows the specification of the welding unit and details on the specimen prepared for the welding. The welding power source used is

Table 3.4: Details of DCSP TIG and ACSQW TIG welding

Sl No	Welding features	Details
1	Name of welding Machine	Miller Make
2	Name of Material used	AA2219 Alloy
3	Size of the specimen	300 X 300 mm
4	Name of filler Material used	ER2319
5	Welding Parameters	Current:210-230A (DCSP),180-220A(ACSQW) Voltage: 18-20 V (DCSP),17-19 V (ACSQW) Travel speed:70-130 mm /min Shielding Gas (DCSP): Helium, (ACSQW) Shielding Gas (ACSQW):Argon+Helium (80:20) Backup bar: Stainless steel

the Miller which produces the AC square wave through the converters. Different weld trials and weld characterization have been made to arrive optimized weld parameters based on DOE procedures. Samples of ACSQW TIG welded and DCSP TIG welded aluminium plates are shown in Figure 3.10. These jonts have been subjected to tensile and microstructural studies as

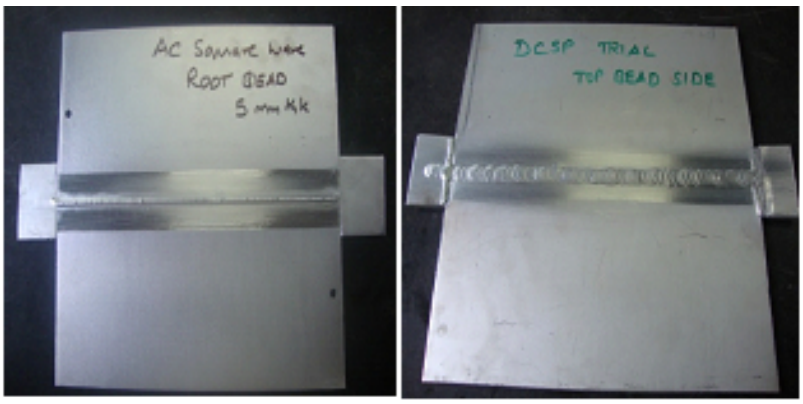

Figure 3.10: Samples of ACSQW and DCSP TIG welded joints

described in section 3.1.1 and 3.1.2.

3.2 Results and Discussion

Overview on various tests conducted under experimental investigations of FSW has been given from section 3.1 to subsection 3.1.3. The result from each studies are explained in the following sections.

3.2.1 Tensile Characteristic Studies

Taguchi orthogonal array has been used to fix the number of experiment. The experiment include formation of friction stir welded joints by controlling the process parameters such as Tool Rotation speed (TR) and Tool Traverse speed (TT) while keeping other parameters constant. These joints have been then subjected to tensile characteristics studies. Table 3.5 indicates the Taguchi orthogonal array selected to fix the number of required experiments. Since for the present study two factors with 3 level for each have been considered, L9 orthogonal array has been fixed. Thus nine friction stir welded joints have been made. Three tensile test specimen as per ASTM E8 standard has been prepared from each and found out the average value of tensile strength from each welded joints. The signal to noise ratio - larger the best option has been selected to optimize the FSW process parameters.Table 3.6 represents the response table for the signal to noise ratio as per the condition-larger the best. Table 3.7 represents the ANOVA table to assess the influence of each process parameters in the response characteristics. Figure 3.11

Table 3.5: Taguchi L9 orthogonal array for FSW

Sl No	Tool rotation Speed (TR) rpm	Tool Traverse Speed (TT) mm/minute	Ultimate Tensile strength of FSW joint MPa
1	1600	80	283.11
2	1600	90	282.20
3	1600	100	284.00
4	1700	80	284.00
5	1700	90	285.00
6	1700	100	286.61
7	1800	80	285.00
8	1800	90	288.00
9	1800	100	293.00

represents main effect plot of SN ratios indicating the optimum process parameters which give

Table 3.6: Response Table - S/N Ratio - FSW

Level	Tool rotation speed (TR) rpm	Tool Traverse speed (TT) mm/ minute
1	49.04	49.07
2	49.10	49.10
3	49.21	49.18
Delta	0.17	0.12
Rank	1	2

Table 3.7: Regression Analysis-ANOVA - TS verses TR and TT

Source	DF	Adj SS	Adj MS	F value	P Value
Regression	3	81.06	27.0352	33.76	0.001
TR	1	8.55	8.5547	10.68	0.022
TT	1	11.06	11.061	13.81	0.014
TR * TT	1	12.638	12.6380	15.78	0.011
Error	5	4.004	0.8009		
Total	8	85.110			

the maximum value of UTS for the friction stir welded joints. Thus,based on the analysis high response value (293 MPa, 67% of parent metal) has been obtained for a TR of 1800 rpm and TT of 100 mm/minute. This might have enhanced the stirring and material transfer between plates to obtain a firm joint. From the analysis it is also seen that TR influences more than that of TT. ANOVA table indicates that the combined effect of both parameter strongly influence the tensile characteristics of the friction stir welded joints obtained. The regression equation obtained from the ANOVA is $TS = 493.1 - 0.1322TR - 2.380TT + 0.001778TR * TS$.

Thus, FSW process is very effective in the joining of aluminium alloys. It is also seen that the surface finishing operations required for the friction stir welded joint is very less.

3.2.2 Microstructural Studies

The microstructure of weld cross sections have been examined at 100 x and photographed using Olympus optical microscopy. Different regions such as weld zone (WZ), interface i.e partially melted zone (PMZ), heat affected zone (HAZ) and parent metal are examined. Figure3.12 shows the micro structure photograph at weld region of friction stir welded joints of AA2219.

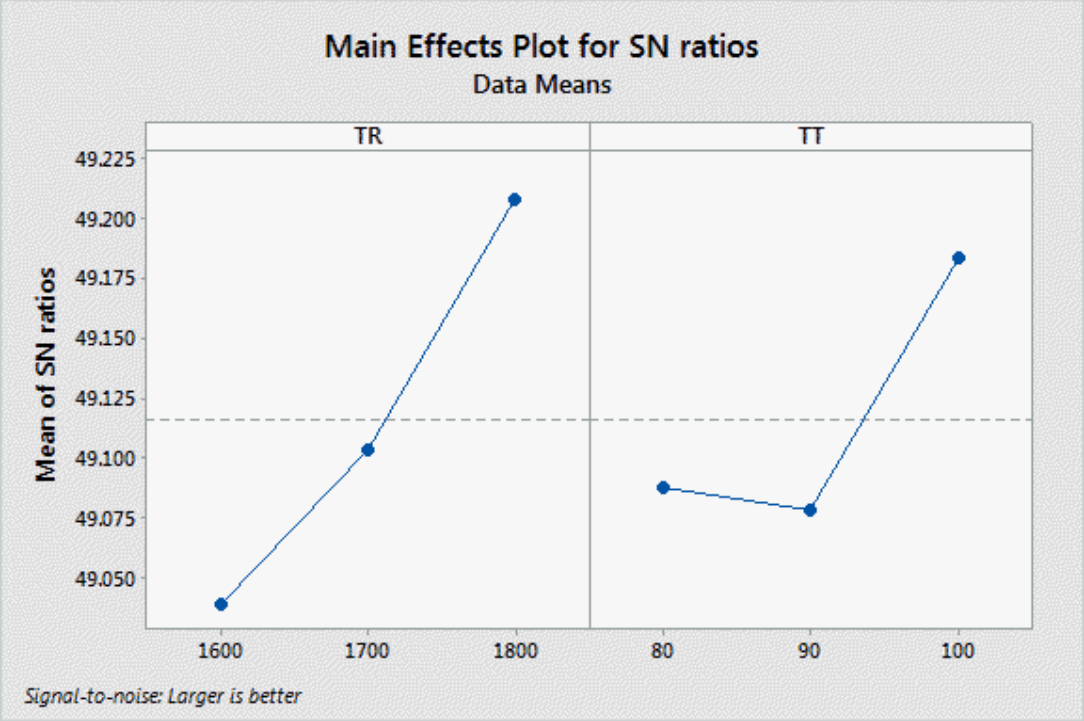

Figure 3.11: Optimum values of process parameters for FSW

Microporosities have not been seen in the microstructure of friction welded joints. Both gas

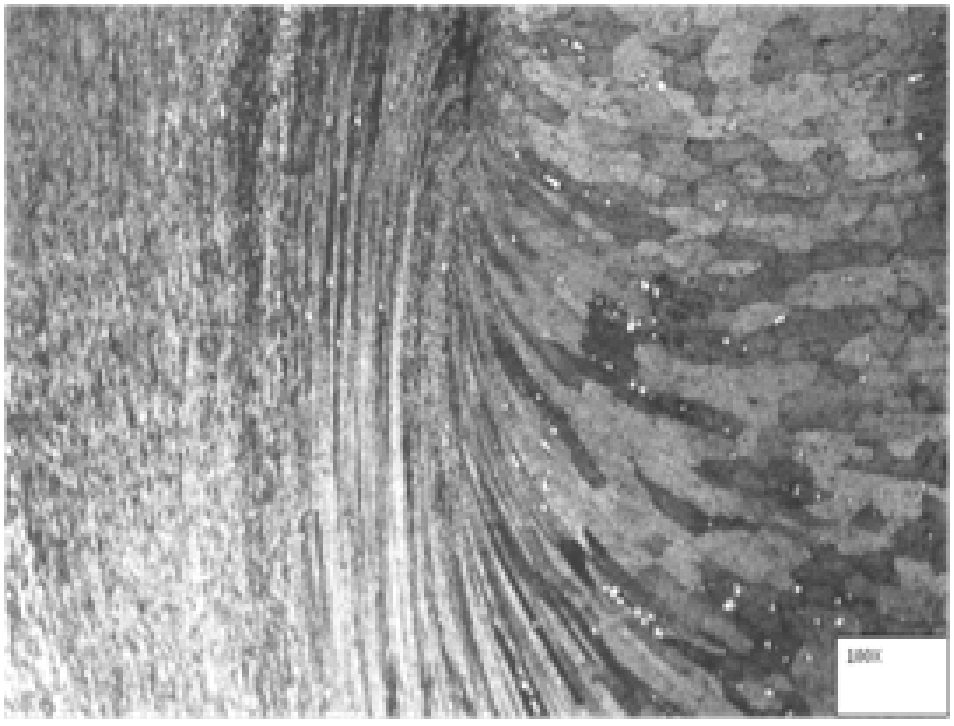

Figure 3.12: Weld region of friction stir welded joint

porosities and inter dentritic porosities are absent in the samples. No interface between the

HAZ and weld regions has been observed. Cu rich films (white coloured cells) along the grain boundaries are found absent in the HAZ region. Flow of grains in the direction of tool movement is also observed.

3.2.3 Comparison of joints by FSW and CW

ACSQW TIG welding involved mainly three factors with 3 levels. Hence L9 Taguchi orthogonal array has been fixed. Table 3.8 represents the parameters with various levels used to obtain the ACSQW TIG welded joints with response as the tensile strength of each joints. Nine

Table 3.8: Taguchi L9 - response table for ACSQW TIGW joints

Sl No	Welding Current (A)	Voltage (V)	Welding speed (mm/minute)	Ultimate Tensile Strength (Mpa)
1	180	17	90	247.78
2	180	18	100	248.05
3	180	19	110	247.86
4	200	17	100	252.51
5	200	18	110	246.84
6	200	19	90	250.63
7	220	17	110	239.39
8	220	18	90	236 .98
9	220	19	100	236.57

ACSQW TIG welded joints have been made. Three tensile test specimen as per ASTM E8 standard have been prepared from each and found out the average value of tensile strength.The signal to noise ratio - larger the best option has been selected to optimize the ACSQW TIG welding process parameters. Based on the analysis high response values have been obtained for welding current as 200A, voltgae as 18 V and welding speed as 100 mm/minutes. Since this combination is not in the L9 orthogonal array a confirmation test has been carried out. According to that the values for UTS strength obtained is 252.51N/mm^2. Since this welding techniques has considered only for the comparative study of tensile characteristics with friction welded joints, influence of its welding parameters has not been investigated further. However from the response table for UTS based on Taguchi (has not presented here) it is observed that the priority of influencing parameters are current, voltage and welding speed respectively.

In the case of DCSP TIG welded joints also, the controlling process parameters are welding current, voltage and welding speed while keeping other parameters constant. Hence for this

also mainly three factors with 3 levels have been considered. Obviously L9 Taguchi orthogonal array has been fixed. Table 3.9 represents the parameters with different levels used to obtain the DCSP TIG welded joints with response as the tensile strength of each joints. Thus, nine DCSP

Table 3.9: Taguchi L9 - response table for - DCSP TIG welded joints

Sl No	Welding Current (A)	Voltage (V)	Welding speed (mm/minute)	Ultimate Tensile Strength (N/mm^2)
1	210	18	80	257.00
2	210	19	100	255.00
3	210	20	120	249.51
4	220	18	100	256.56
5	220	19	120	262.76
6	220	20	80	262.01
7	230	18	120	253.68
8	230	19	80	248.75
9	230	20	100	260.25

TIG welded joints have been made. Three tensile test specimen as per ASTM E8 standard have been prepared from each and found out the average value of tensile strength from each welded joints. The signal to noise ratio - larger the best option has been selected to optimize the DCSP TIGW process parameters. Based on the analysis high response values have been obtained for welding current as 220 A, Voltage as 20 volts and welding speed as 100 mm/minutes. Since this combination has not been in the Taguchi table, a confirmation test has been carried out to find the response values. Thus the values of UTS obtained is 265.25 MPa. Since this welding technique is also considered only for the comparative study of tensile characteristics with FSW joints, influence of its welding parameters has not been investigated further. However from the response table for UTS based on Taguchi (has not presented here) it is inferred that the priority of influencing parameters are current, voltage and welding speed respectively.

A comparison of tensile test result for friction stir welded joints, ACSQW TIG welded joints and DCSP TIG welded joints have been given in the Tables 3.10. Graphs representing comparison of tensile characteristics of welded joints with the parent metal is presented in Figure 3.13. In the case of DCSP TIG welded joints, the UTS has been found 59% and Yield strength has been found 44% near to the parent metal. The percentage elongation has been found less than that of the parent metal. In the case of ACSQW TIG welded joints the UTS and yield strength values are found as 56% and 42% respectively. The percentage elongation in this case has also been found less than that of the parent metal. Thus it is seen that the tensile characteristics of friction stir welded joints are relatively better than that of the conventional

Table 3.10: Tensile test results of friction welded and CW joints

Name of welding technique	Ultimate Tensile Strength (MPa)	Yield strength (MPa)	Percentage Elongation
Friction Stir Welding	293.0	166.8	8.4
ACSQ wave TIG welding	252.5	158.0	5.4
DCSP TIG welding	265.0	165.0	6.4

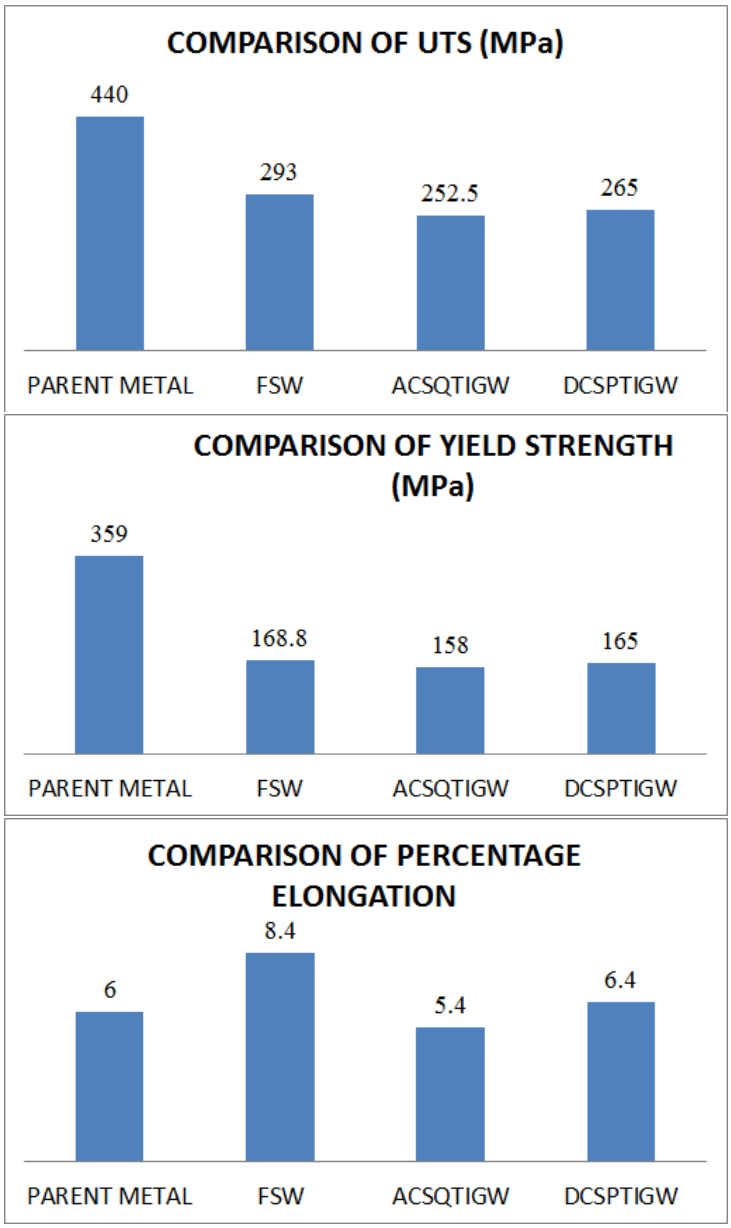

Figure 3.13: Comparison of Tensile characteristics

welded joints. Photograph indicating microstructure features of various zones of ACSQW TIG welded joints are presented in Figures3.14 to 3.17.

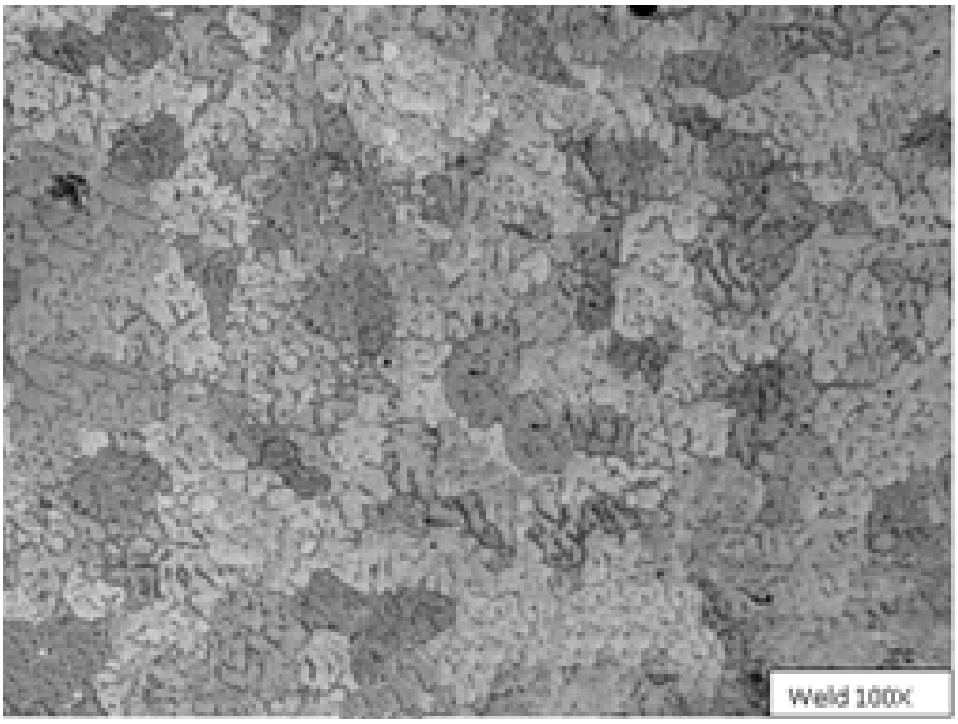

Figure 3.14: Microstructure- WZ- ACSQW TIGW joints

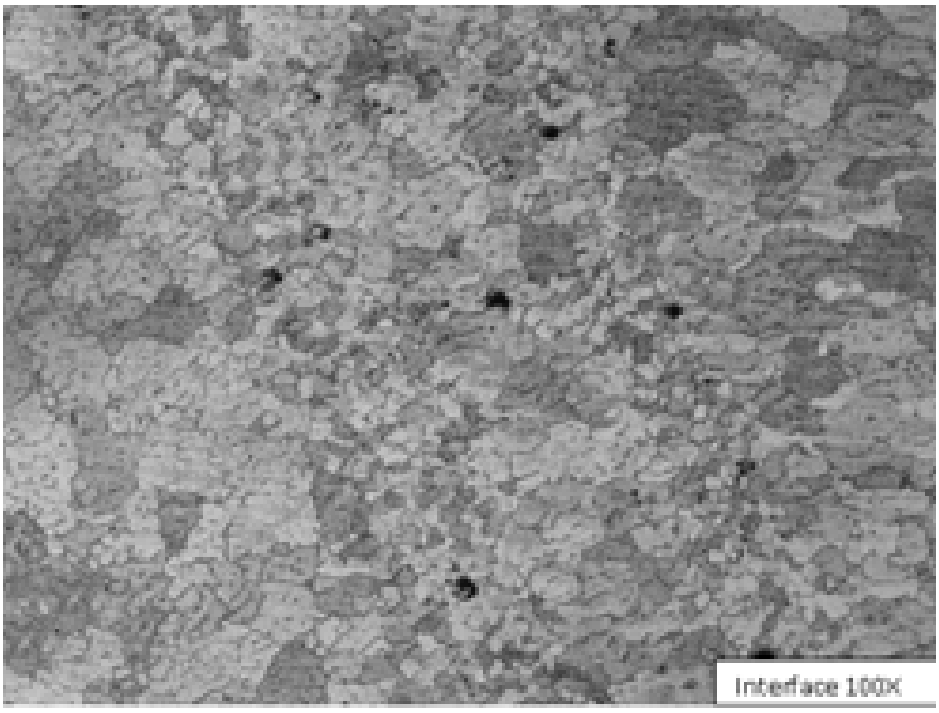

Figure 3.15: Microstructure-interface zone- ACSQW TIG welded joints

Photograph indicating microstructure features of various zones of DCSP TIG welded joints are presented in Figure 3.18 to 3.21.

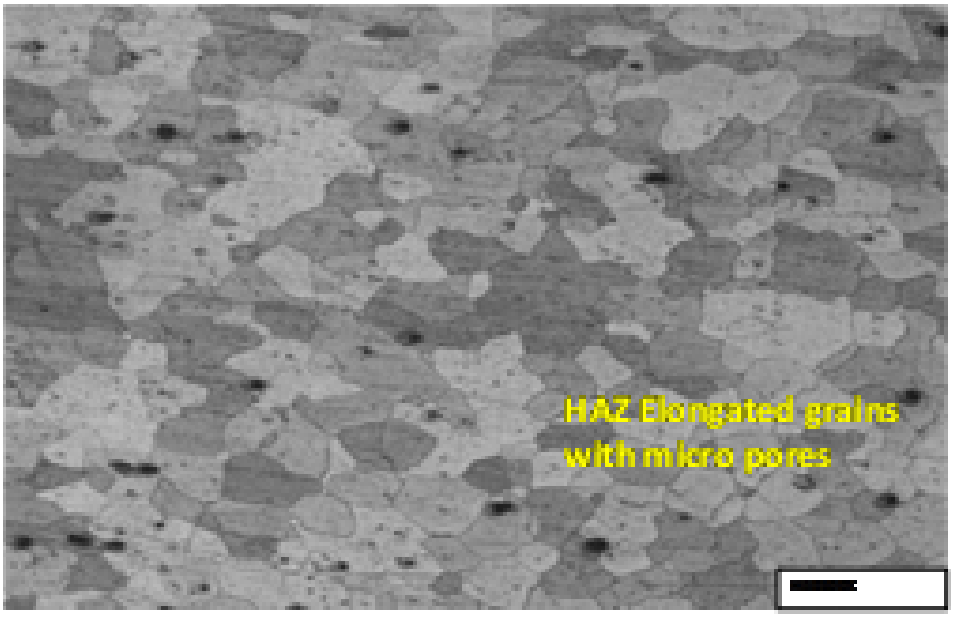

Figure 3.16: Microstructure- HAZ- ACSQW TIG welded joints

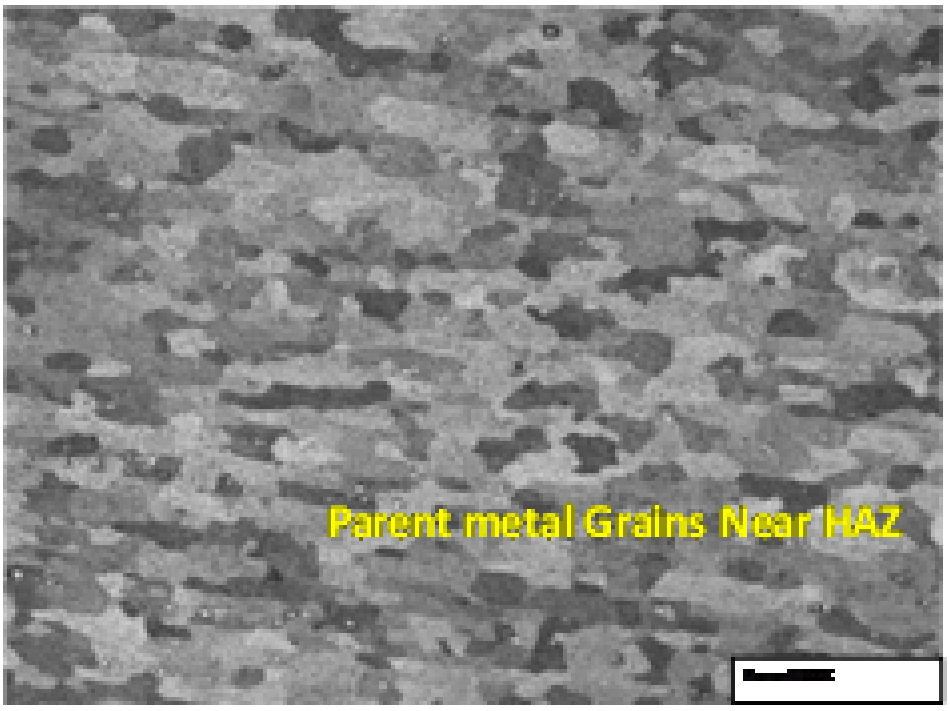

Figure 3.17: Microstructure- parent metal- ACSQW TIG welded joints

Optical micrograph of the ACSQW TIG welded joints have shown cluster of micro porosities in the weld region. Both gas porosities and inter dendrite porosities have been observed in the sample. Cu rich films have also been observed along the grain boundaries in the HAZ region. These films are seen continuous in nature, forming a network along the grain boundaries.

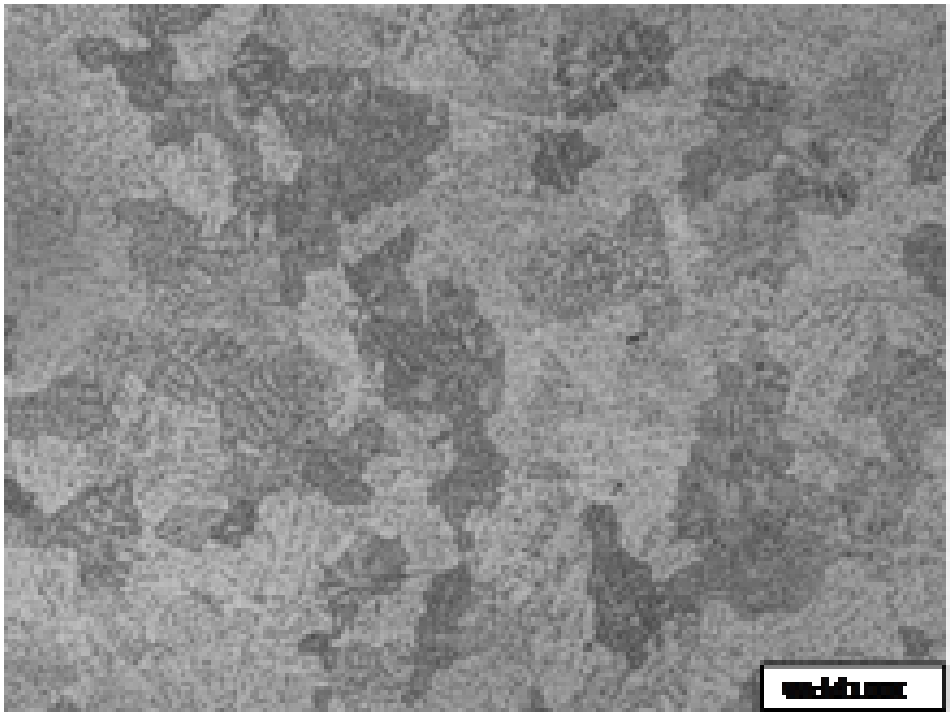

Figure 3.18: Microstructure-WZ-DCSP TIG welded joints

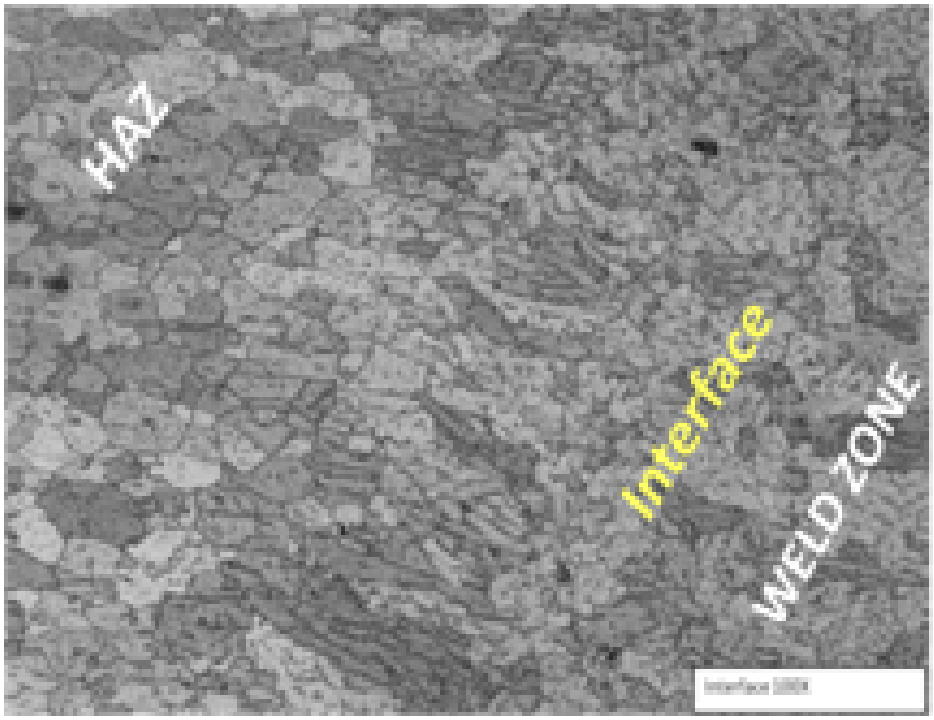

Figure 3.19: Microstructure -interface zone - DCSP TIG welded joint

The continuous network of Cu rich film which forms due to the heat of welding in the HAZ may be the cause for its lowest mechanical properties.

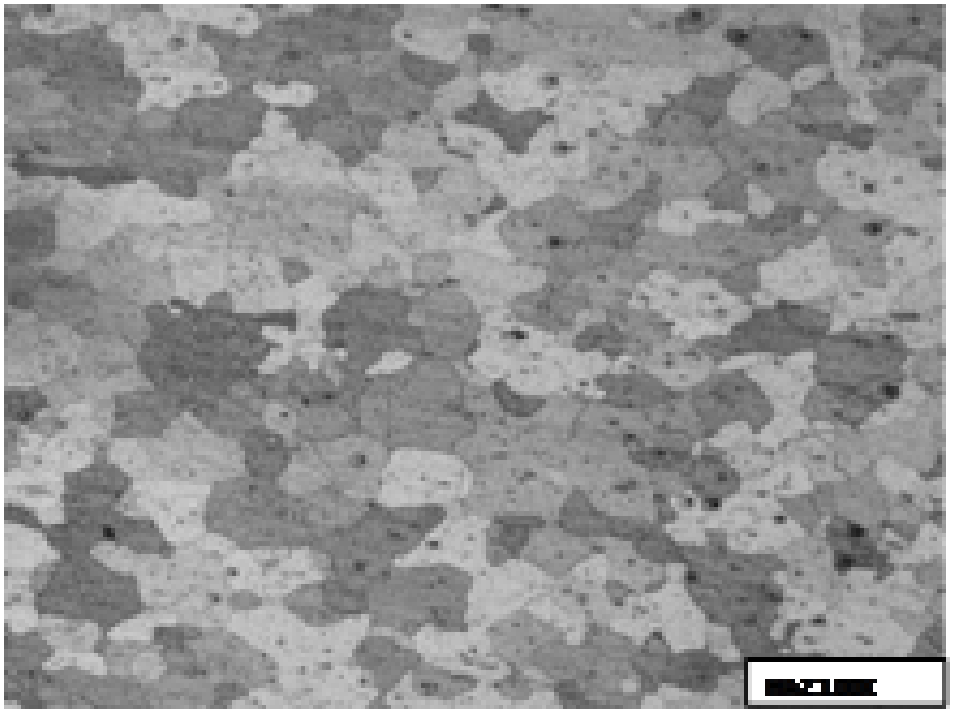

Figure 3.20: Microstructure- HAZ- DCSP TIG welded joint

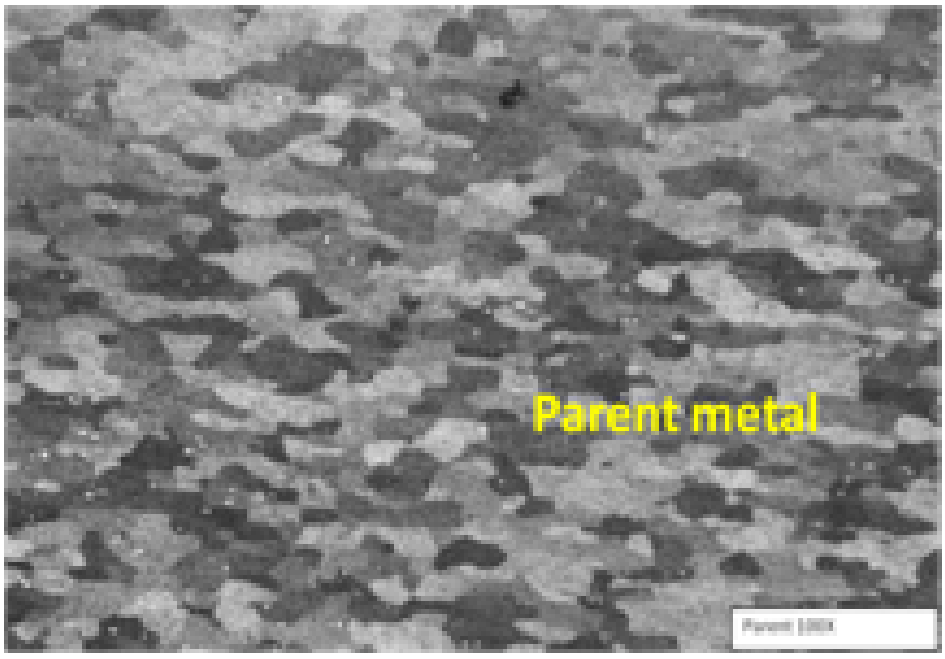

Figure 3.21: Microstructure-parent metal- DCSP TIG welded joint

Optical microstructure of the samples of DCSP TIG welded joints have presented isolated micro porosities. Discontinuous Cu rich film has also been observed along the grain boundaries in the HAZ region. Fine elongated grains has been noted in the parent material region. Second

phase particles of $(Fe, Mn)_3$,$SiAl_2$ and coarse $CuAl_2$ have been observed in the matrix of the parent material. Hence samples made from DCSP TIG welded joints shows better mechanical properties. However the highest mechanical properties including percentage elongation of more than 8, have been found in the samples from friction stir welded joint as they don't have micro porosities and brittle Cu rich films.

Thus from the tensile and micro structural characteristic studies, it is inferred that the properties of friction stir welded joints are very much close to the parent metal. Hence it can be inferred that FSW is very suitable for the joining of low weight and high strength materials like aluminium alloys, than conventional welding techniques.

3.3 Friction Welding

A FW setup has been developed initially for the research purpose. Preliminary studies have been carried out to evaluate the time taken for the formation of friction welded joints. Influence of speed on the tensile characteristics of friction welded joints has also been studied. In addition comparative study of friction welded joints and the conventional welded joints has also been studied. Details of this study are given as a separate section in Appendix A (page 111). Since only a few studies on influence of various interface geometries on the tensile characteristics of friction welded joints are available this research concentrates on this aspect. Followed with that, experiments have also been carried out to find the optimum interface angle for the friction welded joints obtained with tapered interface geometry for desired mechanical and microstructural characteristics.

3.3.1 Development of FW Setup

The basic frame work of the friction welding setup is a medium duty lathe. The tail stock of the same has been replaced with a hydraulic loading system integrated with a work holding arrangement as per the requirement of the FW process. Special fixtures have also been made to hold the hydraulic loading system unit. Figure 3.22 shows the FW setup developed for the present study The FW setup is suitable to hold workpieces diameter ranges from 0.75 mm to 30 mm. Hydraulic system can provide a pressure up to 30 MPa. The specification of the FW setup developed is shown in Table 3.11.

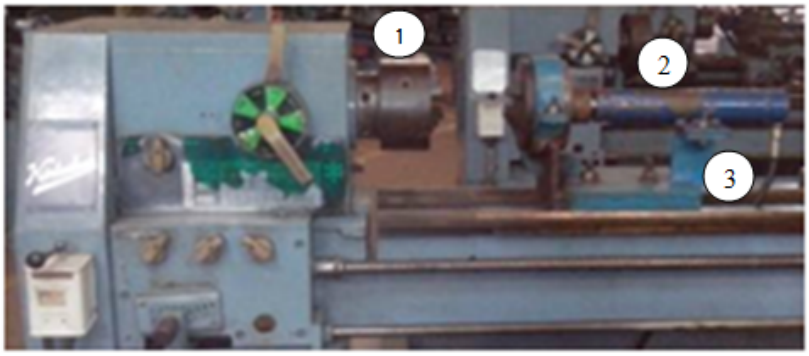

1. Chuck for rotating specimen, 2. Work holding device for stationary specimen, 3. Connection to hydraulic loading system

Figure 3.22: Friction welding setup developed

Table 3.11: Specification of the FW setup

Specification	Type/ Value	Specification	Type/ Value
Type of Transmission	Gear	Distance between centers	800 mm
Swing over bead	170 mm	Spindle bore	41 mm
Motor Power	2.2kW	Hydraulic load range	up to 30 MPa
Motor Speed	1500 rpm	Diameter of specimen	up to 30 mm

3.3.2 Material

The material used is Aluminium 6061 which is a precipitation hardening aluminium alloy, containing magnesium and silicon as its major alloying elements. Originally called ”Alloy 61S”. It was developed in 1935. It has good mechanical properties and exhibits good weldability. It is one of the most common alloys of aluminium for general purpose use. The chemical composition of the Al 6061 is given in Table3.12.

Table 3.12: Chemical composition of the Al6061 alloy

Element	Al	Mn	Si	Ti	Mg	Zn	Fe	Ni	Cu	Cr	Bal
Weight (%)	96	0.04	2.1	0.022	0.95	0.014	0.33	0.04	0.013	0.66	0.01

3.3.3 Preliminary Studies

Preliminary studies on FW welding have been carried out mainly to check the feasibility of obtaining friction welded joints from the setup developed. FW process has been carried out by

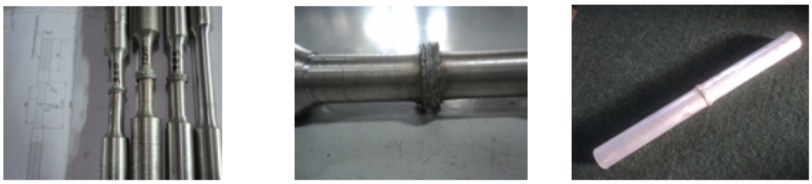

Figure 3.23: Friction welded joints from preliminary studies

keeping the rotating specimen in the head stock and the stationary specimen in the work holder of hydraulic loading system. The process has been started with a speed of 500 rpm for the rotating specimen. During this time the stationary specimen has been let to come gradually in contact with the rotating specimen with a constant axial loading of 3 MPa. Due to the friction between rotating and stationary specimen the temperature at the inter faces of the specimens has been raised to make the contact region in a plastically deformed form. At that moment, the rotation has been stopped and an axial forging upset pressure of 5 MPa has been applied on the stationary specimen. The combination of pressure and heat forges a solid state bond at the interface of the two joining parts. Figure 3.23 shows the samples of friction welded joint obtained in the preliminary studies. For this studies the specimen to be friction welded are initially modified according to the ASTM standard required for the tensile characteristic studies. The friction welded joints thus obtained with various speed for the rotating specimen have then been subjected to tensile and hardness characteristic studies. In addition to that, microstructural studies of the same have also been carried out as described in the following paragraph.

Preparations for the micro-structural study samples have been started by cutting a 30 mm portion from the welded specimen in which weld will be at the centre. This sample is again cut longitudinally and then subjected to polishing. The inner surface of the specimens has been polished using emery paper of grade 250 for 20 minutes each, emery paper of grade 600 for 20 minutes each and emery paper of grade 1000 for 20 minutes each. The specimens has been washed and dried after that. These preliminary polished surfaces have been then subjected to fine polishing process using Econet 3 variable speed grinder polisher. For that, initially using lapping cement as 6μ diamond suspension paste at 250 rpm and kerosene as lubricant, polishing has been carried out for one hour for each specimen. After that, using lapping cement as 3 diamond suspension paste at 250 rpm and kerosene as lubricant the same have been polished for one hour. Finally using Metaserv 2000 Grinder/ Polisher, the above polished materials have been fine polished by lapping cement as 0.5μ paste at 250-350 rpm and kerosene as lubricant. Selvate cloth has been used in these machines for polishing. The specimen has then been washed with mineral water and dried. The same have been subjected to etching using HF solution for 50 seconds. For the microstructure visualization Leica DMRX

optical microscope has been used. The results for the preliminary studies has been presented in section 3.4.1.

3.3.4 Influence of Interface Surface Geometries

A number of research have been conducted by various researchers on FW. Major studies includes the mechanical and microstructure characteristics of friction welded joints from similar and dissimilar metal combinations. Almost all the research work are discussing about the optimization of process parameters especially speed of rotating specimen, axial loading on stationary specimen and upset loading. Research work related to the study on the influence of interfacing surface geometry on the characteristics friction welded joints are seen very less. Hence present study mainly aimed to check whether the interface geometry influence the characteristics of friction welded joints.

Various interface surface geometries considered are Flat-Flat (F-F), Taper-Taper (T-T), Convex-Convex (Cx-Cx) and Convex-Concave (Cx-Cv). Different speeds considered are 500, 775, 1000 and 1200 rpm. Various axial loading considered are 2, 2.5, 3 and 3.5 kN. Figure 3.24 shows various combinations used under this study. FW process has been carried out as

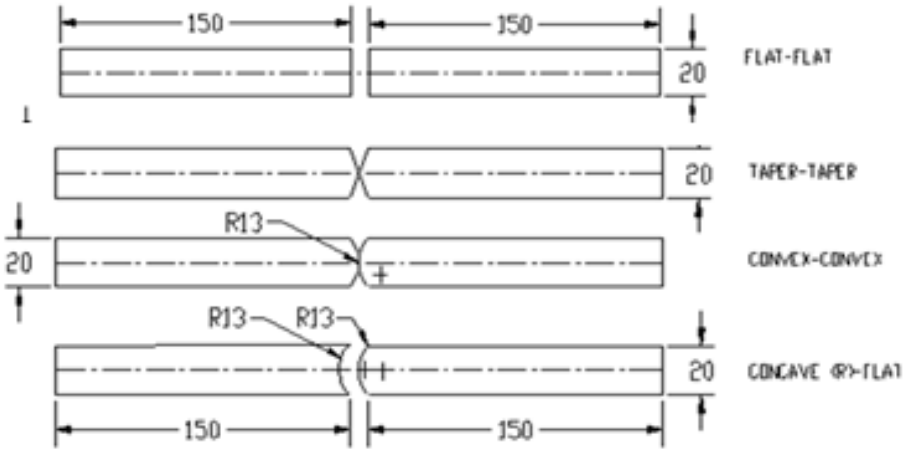

Figure 3.24: Interface geometry combinations for FW

per the procedures described in section 3.3.3, page 45. Specimen with taper interface geometry has been made by taper tuning facility available in lathe. Samples of specimen prepared for these studies are shown in Figure 3.25. Samples of friction welded joints for the tensile, torsion and hardness studies are presented in Figure 3.26. Photograph of testing machines used are presented in Figure 3.27. Torque of friction welded joints has been calculated for 5°and 10°angles of twist. Modulus of rigidity for these joints have been calculated using torsion equation, T/J = G/L. A 50 mm portion of specimen of different interface geometries with weld joint

Figure 3.25: Specimens for FW with modified interfaces

Figure 3.26: Tenslie,torsion and hardness test specimens

Figure 3.27: Machines used for tension,torsion and hardness tests

as centre is taken for hardness test. It is then longitudinally cut and various region (three points along the weld line and its average for a single tabulation) in the flat face has been subjected for brinell hardness test. The brinell hardness number has been calculated using the formula, B.H.N $= 2F/\pi D(D - D^2 - d^2 1/2)$. Results from this studies have been discussed in section 3.4.2

3.3.5 Optimum Interface Taper Angle

It is observed that interface geometries are influencing the strength characteristics of friction welded joints. In that T-T interface geometry exhibited good results (see section 3.4.2). Hence further experiments have been conducted to observe optimum dimensions for the tapered geometry which give good desired characteristics for the friction welded joints. Different interface tapered angles considered are 0°, 15°, 30°, 45°and 60°. The friction welded joints obtained in

this manner have been subjected to various mechanical characteristic tests like tension, hardness, torsion and impact toughness. Considering the factors and levels required for the design of experiment procedures even though tests for specimen with flat geometry (0°taper angle) have been carried out, results found for them have not been considered for the analysis. Table 3.13 shows the parameters considered for the FW. A close view of tapered angles considered

Table 3.13: Parameters for FW specimen with T-T interface geometry

Specimen diameter(mm)	Axial Loading (MPa)	Forging pressure (MPa)	Speed (rpm)	Interface Angles(°)
20mm	2 to 3.5	5	500,775, 1000 and 1200	15,30, 45 and 60.

for the specimen are shown in Figure3.28. In order to make a perfect align with the rotating and stationary specimen the tip of the tapered interfaces have been made a little flat. Samples of specimen prepared with various taper angles are shown in Figure 3.29. All the joints obtained in this manner have been subjected to mechanical characteristic studies (tensile, torsion, hardness and impact toughness tests etc.). Figure 3.30 shows the samples of friction welded joints obtained with various tapered angles.

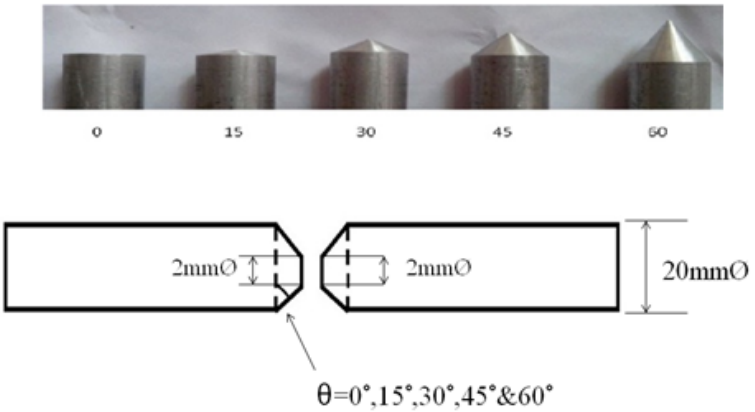

Figure 3.28: Various tapered interfaces

Toughness of the friction welded joints have been found using charpy impact test. A specimen with weld as centre having length equal to 55 mm has been cut and made it to a square prism with cross section as $10mm \times 10mm$, required as per ASTM standard for impact test initially. A v-notch of 2 mm depth has then been provided at the weld area along one of the faces in all specimens. Figure 3.31 shows the specimen prepared from friction welded joints for charpy impact testing. The results from these studies are discussed in section 3.4.4 .

In order to establish the result found from mechanical characteristic studies, metallurgical

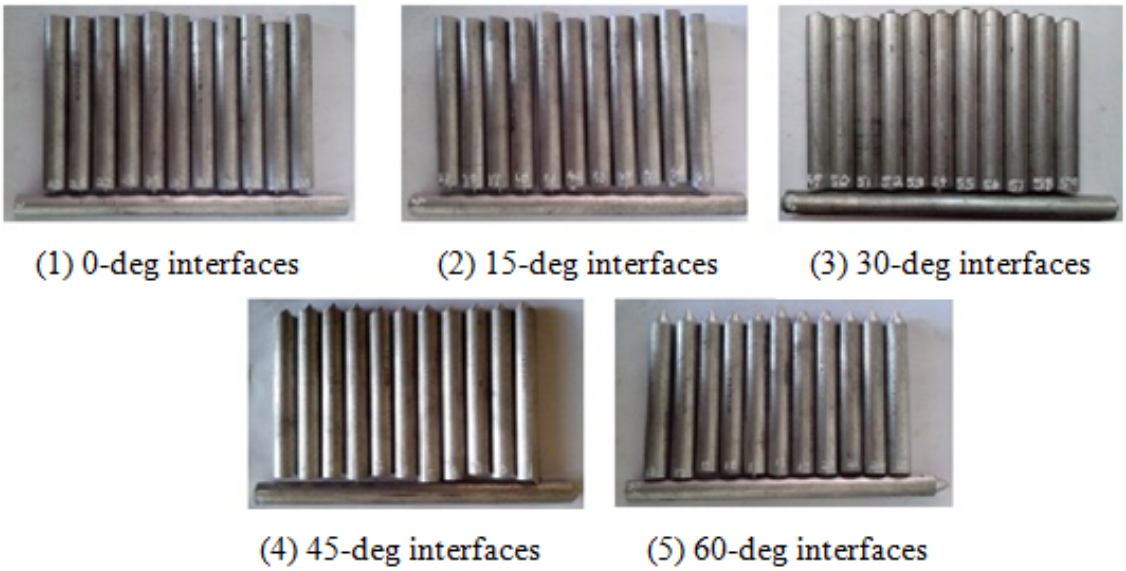

Figure 3.29: Samples of FW specimen with various taper angles

Figure 3.30: Friction welded joints obtained with various taper angles

studies of friction welded joints obtained with various interface angles have also been carried out. Sample preparation for the microstructure studies is almost same as explained in section 3.3.3, page 46. Here also the material preparation has been started with cutting of centre portion of 5 mm length including the weld as centre from the friction welded specimens in lathe. These are machined so as to obtain cross section of the weld region through milling. Flatness is provided to the curved surface so that it can be suitably placed for observation. All the sharp edges have been chamfered for safety during polishing process.

Surfaces of the samples to be examined have been polished using emery papers of grade 320

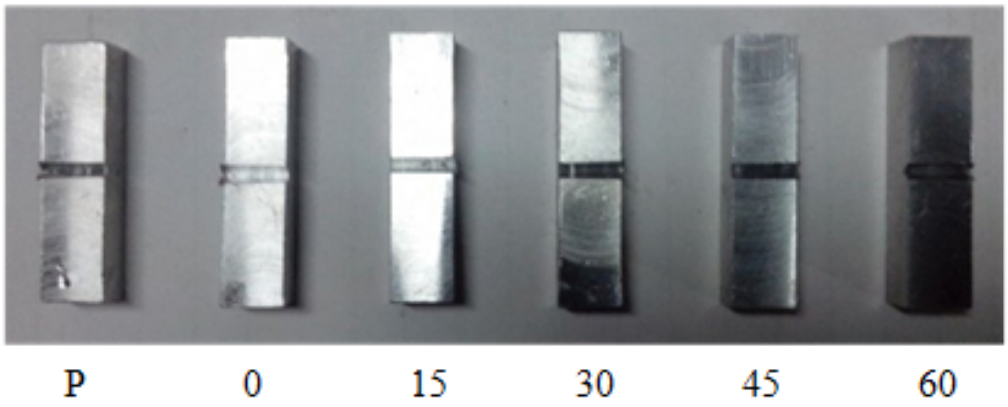

Figure 3.31: Charpy impact test specimens

for 10 minutes each, 600 for 10 minutes each, 1000 for 20 minutes each and finally 1500 for 20 minutes each. The emery paper with grade 1500 has been attached to disc polishing machine. Machine polishing has been carried out in Ecomet twin variable speed grinder-polisher at 250 rpm. First polishing has been done using alumina polishing suspension of 0.05μ for 20 minutes for each specimen. Final polishing has been carried out using diamond suspension paste of 1 μ as lapping cement and kerosene as lubricant. After that the specimens have been washed with mineral water and dried. Figure 3.32 shows the microstructure test specimen after machine polishing.

Figure 3.32: Microstructure specimens after machine polishing

Etching has been carried out using HF solution (10% HF, 90% distilled water) for 30 sec. Followed with etching, each specimen has been dried. The prepared samples for microstructural studies shows white pattern at weld zone. Figure 3.33 shows microstructure test specimen after etching. These samples have been subjected to optical studies.

Figure 3.33: Microstructure test samples after etching

All the experimental studies have been carried out as per the suitable design of experiment procedures with the help of Minitab software package.

3.4 Results and Discussion

Overview on experiments conducted on friction welding process have been discussed from section 3.3 to subsection 3.3.5. The result and discussion on those experiments has been explained in the following sections

3.4.1 Preliminary studies

Tensile characteristics study of friction welded joints has been carried out initially. Figure 3.34 represents the dimensions of tensile test specimen prepared as per ASTM standards (B557M). The average value obtained for maximum load, breaking load and percentage elongations have been tabulated. For the parent metal the values found are 25.849 kN, 22.4 kN and 22 kN respectively. Two levels of speed for the rotation specimen have been considered, 775 rpm and 1200 rpm. Friction welded joints obtained with 1200 rpm possessed comparable result with the parent metal (21.24 kN, 19 kN and 17). Thus a scope for further research has been realized from the preliminary studies.

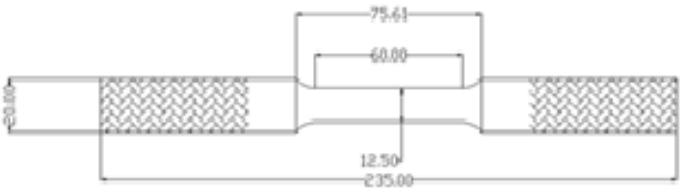

Figure 3.34: Standard specimen for tension test

3.4.2 Influence of Interface Surface Geometries

Taguchi Orthogonal array has been used to fix the number of experiment. The experiment includes formation of friction welded joints by controlling the process parameters such as Speed of the Rotating specimen (SR), Axial loading on the stationary specimen (AL), Interface Geometry of the welding specimens(IG) while keeping other parameters constant. These joints

have been subjected to mechanical characteristics studies. Since for the present study three factors with 4 level for each have been considered, Taguchi L16 orthogonal array has been fixed. Parameters with different levels used to obtain the friction welded joints with responses as the UTS, hardness and torsional rigidity are given in Table 3.14 .

Thus forty eight friction welded specimen have been made (sixteen numbers of specimens for tensile test, sixteen numbers for hardness test and sixteen numbers for torsion testing). Grey Relational Analysis (GRA) has been used to observe the effectiveness of process parameters on the response characteristics with different units. GRA has been started with finding out the normalized values of response characteristics. Three options, namely "larger the best, nominal is the best and smaller the best" have been adopted for normalizing the response characteristics. According to that for UTS and torsional rigidity, "larger the best" option has been selected. For hardness" nominal is the best" has been adopted. Thus the formulae used to find out the normalized values of these response characteristics are presented below.

$$UTS_{norm} = (UTSx_i - UTSx_{min})/(UTSx_{max} - UTSx_{min}) \tag{3.1}$$

$$TR_{norm} = (Tx_i - Tx_{min})/(Tx_{max} - Tx_{min}) \tag{3.2}$$

$$H_{norm} = 1 - |(Hx_i - 20)/(Hx_{max} - Hx_{min})|). \tag{3.3}$$

where "norm" indicates normalised value of the respective response character. "x_i" indicates an arbitrary value of response character. "min" and "max" indicates the minimum and maximum values of a response character.

Followed with that, the deviation of each normalized values from its maximum value has been calculated. For UTS, this is expressed as ΔUTS_{norm}. Using this, the grey relational coefficient of each response characters has been found out by following equation.

$$\varphi(UTS) = (\Delta UTS_{norm(min)} + \delta\Delta UTS_{norm}(max))/(\Delta UTS_{norm} + \delta\Delta UTS_{norm(max)}) \tag{3.4}$$

$$\varphi(TR) = (\Delta TR_{norm(min)} + \delta\Delta TR_{norm}(max))/(\Delta TR_{norm} + \delta\Delta TR_{norm(max)}) \tag{3.5}$$

$$\varphi(H) = (\Delta H_{norm(min)} + \delta\Delta H_{norm(max)})/(\Delta H_{norm} + \delta\Delta H_{norm(max)}) \tag{3.6}$$

Here "φ" is the grey relational coefficient. "norm(min)" indicates the minimum value of normalised value of a response character. "norm(max)" indicates the maximum value of normalised value of a response character. "δ" is the weightage given as per "larger the best" option. From the grey relational coefficients, we can calculate the Grey Relational Grade(γ_i) using the

following equation.

$$\gamma_i = (1/n)\Sigma\varphi(k) \tag{3.7}$$

$$i.e.....\gamma = (1/3)(\varphi(UTS) + \varphi(TR) + \varphi(H) \tag{3.8}$$

Table 3.15, Table 3.16 and Table 3.17 represents the grey relational coefficients corresponding to each response characters. Table 3.18 represents the grey relational grade and ranking of each combination of process parameters. First rank corresponds to highest value of grey grade among 16 sets. Based on the ranking, the most influencing process parameters has been identified.

Table 3.14: Response table as per Taguchi L16 orthogonal array

Sl.No	Speed (rpm)	Axial Load (MPa)	Interface Geometry	UTS (MPa)	TR $\times 10^4(N/mm^2)$	Hardness (BHN)
1	500	2.0	FF	103.25	0.94	23
2	500	2.5	TT	113.00	1.20	21
3	500	3.0	XX	117.00	1.10	21
4	500	3.5	VX	60.59	0.98	20
5	775	2.0	TT	127.00	1.30	21
6	775	2.5	FF	112.00	0.98	22
7	775	3.0	VX	70.40	1.29	20
8	775	3.5	XX	112.00	1.21	19
9	1000	2.0	XX	103.00	0.98	21
10	1000	2.5	VX	065.22	0.90	22
11	1000	3.0	FF	108.00	0.94	21
12	1000	3.5	TT	118.20	0.97	22
13	1200	2.0	VX	065.22	1.23	20
14	1200	2.5	XX	100.00	0.97	21
15	1200	3.0	TT	122.00	1.10	20
16	1200	3.5	FF	109.00	0.96	22

Table 3.15: Calculation of grey relational coefficients - UTS

Sl.No	UTS_{norm}	ΔUTS_{norm}	UTS_{grc}	Sl.No	UTS_{norm}	ΔUTS_{norm}	UTS_{grc}
1	0.6424	0.3576	0.5380	9	0.6386	0.3614	0.5805
2	0.7892	0.2108	0.7034	10	0.0697	0.9303	0.3496
3	0.8494	0.1506	0.7685	11	0.7139	0.2861	0.6361
4	0.0000	1.0000	0.3333	12	0.8675	0.1325	0.7905
5	1.0000	0.0000	1.0000	13	0.0697	0.9303	0.3496
6	0.7741	0.2259	0.6888	14	0.5934	0.4066	0.5515
7	0.1477	0.8523	0.3697	15	0.9244	0.0753	0.8691
8	0.7741	0.2259	0.6888	16	0.7290	0.2710	0.6485

Table 3.16: Calculation of grey relational coefficients-Torsional Rigidity

Sl.No	TR_{norm}	ΔTR_{norm}	TR_{grc}	Sl.No	TR_{norm}	ΔTR_{norm}	TR_{grc}
1	0.000	1.000	0.1000	9	0.1143	0.8857	0.1275
2	0.7429	0.2571	0.4271	10	-0.1143	1.1143	0.0764
3	0.4751	0.542	0.2462	11	0.0000	0.0000	0.1000
4	0.1143	0.8857	0.1275	12	0.0825	0.8257	0.1202
5	1.0286	-0.0286	0.8273	13	0.8286	0.8286	0.5114
6	0.1143	0.8857	0.1275	14	0.0857	0.0857	0.1202
7	1.0000	0.0000	0.7667	15	0.4571	0.4571	0.2462
8	0.7714	0.2286	0.4530	16	0.0571	0.0571	0.1132

Table 3.17: Calculation of grey relational coefficients-Hardness

Sl.No	$(H_x i - 20)$	H_{norm}	H_{grc}	Sl.No	$(H_x i - 20)$	H_{norm}	H_{grc}
1	3.0000	0.2500	0.3333	9	1.0000	0.7500	0.6000
2	1.0000	0.7500	0.6000	10	2.0000	0.5000	0.4286
3	1.0000	0.7500	0.6000	11	1.0000	0.7500	0.6000
4	0.0000	1.0000	1.0000	12	2.0000	0.5000	0.4286
5	1.0000	0.7500	0.6000	13	0.0000	1.0000	0.6000
6	2.0000	0.5000	0.4286	14	1.0000	0.7500	1.6000
7	0.0000	1.0000	1.0000	15	0.0000	1.0000	1.0000
8	1.0000	0.7500	0.6000	16	1.0000	0.7500	0.6000

Table 3.18: Grey relational grade and ranking

Sl. No	Speed (rpm)	Axial Load (MPa)	Interface Geometry	UTS_{grc}	TR_{grc}	H_{grc}	GRG	Rank
1	500	2.0	FF	0.3580	0.1000	0.3333	0.3388	15
2	500	2.5	TT	0.7034	0.4271	0.6000	0.5678	5
3	500	3.0	XX	0.7685	0.2462	0.6000	0.5382	6
4	500	3.5	VX	0.3333	0.1275	1.0000	0.4870	8
5	775	2.0	TT	1.0000	0.8273	0.6000	0.8091	1
6	775	2.5	FF	0.6888	0.1275	0.4286	0.4150	14
7	775	3.0	VX	0.3697	0.7667	1.1000	0.7121	2
8	775	3.5	XX	0.6888	0.4530	0.6000	0.5806	4
9	1000	2.0	XX	0.5805	0.1275	0.6000	0.4360	12
10	1000	2.5	VX	0.3446	0.0764	0.4286	0.2849	16
11	1000	3.0	FF	0.6361	0.1000	0.6000	0.4454	11
12	1000	3.5	TT	0.7905	0.1202	0.4286	0.4464	10
13	1200	2.0	VX	0.3496	0.5114	0.6000	0.4870	8
14	1200	2.5	XX	0.5515	0.1202	1.6000	0.4239	13
15	1200	3.0	TT	0.8691	0.2462	1.0000	0.7051	3
16	1200	3.5	FF	0.6485	0.1132	0.6000	0.4359	9

3.4.3 ANOVA of Process Parameters

ANOVA is started with calculating the mean of grey relational grade ($GRG_(mean)$) corresponding to each process parameters in various levels. The difference between the maximum and minimum value of these mean of GRGs($\delta GRG_(mean)$) have been further calculated as explained below

At level 1, the GRG s corresponding to the speed 500 rpm are 0.3388, 0.5678, 0.5382 and 0.4870. The mean of these GRGs are 0.4852. Similarly the $GRG_(mean)$ for 775 rpm, 1000 rpm and 1200 rpm have been calculated as 0.6292, 0.4302 and 0.5175 respectively. Hence the difference between maximum and minimum values of mean of GRGs is 0.1953. Similarly for axial load, the GRGs corresponding to the 2 MPa are 0.3388, 0.8091,0.4360 and 0.4870. Mean of these GRGs are 0.5177. Followed with that the mean of GRGs corresponding to 2.5 MPa, 3 MPa and 3.5 MPa have been calculated. The mean of GRGs for FF has also been calculated in this manner. (ie.the mean of GRGs corresponding to each level of parameters have been calculated and the difference between maximum value of mean of GRGs and minimum value of GRGs have been noted). All these data are then tabulated (see Table3.19) for the ranking of process parameters. From the ranking the most influencing process parameters have been identified. From the ranking we can see that the most influencing process parameter is the speed of rotation. It is then followed with interface geometry and axial loading. It can also be inferred that the maximum value of mean of GRGs for speed of rotation, axial loading and interface geometry are seen in Level 2, Level 3 and Level 2 respectively. It indicates that the best combination of process parameters which give desired results are speed of rotating specimen as 775 rpm, axial laoding as 3 MPa and interface geometry as T-T. A confirmation test has been done to find out the response characters from this combination of process parameters. Table 3.20 represents the result obtained from the confirmation test

Table 3.19: Response table for grey relational grade

Parameters	MEAN OF GREY RELATIONAL GRADES					
	LEVEL 1	LEVEL 2	LEVEL 3	LEVEL 4	MAX-MIN	RANK
Speed of Rotation	0.4852	0.6292*	0.4032	0.5175	0.1953	1
Axial loading	0.5177	0.4251	0.6002*	0.4920	0.1082	3
Interface Geometry	0.4133	0.6144*	41.53	0.4947	0.1416	2
*Grey relational grade corresponding to optimum process parameters						

Table 3.20: Result from the confirmation test

Exp No	Speed (rpm)	Axial Load (MPa)	Interface Geometry	UTS MPa	TR $\times 10^4 N/mm^2$	Hardness BHN
1	775	3.0	TT	132	1.35	24

The steps involved in the calculation of percentage contribution by the process parameters are as follows.

- Calculation of total sum of squares of process parameters (SS_T)
  For the present calculation

$$SS_T = \sum (GRG - TGRG_{mean})^2 \tag{3.9}$$

$$\text{i.e., } SS_T = (0.3388 - 0.5088)^2 + (0.5768 - 0.5088)^2 + \ldots + (0.4927 - 0.5088)^2$$

$$\text{i.e., } SS_T = 0.8788$$

- Calculation of sum of squares of process parameters, for speed, SS_{SP} has been found out by the following relation.

$$SS_{SP} = \sum_{i=1}^{4} k_i \times (GRG_{SPi} - TGRG_{mean})^2 \tag{3.10}$$

where, i - number of levels, k - number of experiments in a level, GRG_{SPi} - Grey relational grade for speed in a particular level, $TGRG_{mean}$ - mean of grey relational grades of all the process parameters,

$$\text{i.e., } SS_{SP} = (4 \times (0.4852 - 0.5088)^2) + \ldots + (4 \times (0.5175 - 0.5088)^2)$$

$$\text{Thus, } SS_{SP} = 0.1052$$

Similarly, for sum of squares of axial load,

$$SS_{AL} = 0.0629$$

and sum of squares of interface geometry

$$SS_{IG} = 0.1014$$

- Calculation of the variance of process parameters

Variance of speed of rotation, V_{SP}

$$\begin{aligned} V_{SP} &= SS_{SP}/DOF \\ &= 0.1052/3 \\ &= 0.0350 \end{aligned} \tag{3.11}$$

similarly, Variance of Axial load,

$$V_{AL} = 0.0210$$

Variance of interface Geometry,

$$V_{IG} = 0.0038$$

- Calculating sum of square error SS_E

$$\begin{aligned} SS_E &= SS_T - (SS_{SP} + SS_{AL} + SS_{IG}) \\ \text{i.e., } SS_E &= 0.8788 - (0.1052 + 0.0629 + 0.1014) = 0.6094 \end{aligned} \tag{3.12}$$

- Calculation of error variance, V_E

$$\begin{aligned} V_E &= SS_E/DOF \\ &= 0.2031 \end{aligned} \tag{3.13}$$

- Finding F Ratio for each process parameter F_{SP}

F ratio for speed of rotation,

$$\begin{aligned} F_{SP} &= V_{SP}/V_E \\ &= 0.0350/0.2031 = 0.1727 \end{aligned} \tag{3.14}$$

Similarly F Ratio for other process parameters, $F_{AL} = 0.1032$ and $F_{IG} = 0.1664$

- Finding percentage contribution of process parameters

Percentage contribution by speed of rotating specimen, PC_{SP}

$$\begin{aligned} PC_{SP} &= F_{SP}/(F_{SP} + F_{AL} + F_{IG}) * 100 \\ &= (0.1725/(0.1725 + 0.1032 + 0.1664)) * 100 = 39.02\% \\ \text{Thus} PC_{AL} &= 23.34\% \\ \text{and} PC_{IG} &= 37.64\% \end{aligned} \tag{3.15}$$

From these analysis it is seen that interface geometry has key influence in making friction welded joints with good mechanical characteristics. It is also seen that interface geometry with taper-taper configuration has got relatively better mechanical characteristics than others. Hence the next study on friction welded joints has been fixed to evaluate the suitable taper angle at which good mechanical characteristics will be resulted.

3.4.4 Optimum Interface Taper Angles

Here also Taguchi orthogonal array has been used to fix the number of experiment. The experiment involved formation of friction welded joints by controlling the process parameters such as speed of the rotating specimen (SR), Axial loading on the stationary specimen (AL),Various Interface taper angles (TA) as 15°, 30°,45°and 60°, while keeping other parameters constant. These joints have been subjected to mechanical characteristics studies. L16 orthogonal array has been fixed. Table 3.21 represents the parameters with different levels used to obtain the friction welded joints with responses as the UTS, hardness, torsional rigidity and impact toughness. Thus sixty four specimen have been made with various combinations. Grey relational analysis and ANOVA have been conducted to find out optimum taper angles and percentage contribution of each parameters in response characteristics respectively as mentioned in previous section. Table 3.22and Table 3.23 represents the calculations made in this regard.

From the grey relational grade table, the most suited combination of process parameters have been found. It is seen that the order of taper angles which gave higher values for tensile, torsional and impact characteristics are 30°, 60°, 45°and 15°. However friction welded joints obtained with 30°taper angle showed good tensile strength and torsional characteristics, friction welded joints obtained with 45°taper angle possessed high hardness value near to weld region, friction welded joints obtained with 60°taper angle showed good impact characteristics. From the analysis, it is inferred that suitable taper angle for the interface geometry can influence various mechanical characteristics for the friction welded joints. Here also a confirmation test has been carried out to find out the response characters from the optimum process parameters. Table 3.24 represents the result obtained from the confirmation test. In addition to this tests

Table 3.21: FW parameters and mechanical characteristics

Sl. No	Speed (rpm)	Axial Load (MPa)	Taper angle (°)	UTS (MPa)	TR $\times 10^4 (N/mm^2)$	Hardness BHN	IT Nm
1	500	2.0	15	115.21	1.50	18.23	5.8
2	500	2.5	30	118.34	2.10	20.31	4.2
3	500	3.0	45	117.21	1.81	23.12	7.0
4	500	3.5	60	108.68	2.00	18.00	9.8
5	775	2.0	30	122.15	2.30	21.36	4.1
6	775	2.5	15	120.26	1.83	22.00	6.5
7	775	3.0	60	123.23	2.28	24.80	10.8
8	775	3.5	45	122.23	1.85	24.12	8.0
9	1000	2.0	45	120.21	1.73	21.23	7.1
10	1000	2.5	60	121.21	1.70	24.00	10.3
11	1000	3.0	15	118.00	2.27	21.00	6.4
12	1000	3.5	30	121.25	1.45	22.12	3.6
13	1200	2.0	60	110.21	1.60	18.00	9.1
14	1200	2.5	45	117.34	1.62	21.23	7.2
15	1200	3.0	30	119.00	2.10	23.12	4.2
16	1200	3.5	15	112.27	1.48	20.15	5.4

Table 3.22: GRGs - friction welded joints with various taper angles

Sl. No	Speed (rpm)	Load (N/mm^2)	Taper Angle(°)	UTS grc	TR_{grc}	H_{grc}	IT_{grc}	GRG	Rank
1	500	2.0	15	0.4761	0.1136	0.5379	0.4186	0.3866	16
2	500	2.5	30	0.5985	0.4467	0.8692	0.3529	0.5668	4
3	500	3.0	45	0.5477	0.2363	0.5869	0. 5625	0.4834	11
4	500	3.5	60	0.3333	0.3529	0.5074	0.7826	0.4941	9
5	775	2	30	0.8709	0.7667	0.6023	0.3495	0.6474	2
6	775	2.5	15	0.7105	0.2416	0.5074	0.4557	0.4788	12
7	775	3	60	1.0000	0.7218	0.3399	1.0000	0.7654	1
8	775	3.5	45	0.8794	0.2524	0.3333	0.5695	0.5069	7
9	1000	2	45	0.7071	0.1938	0.6261	0.4931	0.5051	8
10	1000	2.5	60	0.7831	0.1813	0.3399	0.8781	0.5456	6
11	1000	3	15	0.5823	0.7008	0.6732	0.4500	0.6016	3
12	1000	3.5	30	0.7864	0.1136	1.0000	0.3462	0.5616	5
13	1200	2	60	0.3589	0.1445	0.5074	0.6793	0.4225	15
14	1200	2.5	45	0.5531	0.1813	0.6261	0.5000	0.4651	13
15	1200	3	30	0.6328	0.4467	0.5074	0.3529	0.4850	10
16	1200	3.5	15	0.3995	0.1081	0.9321	0.4000	0.4599	14

Table 3.23: Response table for GRGs

Process Parameters	MEAN OF GREY RELATIONAL GRADE					
	LEVEL 1	LEVEL 2	LEVEL 3	LEVEL 4	MAX-MIN	RANK
Speed of Rotation	0.4827	0.5996*	0.5468	0.4629	0.1368	1
Axial Loading	0.4904	0.5169	0.5791*	0.5056	0.0887	3
Taper Angle	0.4722	0.5699*	0.4901	0.5597	0.0977	2
	*grey relational grades corresponding to optimum process parameters					

have also been carried out to check any effects by other taper angles with the medium speed and the axial loading. The result obtained from those studies are also presented in the same table. From the aforementioned tests, it is inferred that interface geometry also have the influence

Table 3.24: Confirmation test results

Exp. No	Speed (rpm)	load (MPa)	Taper angle(°)	UTS (MPa)	TR (MPa)	Hardness (BHN)	IT (Nm)
1	775	3.0	30	135	1.7	24	6.7
2	775	3.0	15	123	1.8	25	6.5
3	775	3.0	45	127	1.72	25	8.2
4	775	3.0	60	124	2.4	24	11.2

on the strength characteristics of friction welded joints. In that friction welded joints with T-T interface geometry exhibited comparable results with the parent metal. It is also inferred that desired characteristics for the friction welded joint can be obtained by providing suitable taper angle for the interface.

3.4.4.1 Microstructure studies

The results from the micro structure studies obtained as microstructure photographs for the friction welded joints with various interface taper angles are presented from Figure 3.35 to Figure 3.38. All the photographs have been taken in 200X.

Figure3.35 shows the photograph taken for the friction welded joints obtained with 15°degree interface taper angle. Twelve points (an array of 4 $\times$ 3) have been considered for the observation. The weld regions (both longitudinal and transverse direction) are filled with denser particles. The HAZ in the rotating specimen region possessed about 80% of the denser particles. In the case of HAZ of stationary specimen it is about 40%. Also at the outer regions above

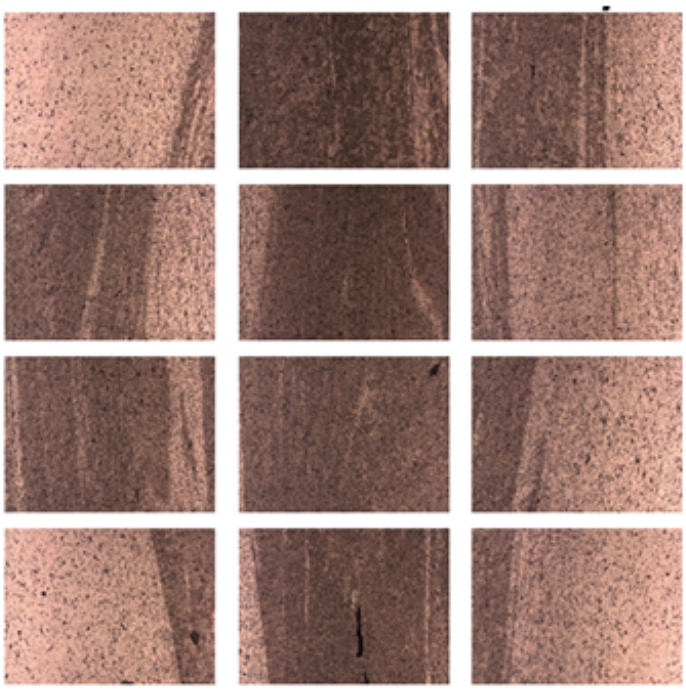

Figure 3.35: Microstructure - friction welded joints by 15°taper angle

HAZ, in the stationary specimen, are seen filled about 60% of denser particles. Due to this reason the joint is seems to be sufficiently strong and hence it is having high tensile strength than the joint with flat interface. Due to the same reason it showed almost equal hardness and high modulus of rigidity compared to the parent metal. Cracks in microlevel have been observed at the outer region.This may be due to the faster cooling of outer surface by convective heat transfer, which may lead to non uniform bonding. Figure 3.36 shows the microstructure of friction welded joints obtained with 30°interface taper angle. Here also twelve points (an array of 4 $\times$ 3) have been considered for the observation. Weld region and 70% of HAZ in the stationary specimen are thickly packed with denser particles. The dispersion of denser particles in HAZ and WZ looks like the tip of a firing bullet. In the stationary specimen side, towards the HAZ it is seen like a piercing effect. In addition to the above observation it is also seen that all other regions are equally dispersed with denser particle. Due to that, those areas are not easy to distinguish with parent material particles. This may be the reason for the equal hardness with the parent metal, its high tensile strength and torsion compared to friction welded joints with other interface taper angles. The reduction in impact toughness value may be due to the orientation of large amount of denser particles at the weld region towards the stationary specimen. Micro level crack are also visible towards the outer region in the weld line.

Figure 3.37 shows the microstructure of friction welded joints obtained with 45°interface taper angle. The micro structure photograph has been presented as a 4 $\times$ 3 array (photograph

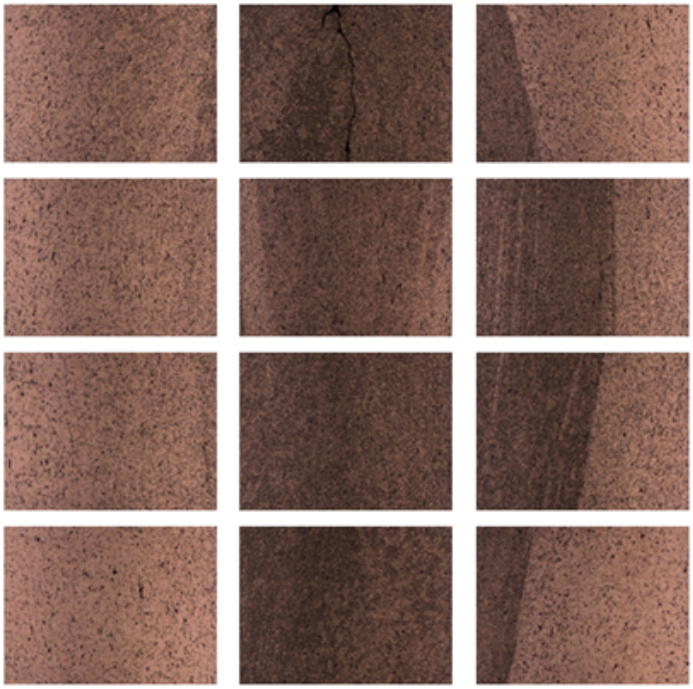

Figure 3.36: Microstructure - friction welded joints by 30°taper angle

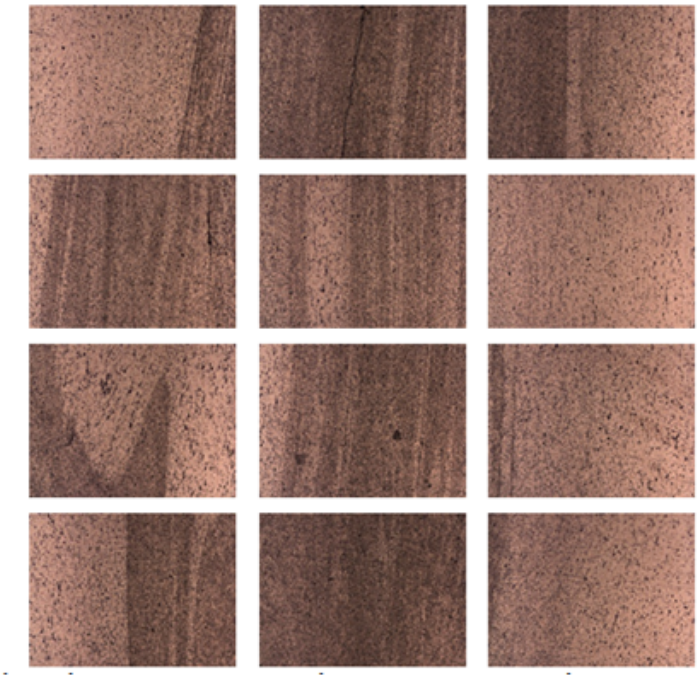

Figure 3.37: Microstructure -friction welded joints by 45°taper angle

from 12 points). Here denser particles are seen as layers, much concentrated at weld region. Thick patterns are visible towards the outer region. At the centre, it is comparatively less. Even though denser particles are not seen as thick layer everywhere, we can see a uniform dispersion

of particles. It is also seen that, the dispersion of denser particle as thick layers resemble like piercing effect towards left due to axial loading. It is also observed that almost all the areas are seen like the microstructure of the parent metal itself. This may be the reason for its quality having second highest UTS relative to other joints, higher hardness and higher torsion characteristics, high impact toughness value than the parent metal. Here also miner cracks are visible at the outer region.

Figure 3.38 shows the microstructure of friction welded joints obtained with 60°interface taper angle. The micro structure photograph presented as a 4 $\times$3 array (photograph from 12

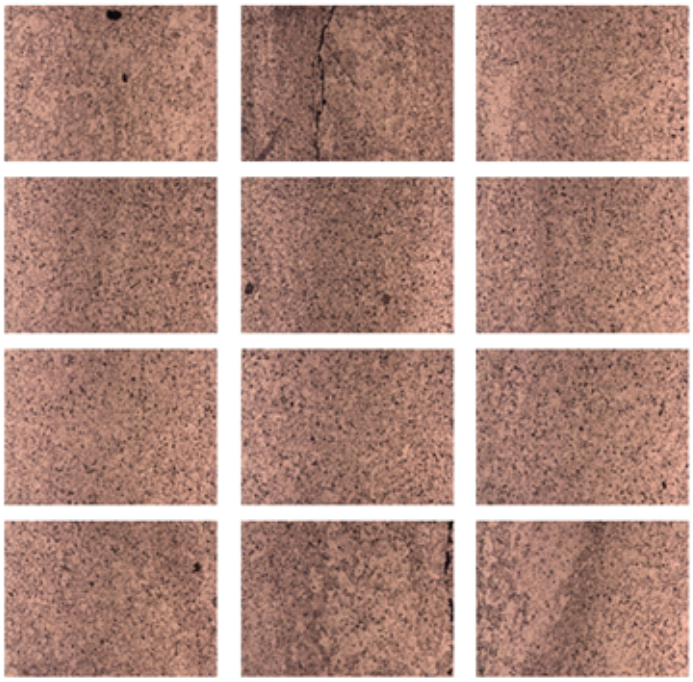

Figure 3.38: Microstructure- friction welded joints by 60°taper angle

points). All the regions including weld zone as well as heat affected zones looks alike. All regions are dispersed with dense particles not like layers. But the concentration of dense particles are seen high in all regions. This may be the reason for having about 50% tensile strength, reasonable hardness, high torsion and very high impact toughness characteristics compared to the parent metal. Here also micro cracks are observed at the outer region of the weld line.

3.4.4.2 Microhardness Evaluation

Microhardness evaluation of specimens with various interface taper angle has been carried out with optimized values for speed and axial load. However different taper angles have been considered to observe any influence of the same in microhardness. The result from Vickers

micro hardness test was obtained as microhardness number corresponding to the indentation made by the hardness tester by making impinges. These impinges, see Figure 3.39 have been made on the specimen by a loading of 0.05 kgf. The load is applied for 15 seconds at weld

Figure 3.39: Indentations on Vickers microhardness test specimen

zone, HAZ and the parent metal region in all specimens. The diagonal length of impressions (3 Nos) made by the impinges has been measured through microscope and the average values of all have been found.

The results obtained from micro hardness test at weld zone, heat affected zone and parent metal region of each specimen have given in Table3.25. Specific comparison of the microhard-

Table 3.25: Vickers microhardness number for friction welded joints

Taper Angle	0°	15°	30°	45°	60°
Parent metal region	89.2	82.0	89.4	88.9	85.2
Weld zone	81.0	80.8	84.4	86.0	87.9
Heat affected zone	87.8	83.3	82.0	87.5	89.7

ness values at various region corresponding to respective welded joints formed with various interface angles have been presented as histograms shown in Figure 3.40 to Figure 3.42.

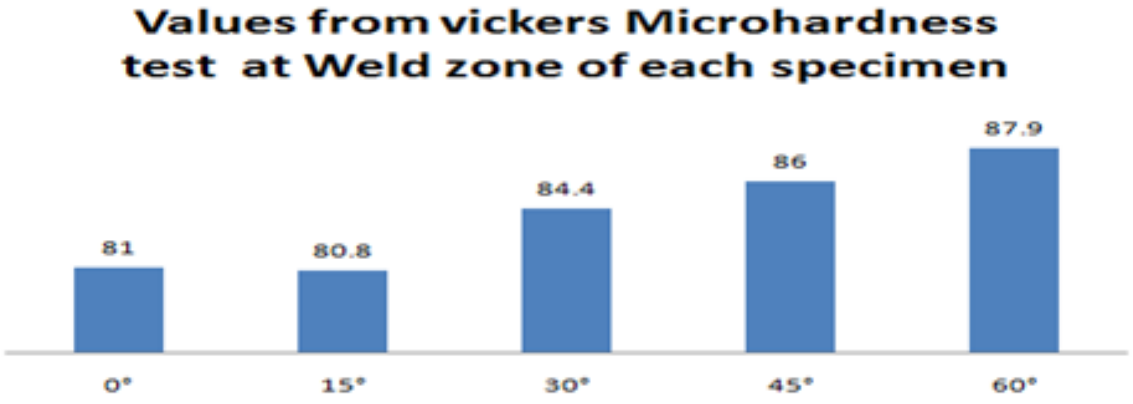

Figure 3.40: Microhardness distribution- weld zone

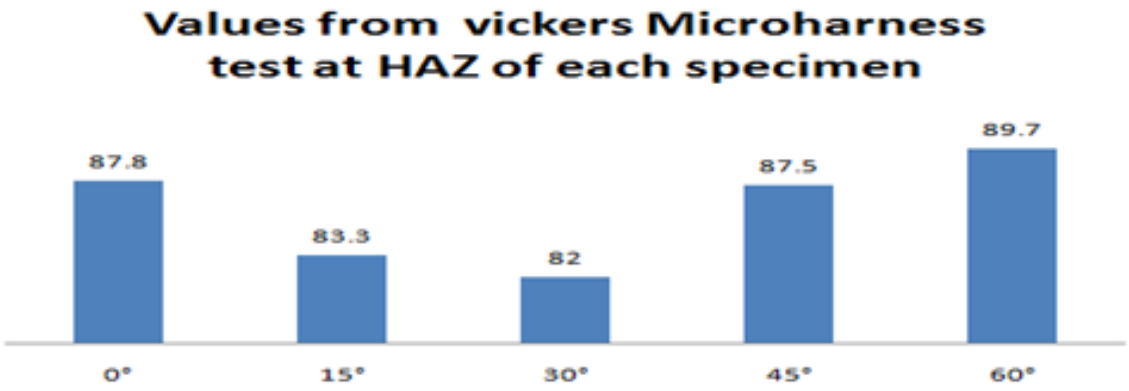

Figure 3.41: Microhardness distribution -heat affected zone

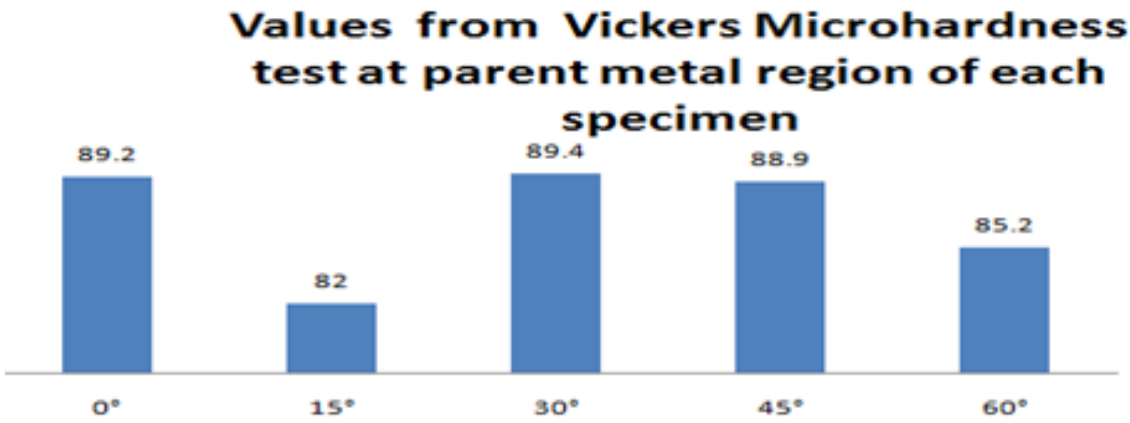

Figure 3.42: Microhardness distribution -parent metal

From the microhardness distribution at the weld zone of various specimen it is seen that the value ranges from 80 to 88. It is also seen that the Vickers micro hardness value increases with the increase in interface taper angle except for 15°. The value was found maximum corresponding to welded joints formed with interface taper angle of 60°. It may be due to the appropriate material transfer with the development of temperature by friction to form strong welded joints. It may also attributed to the higher value of torsion and impact toughness characteristics.

From the histogram showing the microhardness distribution at HAZ of welded joints formed with various interface angles, it is seen that the values are higher except for the specimen formed with interface angle 15°and 30°. It is also seen that the highest value is for the specimen formed with taper angle of 60°similar to the result found in the case of weld zone. The same has been comparable with the result obtained for BHN values.

Thus, by conducting the above said experiments (comparative studies with conventional welding techniques (in the case of friction stir welded joints), influence of interface geometries in friction welding process, studies to find out optimum interface angles for strong friction

welded joints and microstructural studies) it is clear that friction stir welding and friction welding are the most suited joining process for the plates and rods respectively for the aluminium alloys. In addition to that it is also inferred that with proper interface geometry variation especially as tapered geometry, strong friction welded joints can be made from FW setup developed in a medium duty lathe.

Chapter 4

ANALYTICAL INVESTIGATIONS

This chapter explains the analytical investigations carried out. Aim of analytical investigations is to study the influence of process parameters in the formation of friction stir welded and friction welded joints. Various software tools used for this by researchers all over the world are Abaqus, Forge etc. A number of research papers on analytical investigations on FSW are now available. Very few papers are available regarding the analytical investigations on friction welding. Hence for the present work, analytical investigations are mainly focused on the study of FW process. However a review on the developments in analytical investigations on FSW has been carried out prior to the numerical investigations on friction welding.

4.1 Analytical Investigations on FSW

The analytical modelling of FSW is a complex procedure as it involves frictional heat generation due to the rotation of the tool, its piercing effect in to the material and its simultaneous traverse along the surface to be joined, axial loading and resistive force due to the firm fixing of the specimen and its material property. Due to these effects, high frictional heat is developed at the contact surface of FSW tool and specimen. It also causes for the plastic deformation of materials and its transfer from advancing side to retreating side, due to the stirring effect of the tool. On cooling a strong bonding between FSW specimen will be developed. Hence FSW is a coupled thermal and structural problem. The main objective of this numerical modelling is the thermal modelling of FSW process to assess the temperature developed in the FSW specimen during FSW process. An available inbuilt procedures under heat transfer module in Comsol Multi Physics software package has been used for the thermal modelling of FSW process. The main highlights behind this procedure are as follows.

- The model geometry is symmetric around the weld. Hence half of the portion only should be modelled.
- The plates are surrounded by two infinite domains.
- The heat transfer in the plate is represented by

$$\nabla = (-k\nabla T) = Q - \rho C_p u \Delta T \tag{4.1}$$

where k is the thermal conductivity, ρ is the density, C_p is the specific heat capacity and u is the velocity of tool traverse.

- The heat generated in the interface between the tool pin and the work-piece as a surface heat source can be expressed as

$$q_{pin}(T) = \frac{\mu \times r_p \omega Y(T)}{\sqrt{3(1+\mu^2)}}\, W/m^2 \tag{4.2}$$

where μ is the coefficient of friction, r_p is the friction stir tool pin radius, ω is the angular velocity in rad / sec, $Y(T)$ is the average shear stress of material which is a function of temperature.

- The heat generated at the interface between the tool shoulder and the workpiece is given by

$$q_{shoulder}(r,T) = \begin{cases} (\mu F_n)/A_s)\omega r; & T < T_{melt} \\ 0; & T > T_{melt} \end{cases} \tag{4.3}$$

where Fn is the normal force,A_s is the shoulder surface area and T is the melting temperature of the specimen.

- Above the melting temperature of the specimen, the friction between the tool and work-piece is very low. Hence, the FE model sets the heat generation from the shoulder and pin to be zero when temperature is equal to or higher than the melting temperature.

- The upper and lower surface of the specimen lose heat due to natural convection and surface to ambient radiation. Then the corresponding heat flux expression is

$$q_{up} = h_u p(T_0 - T) + \varepsilon\sigma(T_{amb}^4 - T^4) \tag{4.4}$$

$$q_{down} = h_{down}(T_0 - T) + \varepsilon\sigma((T_{amb}^4 - T^4)) \tag{4.5}$$

  whereT_0 is the associated reference temperature, ε is the surface emissivity, σ is the stefan- Boltzman constant and T_{amb} is the ambient temperature

- Left hand side of the FE model is provided with an infinite domain. It makes sure that temperature at infinity are in equilibrium with ambient temperature by natural convection and surface to ambient radiation. Hence the boundary condition at that region are set as insulated. Also asumed that resulting temperature distribution is the average of temperature at the advancing and retreating side as stated in literature.

Graphical representation of the 3D model considered by incorporating the above highlights is shown in Figure 4.1. In addition, the global definitions related to the numerical modelling are presented in Table 4.1.

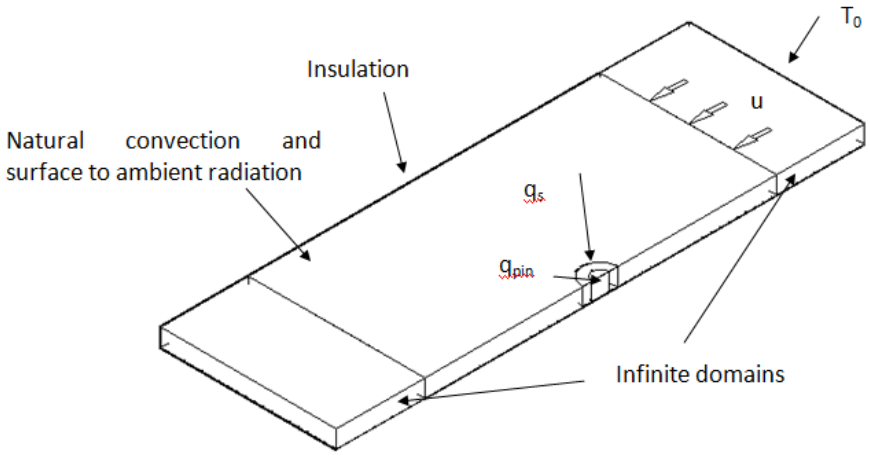

Figure 4.1: 3D model for the numerical modelling of FSW

This procedure has been developed based on the study on the thermal modelling of FSW by Song and Kovacevic (2003). For the present study attempts have been carried out to study this procedure and validate with another numerical study developed using thermal module in NX-5 software package, by Hamilton et al. (2008).

Table 4.1: Global definitions for the FSW numerical modelling

Name	Expression	Value	Description
T_0	300[K]	300 K	Ambient temperature
T_{melt}	933[K]	933.0 K	Workpiece melting Temperature
h_{upside}	12.25$[W/(m^2 * K)]$	12.25$W/(m^2K)$	heat transfer coefficient, upside
epsilon	0.3[1]	0.3000	Surface emissivity
u_{weld}	1.59[mm/s]	0.001590 m/s	Welding speed
mu	0.4 [1]	0.4000	Friction coefficient
n	637 [1/min]	10.621/s	rotation speed
omega	2*pi*[rad]*n	66.71rad/s	Angular velocity
F_n	25[kN]	2.500E4N	Normal Force
r_{pin}	6 [mm]	0.006m	Tool pin radius
$r_{shoulder}$	25 [mm]	0.025m	Tool shoulder radius
A_s	$pi * (r^2_{shoulder} - r^2_{pin})$	0.001850 m^2	Shoulder Surface area

4.1.1 Geometric Model

A 3D model with the boundary conditions assumed as per the highlights mentioned above has been created initially. The model is symmetrical about y-z plane. (see Figure 4.2). Basic entities like block, cylinder and by boolean operations available in the software package has been utilised to generate this geometric model.

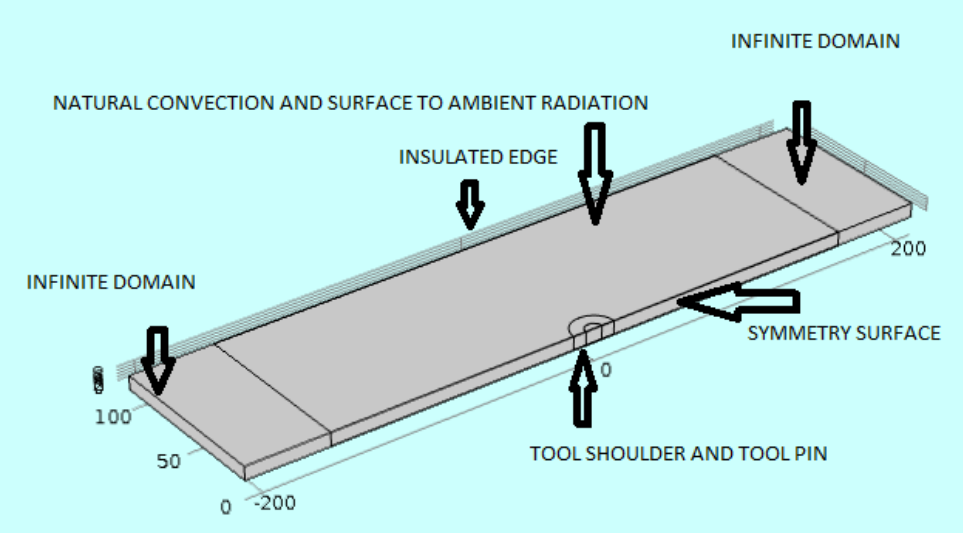

Figure 4.2: Geometric model for the FEA of FSW

4.1.2 Material

The experimental work involved for the present thesis is mainly focussed on the mechanical and microstructure characteristics studies. Hence methods for the measurement of temperature has not been provided in the specimen. Hence in order to validate the numerical procedure, experimental results in referred journal has been considered. According to that the material considered for the present study is Al6061-T6. The material is isotropic and homogeneous with temperature dependent material properties. Table 4.2 represents the thermal properties of this material. Table 4.3 indicate its temperature dependent yield stress values.

Table 4.2: Thermal properties of Al6061-T6 Alloy

Thermal conductivity (k), $(W/(mK)$	Density (rho) (Kg/m^3)	Heat Capacity (Cp) (J/kgK)
42	7800	500

Table 4.3: Temperature dependent yield stress of AA6061-T6 Alloy

Temperature (K)	311	339	366	394	422	450	477	533	589	644
Yield Stress (MPa)	241	238	232	223	189	138	92	34	19	12

4.1.3 Elements

For the meshing of the specimen "Free Quad 1" elements has been used. The tool pin and tool shoulder are meshed with "free triangular 1" elements. "Extremely fine" option has been used to set the size of elements which enables the convergence of FE model. Figure 4.3 shows the meshed model.

4.1.4 Boundary Conditions

Boundary conditions involved specifying the infinite domain, insulation at specimen edges, surfaces subjected to natural convection and radiation, surface heat source developed due to friction between tool shoulder and workpiece (in terms of effect due to rotation, transverse and axial load coming on the tool), surface heat source developed due to friction between tool pin and workpiece etc. Table 4.4 shows the expression for obtaining frictional heat developed at the tool shoulder and tool pin interfaces with the specimen.

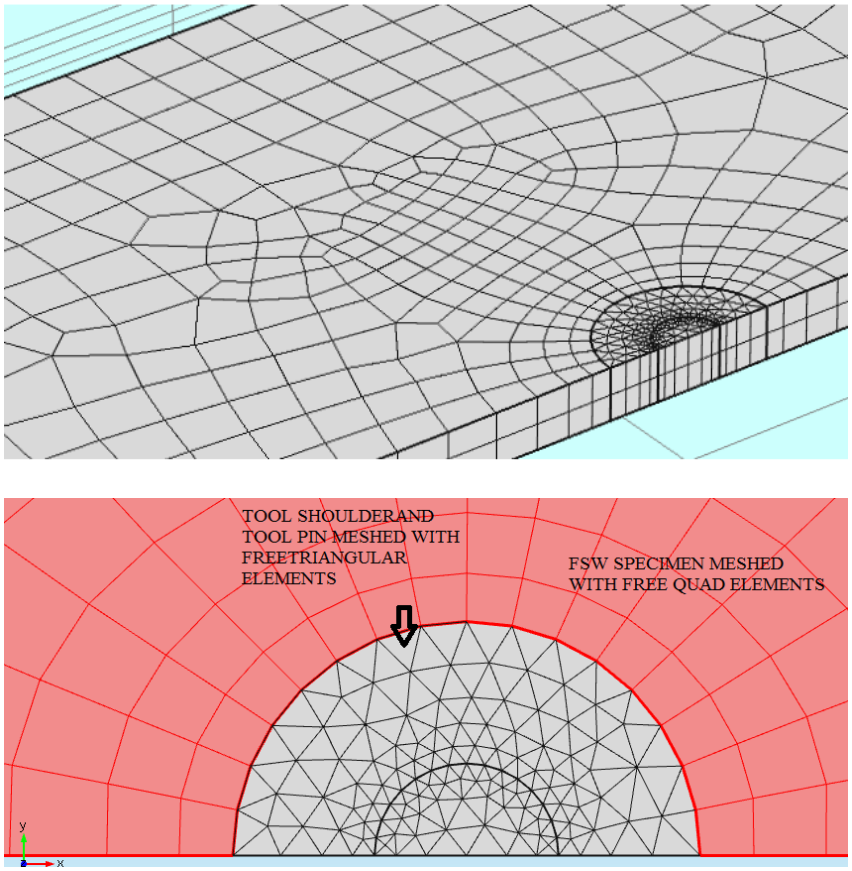

Figure 4.3: Meshed FE model of FSW specimen and tool

Table 4.4: Expressions for calculating surface heat sources

Name	Expression	Unit	Description
R	sqrt$(x^2 + y^2)$	m	Distance in x-y plane from tool center axis
$q_{shoulder}$	$(mu{*}F_n/A_s){*}(R{*}omega){*}step1(T_{melt}-T)[1/K])$	W/m^2K	Surface heat source at tool shoulder work-piece interface
Q_{pin}	$mu/sqrt(3{*}(1{+}mu^2)){*}(r_{pin}{*}omega){*}Ybar(T[1/K]){*}step1(T_{melt}-T)[1/K])$	W/m^2K	Surface heat source at pin-work-piece interface

4.1.5 Result and Discussion

The Temperature distribution and the isothermal contours obtained are the result obtained for the thermal modelling of FSW. Samples of pictures showing the maximum temperature distribution resulted with respect to various tool rotation speed are presented in Figure 4.4 to Figure 4.7.

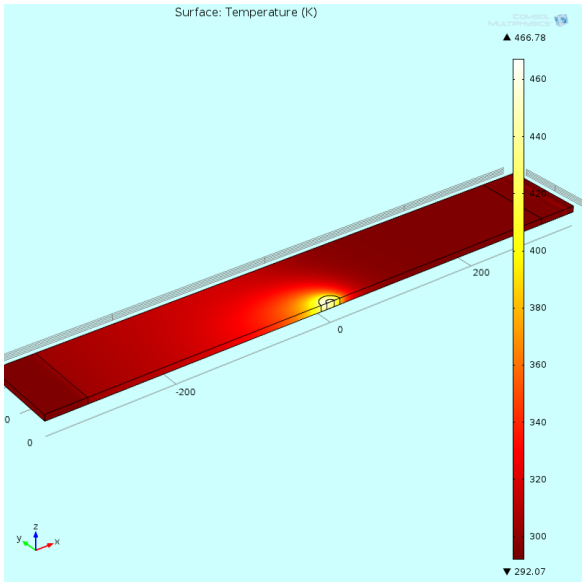

Figure 4.4: Temperature distribution at FSW tool rotations at 50 rpm

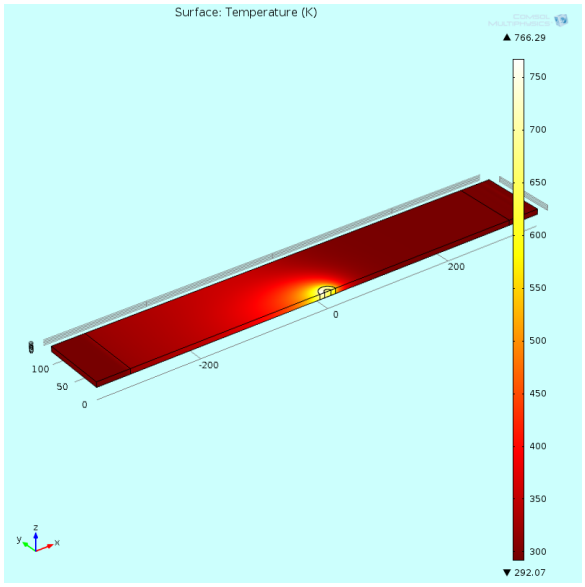

Figure 4.5: Temperature distribution at FSW tool rotations at 200 rpm

The thermal contours showed that maximum higher temperature is at the FSW tool shoulder and workpiece interface. The temperature distribution are seen decreasing towards outer region. Table 4.5 shows the comparison between the predicted temperature distribution as well as the same found by NX5 software package by Hamilton et al. (2008). For the present study, the effect of backing plate has not been considered. Hence for each case, temperature distribution has been calculated as the average of the maximum range of temperatures. In addition to that 15% reduction from the same has been considered from each to compensate the effect of backing plate. Figure 4.8 represent the comparison of temperature distribution predicted by

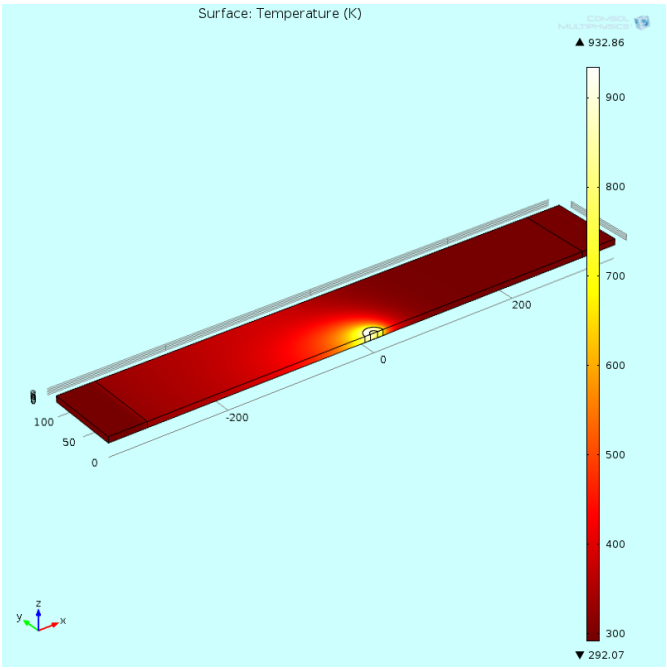

Figure 4.6: Temperature distribution at FSW tool rotations at 300 rpm

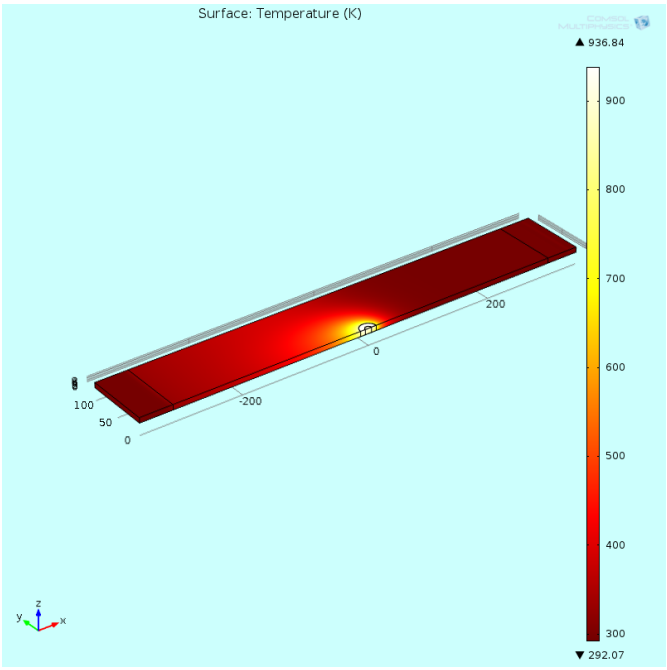

Figure 4.7: Temperature distribution at FSW tool rotations at 550rpm

the present procedure with the same predicted by Hamilton et al. (2008). A close agreement between the values of predicted temperature and the referred values has been noted from this studies. Hence the procedure used for the present study can effectively be utilized for the thermal modelling of FSW process of other materials.

Table 4.5: Comparison of predicted temperature

Sl. No	Tool rotation (rpm)	Predicted Temperature range (°C)	Average Temperature after compensation of back plate effect(°C)	Temperature distribution by Hamilton et al (°C)
1	50	460-466.78	394	398
2	100	550-558.43	471	479
3	175	700-710.22	599	570
4	200	750-766.29	645	594
5	225	800-824.04	690	615
6	250	800-882.45	715	635
7	300	900-932.86	779	667
8	350	900-924.78	780	691
9	450	900-937.59	781	770
10	550	900-936.84	781	776

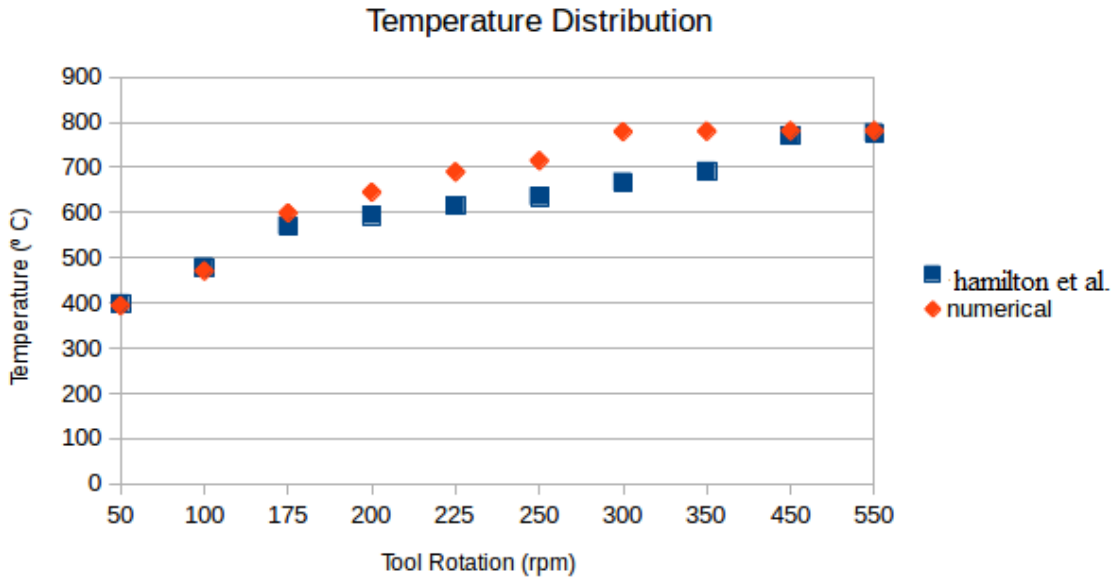

Figure 4.8: Validation plot for the predicted temperature distribution

4.2 Analytical Investigations on FW

Analytical investigation which represent each stages of the FW process is a complicated procedure as it involves the frictional heat generation due to rotating and stationary specimen subjected to axial loading, thermoplastic deformation and there by the upsetting of interface, strain development, material transfer, cooling of heated area etc. Hence like many researchers' work, here also a numerical modelling has been carried out by the coupling of structural as well

as thermal modelling using the temperature dependent material properties. Thus the main objective of the numerical modelling has been fixed as the thermomechanical analysis of the FW process and obtaining distributions of stress, strain, contact friction stress, contact penetration, contact pressure, contact sliding distance, and contact gap distance over time throughout the process. The FEM based software package, Ansys has been used for the study. As an extension to this work, numerical modelling for predicting residual stresses in dissimilar friction welding has also been carried out. The predicted values have been compared with the experimental results available in standard journal papers.

4.2.1 Geometrical Model

A 2D axisymmetrical model, symmetrical about Y axis, as shown in Figure 4.9 has been considered for the numerical modelling.

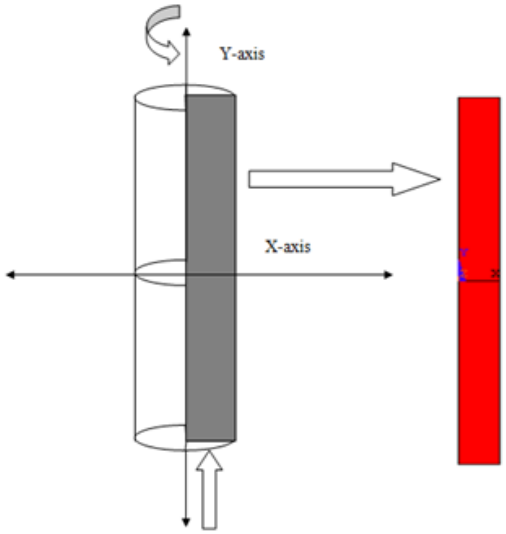

Figure 4.9: Axisymmetricl model for FW

4.2.2 Material

For the present thesis the experimental work are focused for the assessment of mechanical and microstructural characteristics of FSW and FW joints. Attempts have not been made to measure the stresses coming on the specimen during friction welding. Hence a comparison with the experimental work carried out with this numerical modelling has got no much relevance. However, in order to validate the numerical model, available experimental results from the

referred journal has been considered. Thus the material considered for the numerical modelling of FW is AISI 316. The material is assumed as isotropic and homogeneous with temperature dependant material properties. The mechanical properties of AISI 316 are given in Table 4.6. The solidus and liquidus temperature of AISI 316 are 1643K and 1673K respectively. Table 4.7 represents the temperature dependent thermal properties of the same.

Table 4.6: Temperature dependent material properties of AISI316 Alloy

Temperature (K)	Elastic Modulus-(N/m^2)	Temperature (K)	Elastic Modulus-(N/m^2)	Temperature (K)	Elastic Modulus-(N/m^2)
273	2.00E+11	723	1.64E+11	1273	1.19E+11
293	1.96E+11	773	1.60E+11	1323	1.12E+11
373	1.92E+11	823	1.56E+11	1373	1.05E+11
423	1.88E+11	973	1.44E+11	1423	9.44E+10
473	1.84E+11	1023	1.39E+11	1473	2.00E+10
523	1.80E+11	1073	135E+11	1523	1.17E+10
573	1.76E+11	1123	131E+11	1573	7.00E+09
623	1.72E+11	1173	127E+11	1623	5.56E+09
673	1.68E+11	1223	1.23E+11		

4.2.3 Elements

An axisymmetrical 2D model has been created in ANSYS using PLANE 42 quadrilateral elements having four nodal points and two displacement degrees of freedom. The FE model include 918 nodes and 840 elements. For meshing, element edge length has been taken as 0.002 m. Figure 4.10 represents the meshed model. The element has plasticity, creep, swelling, stress stiffening, large deflection, and large strain capabilities. Figure 4.11 shows geometry, node locations and co-ordinate system for the PLANE 42 element. There are four nodes I, J, K and L and two displacement degrees of freedom UX and UY. The element input data includes four nodes, a thickness (for the plane stress option only) and the material properties. For contact pair creation TARGET 169 and CONTACT 171 elements (see Figure 4.12) have been used for rotating and stationary specimens respectively. Using the contact wizard contact element creation has been done. Coefficient of friction at the contact surface has been considered as 0.3. Figure 4.13 represents the FE model incorporated with contact element.

Table 4.7: Thermal properties of AISI316 Alloy

Temperature (K)	Density (kg/m^3)	Specific-heat- (J/kgK)	Thermal-Conductivity (W/mK)	Enthalpy (J/m^3)
273	8038.70	456.28	13.29	9.76E+08
293	8030.47	464.73	13.63	1.05E+09
373	7997.02	494.23	14.99	1.35E+09
473	7954.03	522.74	16.62	1.75E+09
573	7999.76	543.92	18.19	2.16E+19
673	7864.18	599.87	19.72	2.59E+09
773	7817.31	572.69	21.26	3.03E+09
873	7769.13	584.49	22.81	3.48E+09
973	7719.13	597.38	24.42	3.94E+09
1073	7668.90	613.45	26.09	4.41E+09
1173	7616.83	634.82	27.86	4.90E+09
1273	7563.47	663.58	29.76	5.40E+09
1373	7508.81	701.85	31.81	5.93E+09
1473	7452.85	751.72	34.03	6.49E+09
1573	7395.6	815.30	36.46	7.09E+09
1643	7345.75	869.09	38.29	7.54E+09

4.2.4 Boundary Conditions

Here the rotating specimen is held in a chuck and is prevented from movement in the axial direction. In the numerical model the axial movement of rotating specimen has been constrained by arresting movement in the Y direction (UY = 0) of the end nodes. The stationary specimen has only axial motion. The rotation of stationary specimen in numerical model has been prevented by arresting movement in X direction (UX = 0) of the end nodes. Figure 4.14 represents the displacement boundary conditions given. The FE model has been loaded in maximum of 10 sub steps. Loading has been performed in three fold as follows. Initially the inertia load has been applied. For that the rotating specimen has been selected and given an angular velocity of 125.66 rad/s about the Y axis, corresponding to an rpm of 1200. (Angular velocity OMEGAY= $2 * \pi * 1200/60$ = 125.66 rad/s). The axial pressure is the second loading. It has been given by providing a pressure of 100 MPa applied at the end of the stationary specimen. The third loading is the temperature loading. A temperature load of 1673K corresponding to the liquidus temperature of AISI 316 has been given at the contact nodes assuming that heat is generated at the contact interface due to friction. Figure 4.15 represents the given force boundary conditions.

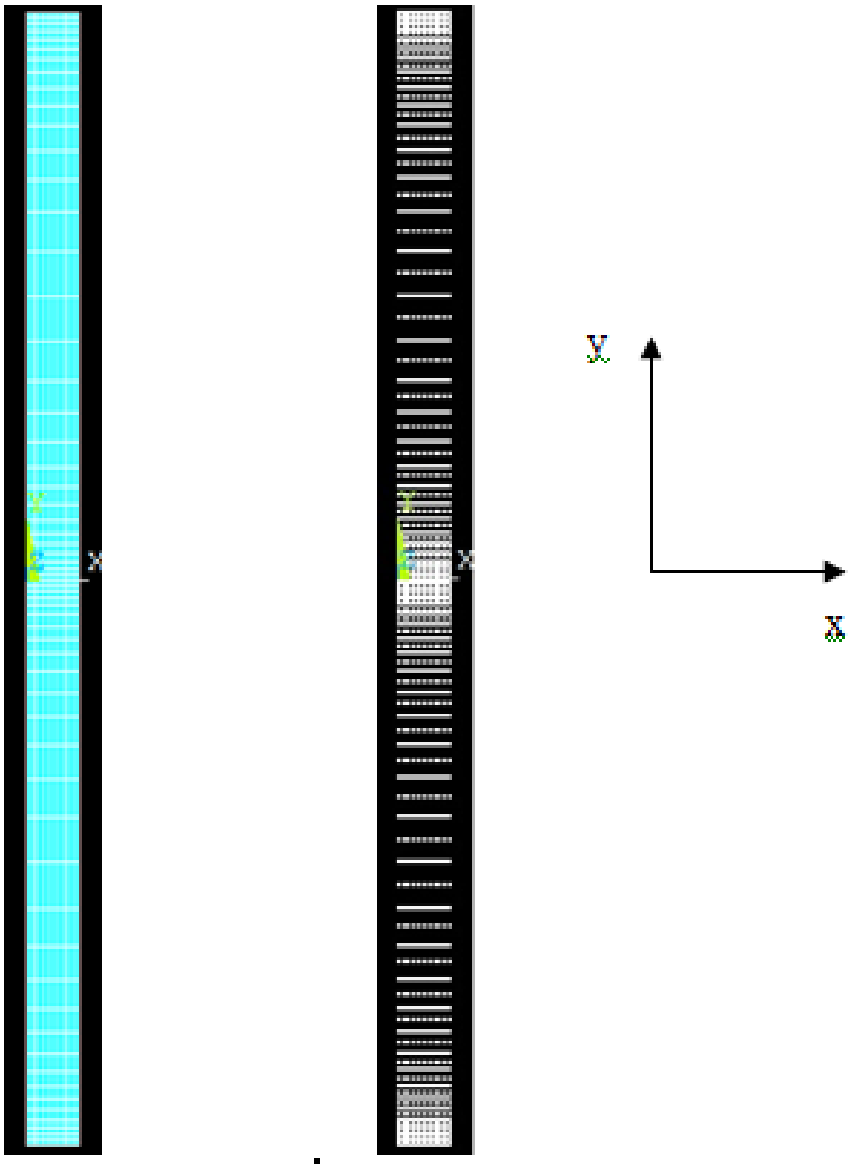

Figure 4.10: Meshed model of FW

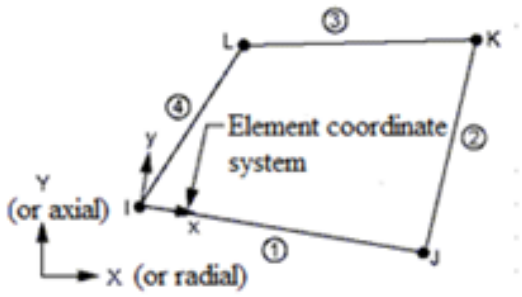

Figure 4.11: Details of plane 42 element

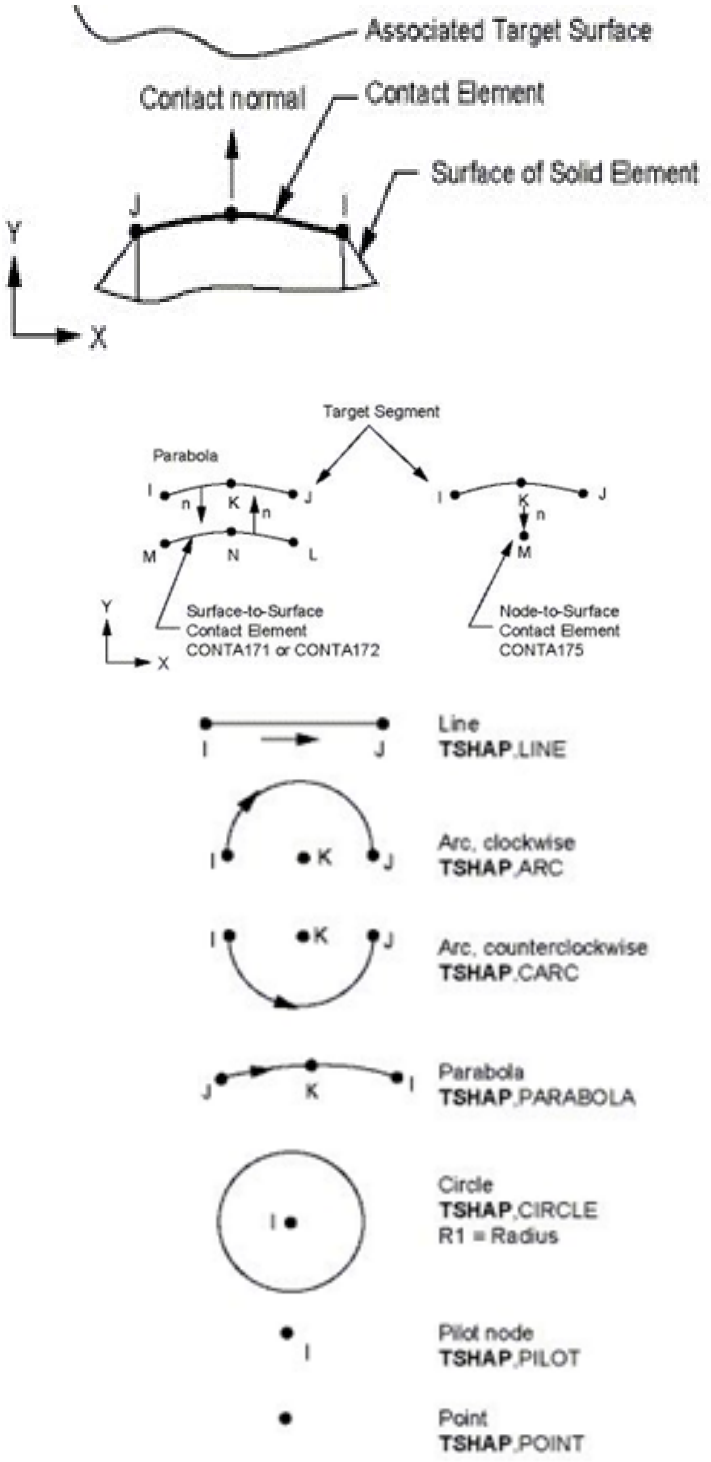

Figure 4.12: Details of contact elements

4.2.5 Convergence Studies

A convergence study has been carried out to assess the equivalent stress (von Mises stress) in the specimen under combined loading. Figure 4.16 indicates the convergence of von Mises stress

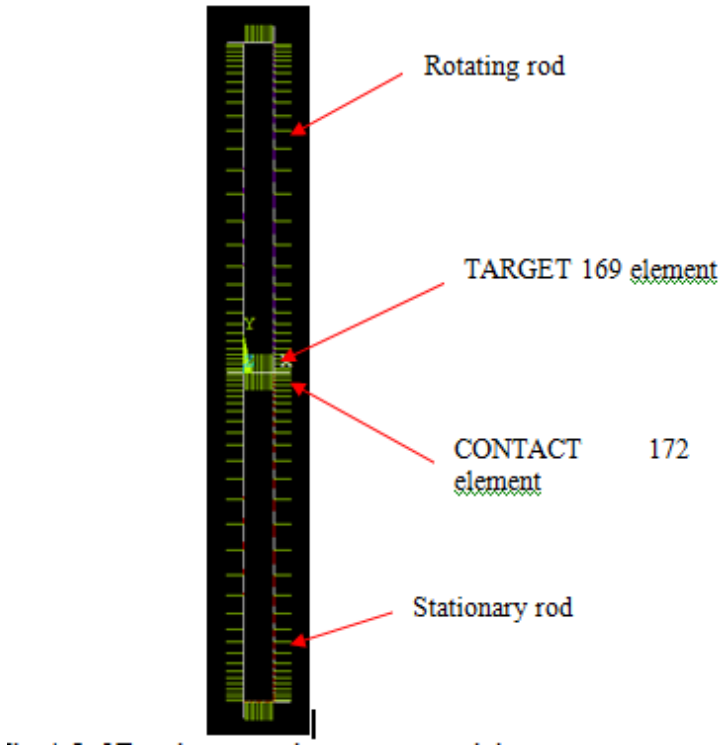

Figure 4.13: FE model incorporated with contact pair

value. Table 4.8 indicates the percentage variation in Von Mises stress value corresponding to number of elements considered. Thus an FE model with finest mesh of 840 Number of

Table 4.8: Convergence of Von Mises stress values

Degree of mesh	SEQVmax MPa	Number of Elements	Number-of nodes	Percentage Change in SEQV max
coarse	74	106	128	-
Fine	120	360	434	62.16
Finer	147	680	712	22.50
Finest	148	840	918	0.6802

elements and 918 number of nodes is found to be suitable for the analysis.

4.2.6 Results and Discussions

The results from preliminary studies are explained based on the contour plots and graphical plots. The results included distribution of von Mises stress, von Mises strain etc. on the specimen, at initial and final stages. In addition to that it also gives the contact sliding distance,

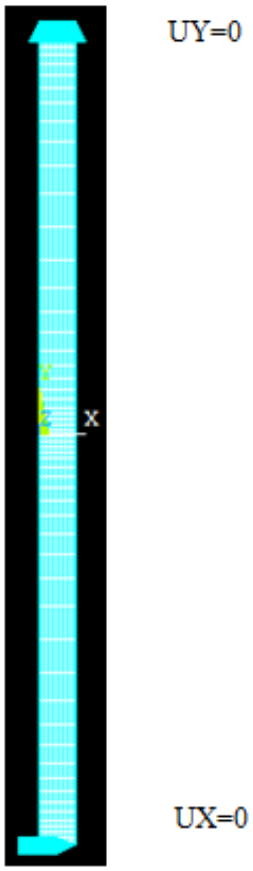

Figure 4.14: Displacement boundary condition

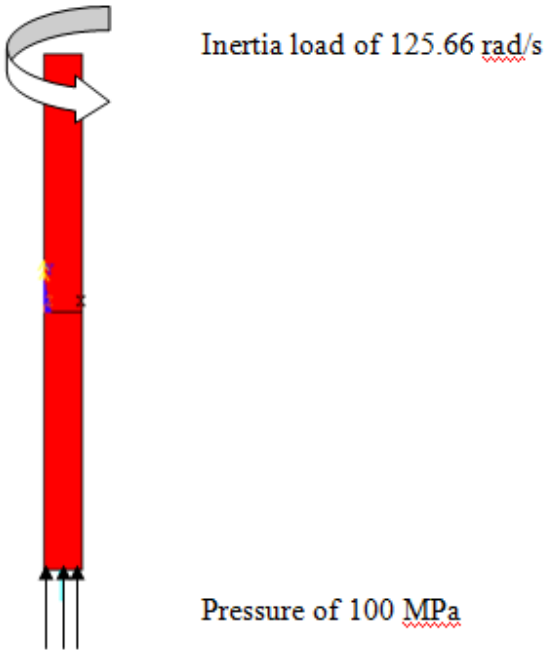

Figure 4.15: Force boundary condition

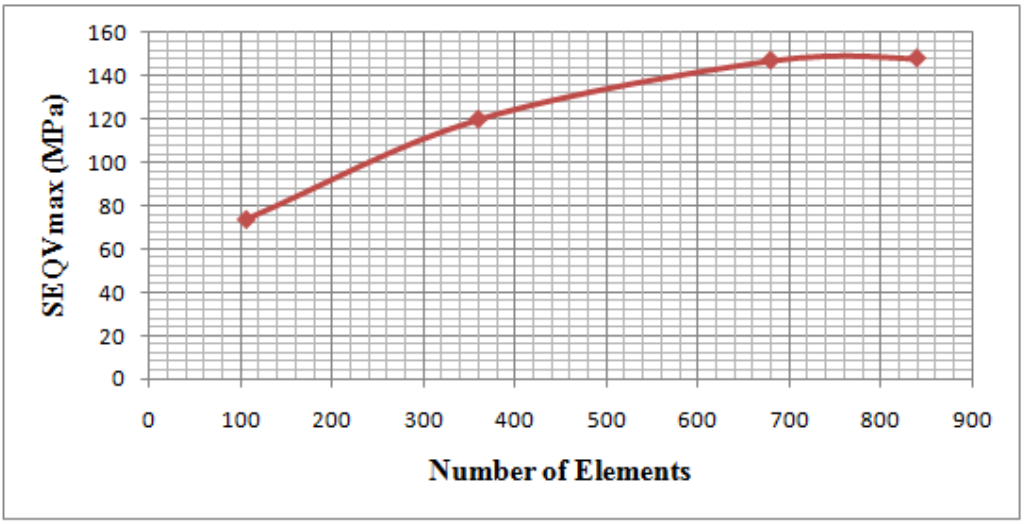

Figure 4.16: Plot of von Mises stress convergence of the FE model

contact friction stress, displacement field, contact penetration and contact pressure over time through out the process. All these are explained in detail in the following sections.

4.2.6.1 Contour plot on Displacement Distribution

The contour plots on displacement at the beginning and end of the process are obtained as shown in Figures 4.17 and 4.18. The maximum displacement value increases from $0.978 * 10^-4m$ to $0.153 * 10^-3m$ towards the end of the process. It shows an increase in the displacement value at the constrained end of stationary specimen from the initial stage to the final stage of the process. The minimum displacement occurs at the constrained end of rotating specimen with a value of $0.561*10^-9m$.. The maximum value of displacement is noted at the constrained end of the stationary specimen. It may be due to the application of axial pressure at that end. The minimum value of displacement at the end of rotating specimen has been caused by the arresting of axial movement at that end.

4.2.6.2 Contour plots on von Mises stress distribution

The stress distribution during the initial and the final stages are shown in Figures 4.19 and 4.20. Figure 4.21 represents the enlarged view of von Mises stress distribution at the final stages. The stress values at the initial stage are seen to be maximum on areas away from the constrained end regions with a value of $0.107 * 10^9 N/m^2$. Towards the end of the process, the stress has been found to be maximum on both sides of the contact region with a value of $0.148*10^9 N/m^2$.

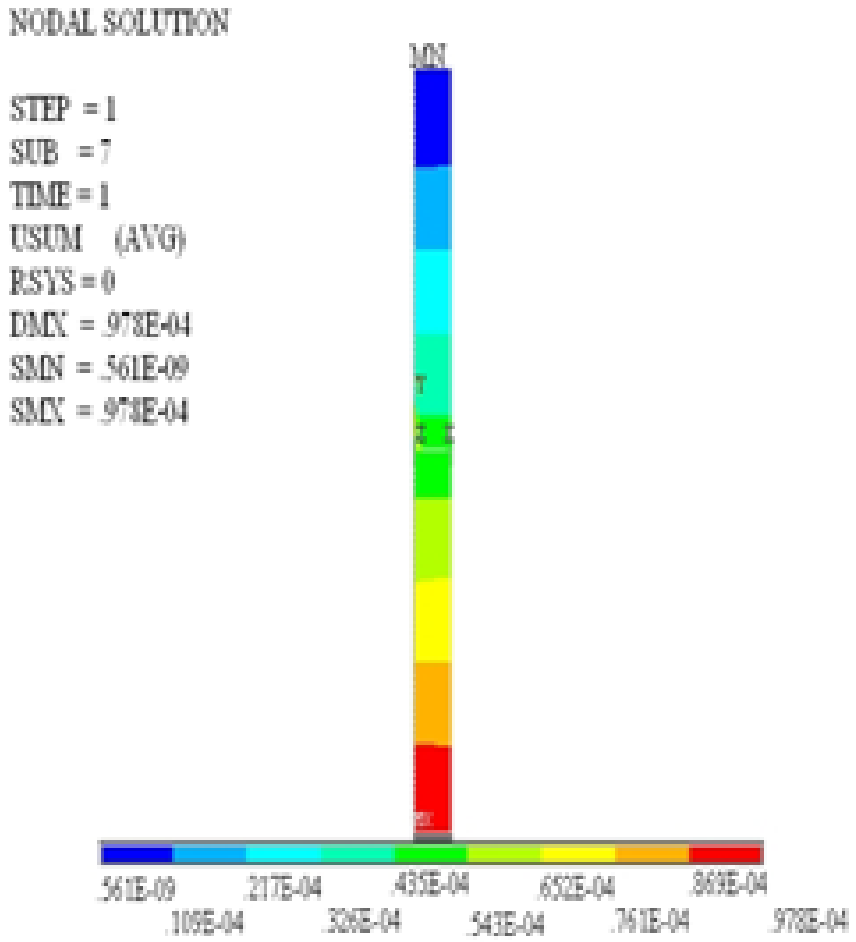

Figure 4.17: Displacement field distribution - initial stages

At the initial stage as well as in the final stage, the minimum values of stress obtained on the constrained end of rotating specimen are $0.616 * 10^7 N/m^2$. The relative motion caused by the rotation of the rotating specimen as well as the axial motion of the stationary specimen along with high temperature load at the contact interface resulted in stress concentrations on both sides of the contact interface towards the end of the process.

4.2.6.3 Contour plots on Strain distribution

The strain values at the initial stage are seen to be maximum on areas away from the constrained end regions with a value of $0.534 * 10^-3$. Towards the end of the process the strain has been found to be maximum on the contact region towards the outer edge with a value of 0.014878. This indicates that maximum change in dimension occurs towards the outer surface of the joint.

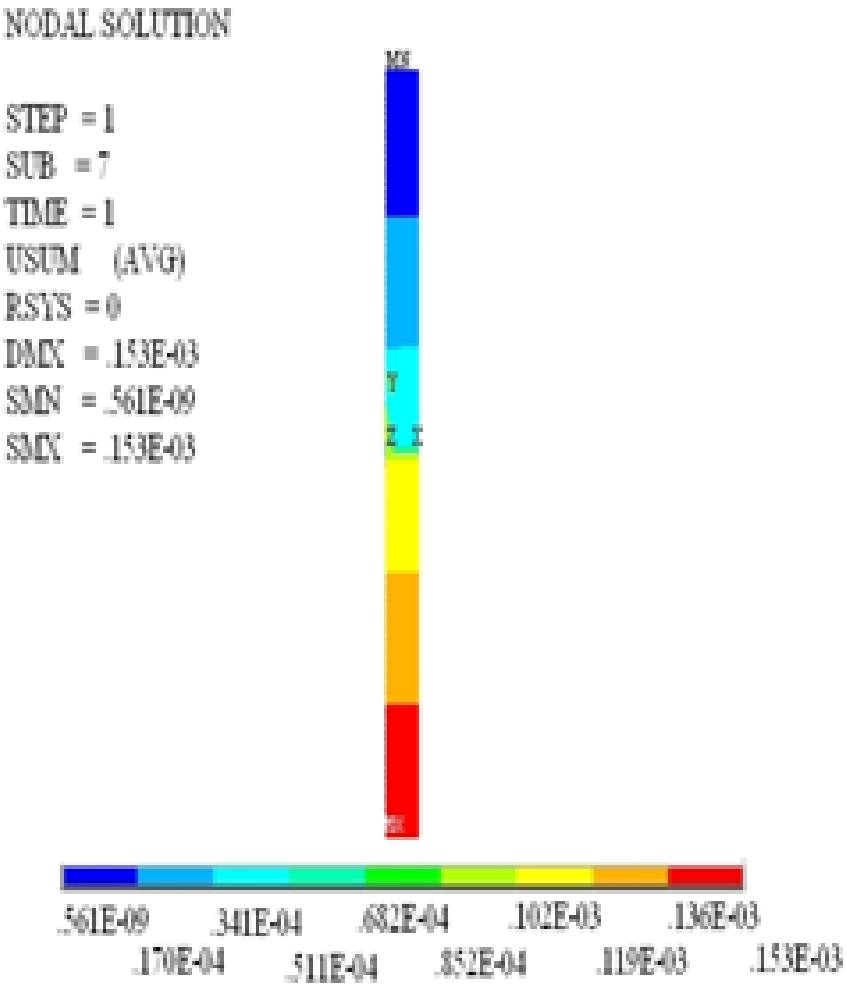

Figure 4.18: Displacement field distribution - final stages

At the initial stage as well as in the final stage, the minimum value of strain has been obtained on the constrained end of rotating specimen with a value of $0.326 * 10^{-}4$. The strains in the model during the initial and final stages are presented in Figures 4.22 and 4.23. The relative motions of rotating and axial loaded stationary specimens along with the high temperature load at the joining faces caused for the development of strain in FW specimen initially. At the final stages it is seen that strain has been increased further due to the upsetting action in the stationary specimen. It is also seen that due to the same reason comparatively larger strain has been developed at the outer surface of the contact region.

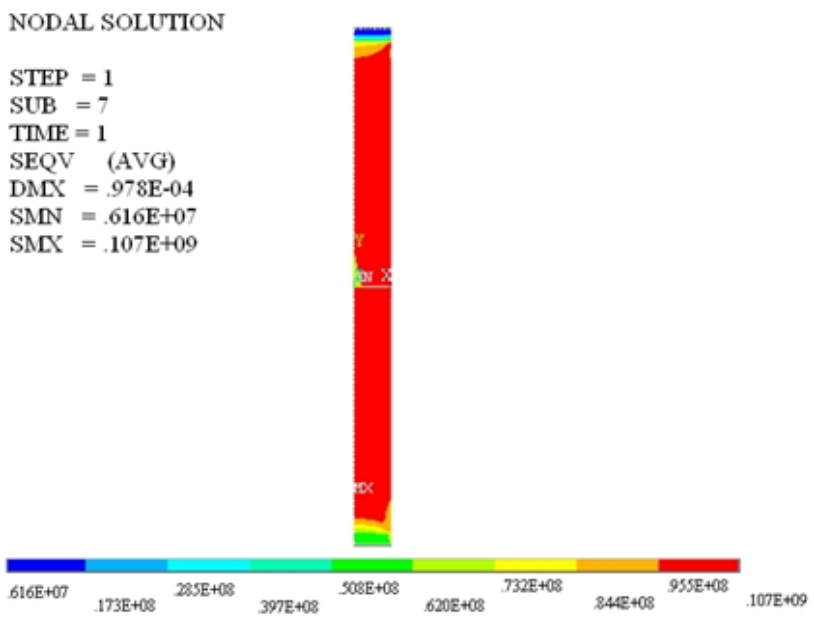

Figure 4.19: von Mises stress distribution - initial stages

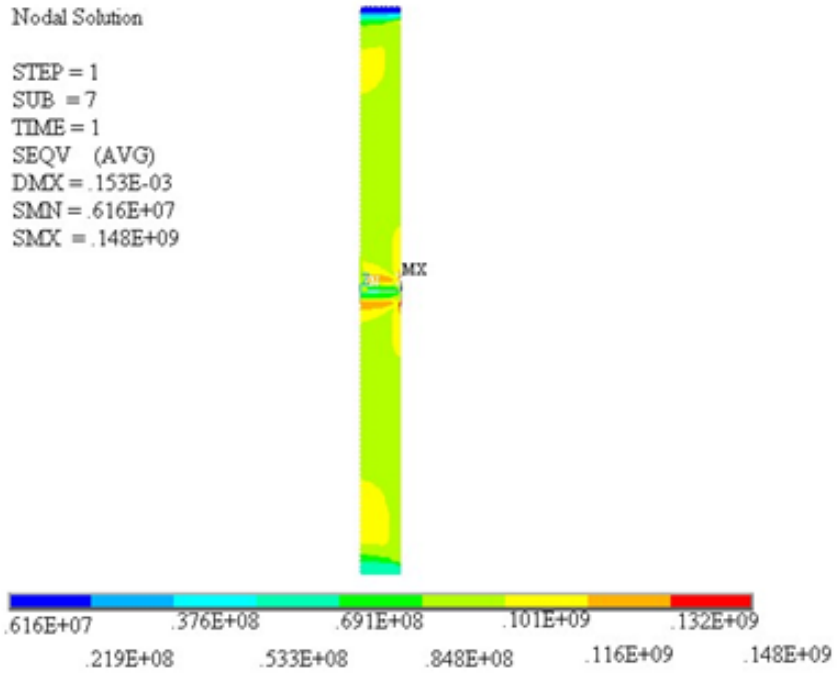

Figure 4.20: von Mises stress distribution - final stages

4.2.6.4 Graphical plot on von Mises stress distribution

A node on the outer surface of the contact interface has been selected and the graphs showing variations of Von Mises stress, strain, contact sliding distance, contact penetration, X component of displacement, Y component of displacement over time of the FW process has been

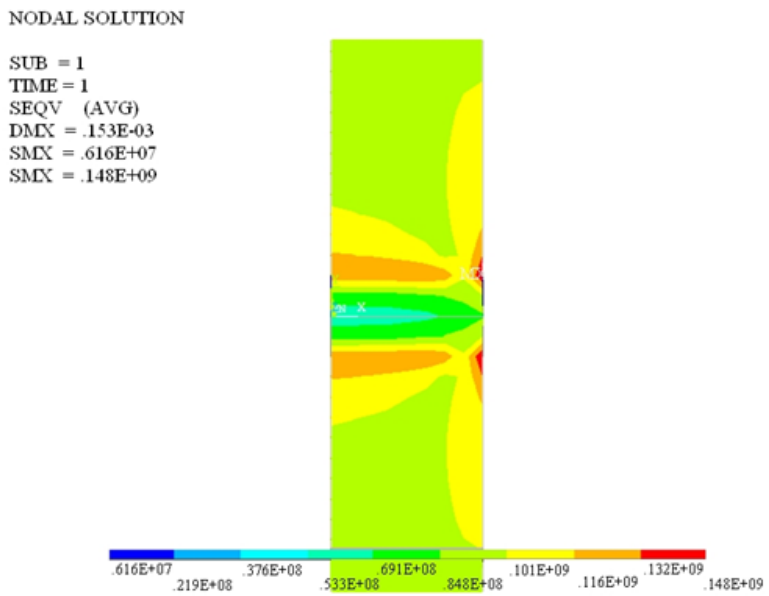

Figure 4.21: von Mises stress distribution near to the joint

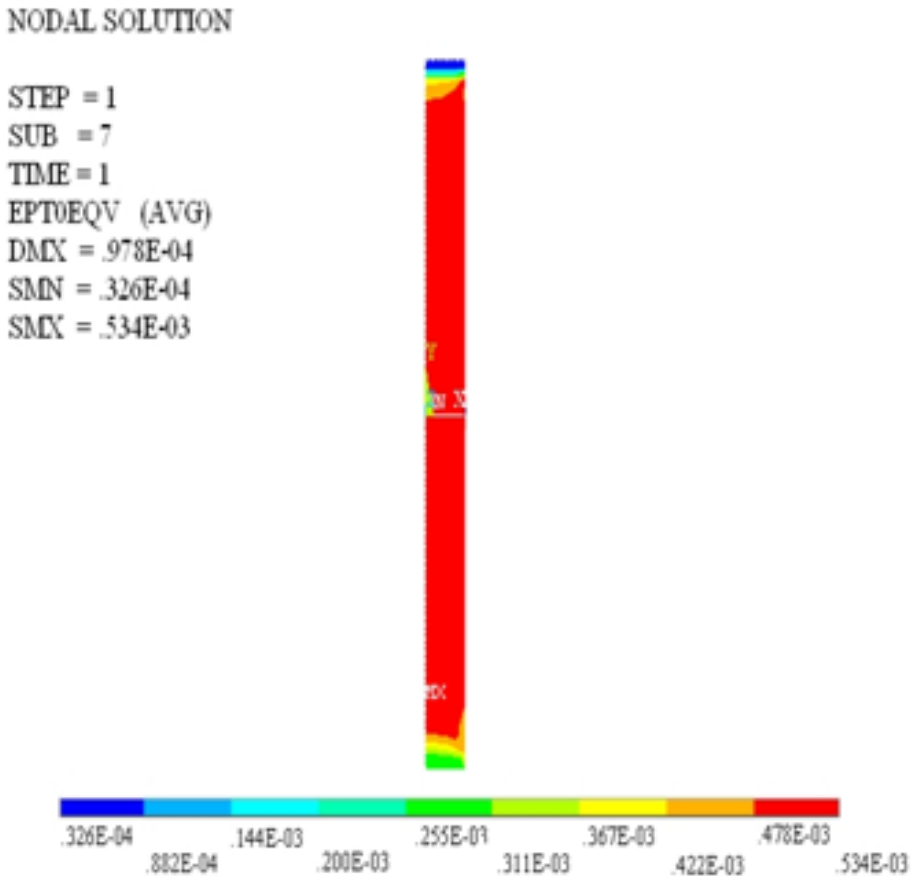

Figure 4.22: von Mises strain distribution - initial stages

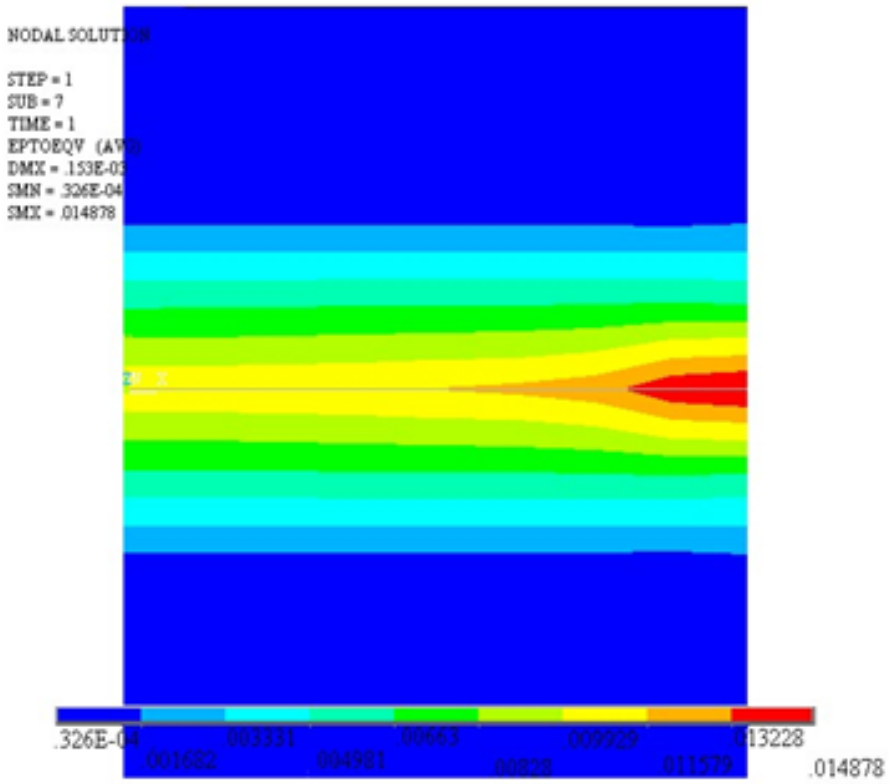

Figure 4.23: von Mises strain distribution at final stages

obtained. All are presented from Figure 4.24 to 4.29. It is seen that von Mises stress value

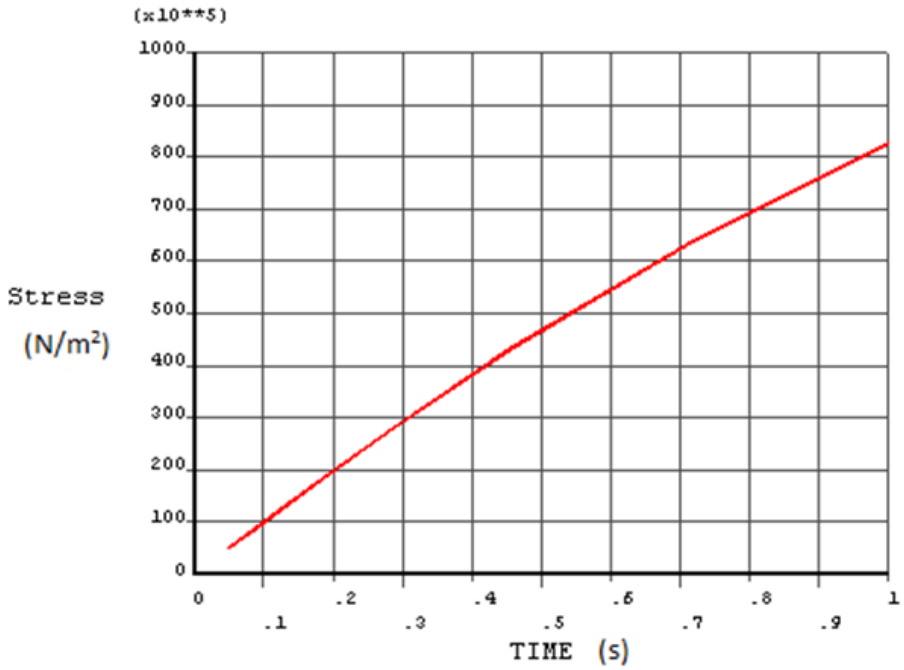

Figure 4.24: variation of von Mises stress over time

variation throughout the process shows an approximately linear increase. Towards the end of the process it shows a decreasing trend 4.24. This might be due to the transformation of the material to plastic state within short period of time due to high temperature and high tangential velocity at the outer region.

4.2.6.5 Graphical plot on Strain distribution over time

Strain at the outer edge of the contact area increases at a smaller rate initially and towards the end of the process, it increases at a faster rate due to the thermoplastic state of the material. Figure 4.25 represents this variation. It is seen that corresponding to von Mises stress, strain also increasing linearly to certain extend of time after that it is seen shoot up within short period of time, corresponding to the node selected at the outer region. This may be due to the loosening of materials at the thermoplastic state due to high temperature and angular velocity.

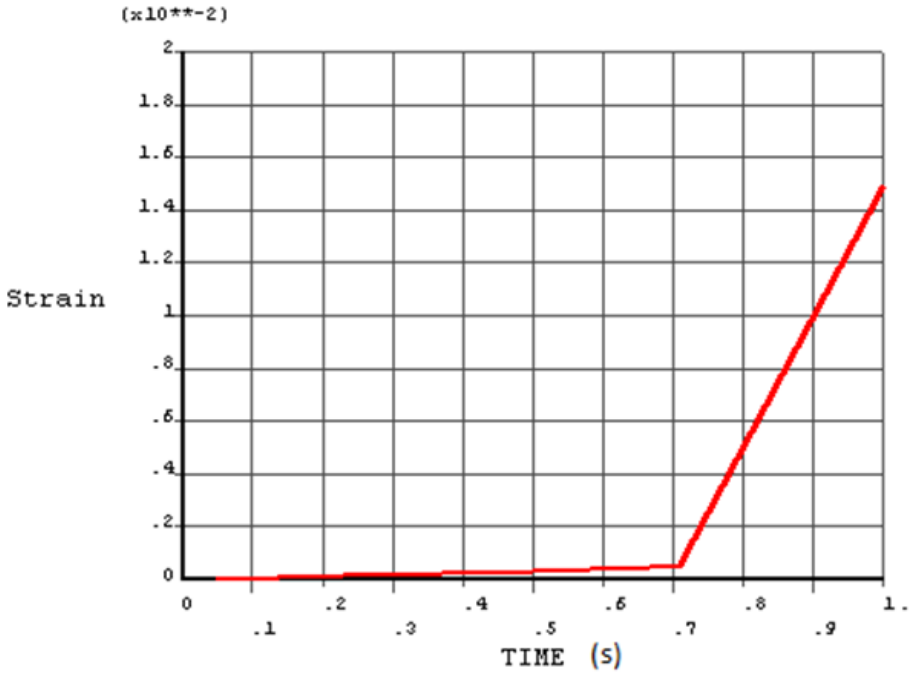

Figure 4.25: variation of von Mises strain over time

4.2.6.6 Graphical plot on Contact sliding distance over time

Contact sliding distance shows a parabolic decrease.(see Figure 4.26). From the picture it is understood that, it is happened due to the high temperature developed and hence the softening of the materials.

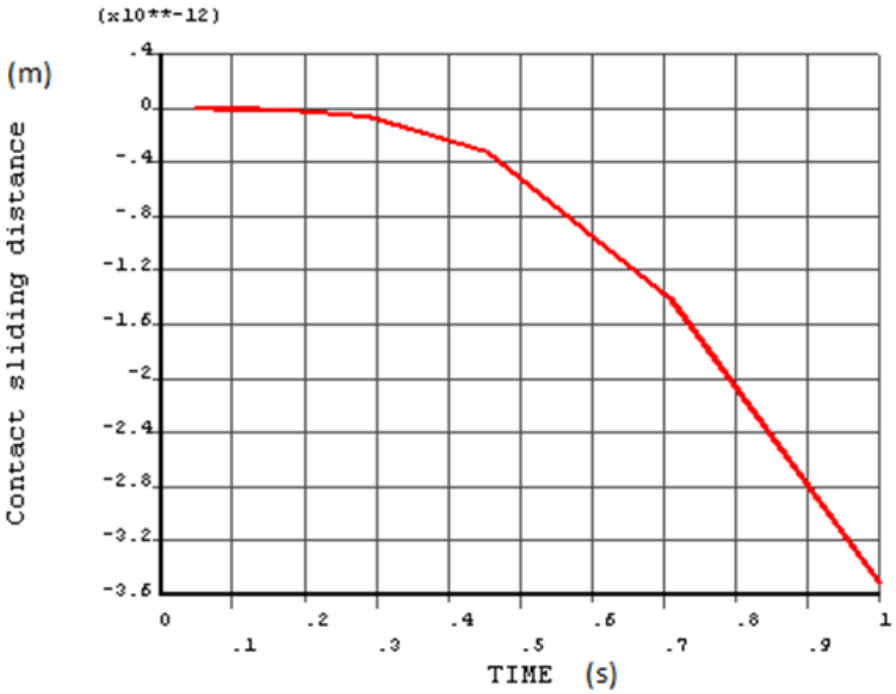

Figure 4.26: variation of contact sliding distance over time

4.2.6.7 Graphical plot on Contact friction stress over time

Contact friction stress shows a parabolic increase as shown in Figure 4.27. This may be due to the reduction in normal area due to the softening of the material.

4.2.6.8 Graphical plot on X and Y components of displacement

It is seen that, both X and Y component of displacements are increases at slower rate initially and within short period of time both get increases rapidly. Here, X component represents the movement along radial direction and Y component of displacement is along the longitudinal direction (see Figure 4.28 and 4.29). Here, Y component of displacement is seen more than that of X component of displacement. This may be due to the softening of material due to the high temperature developed. In addition the upsetting action has also been accelerated the movement of these soft materials.

4.2.7 Validation of the Results

To validate the numerical model, the problem of FW process has been analysed in a manner similar to the case of a rotating shaft. The shaft is of 75 mm diameter and 0.5 m span rotating

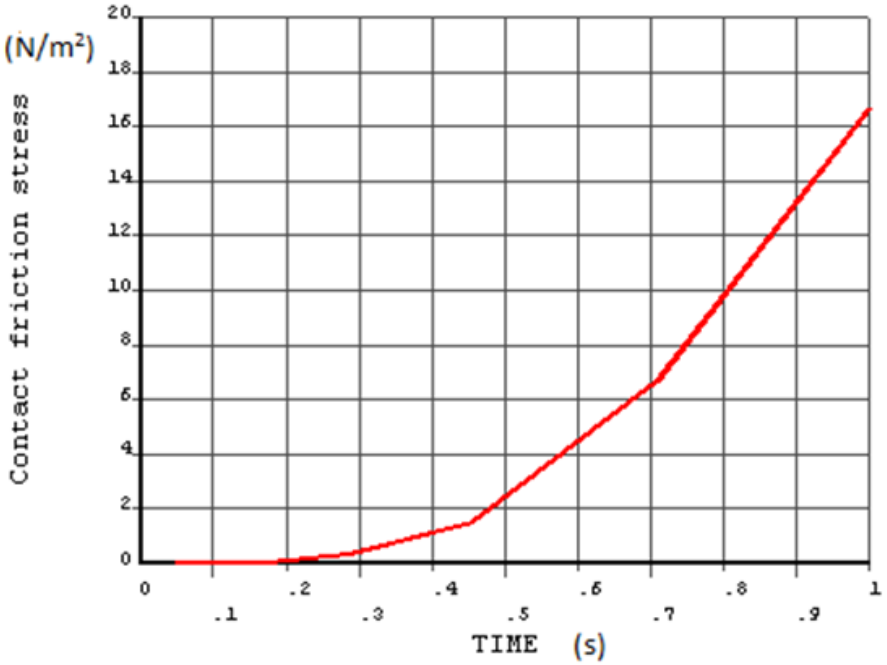

Figure 4.27: variation of contact friction stress over time

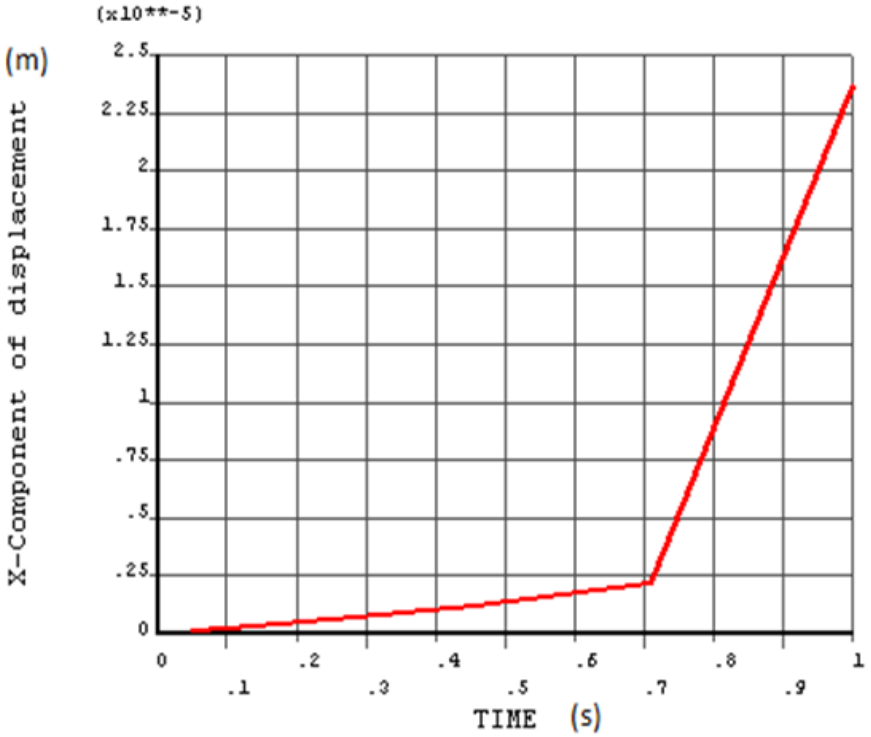

Figure 4.28: Variation of X component of displacement over time.

at 200 rpm (N) and transmitting a power (P) of 35 kW, has been considered. The shaft is subjected to an axial compressive end load of 80 KN. The material is having Youngs modulus of 210 GPa, Poisson's ratio of 0.3 and density of 7800 Kg/m^3. This problem has been solved

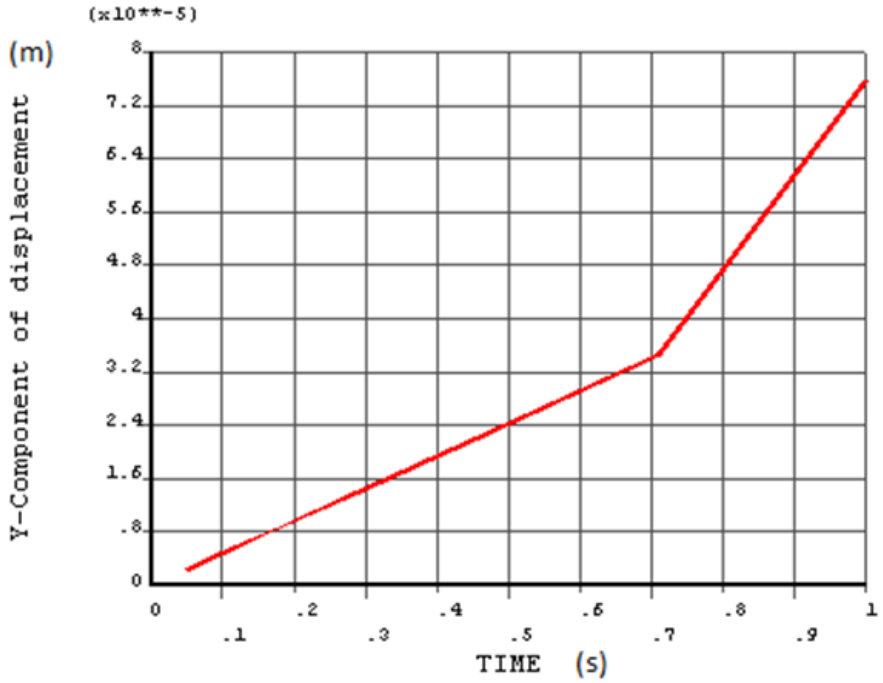

Figure 4.29: Variation of Y component of displacement over time

using FE procedure in Ansys by creating an axisymmetrical model and meshed using PLANE 42 elements by providing requisite boundary conditions. It is seen that, the von Mises stress value noted by the numerical procedure is matching with values found by analytical methods. The steps in the analytical calculations has been given in appendices.

From the numerical modelling and thermo-structural analysis of FW process, it is inferred that the maximum Von Mises stress seemed to be concentrated near the weld zone. Maximum strain is also found to be near the outer surface of the joint. The contact friction stress and contact penetration seemed to be maximum towards the inner surface of the joint and minimum towards the outer surface of the joint as can be observed in the experiment on FW process.

4.3 Residual Stress in a Dissimilar FW joint

Attempts have been made to make a numerical model to assess residual stress developed in dissimilar friction welding. Dissimilar metals considered are ferritic and austenitic steel. The residual stress calculated based on the numerical model, has been validated with the experimentally found result from the referred journal paper (Reddy et al., 2005). In the reference paper, it is reported that welding has been performed on a continuous drive friction welding machine at a speed of 1500 rpm in a continuously and step less variable speed machine of 15

kN capacity. During welding, the primary parameters (friction force, forge force, rotational speed) have been continuously monitored and recorded. Residual stress measurements have been carried out across the interface employing X-ray stress measurement technique. Welding of ferritic to austenitic stainless steels is considered to be a major problem due to difference in coefficient of thermal expansion, which may lead to crack formation at the interface, formation of hard zone close to the weld interface, relatively soft regions adjacent to the hard zone, large hardness difference between the hard and soft zones and expected differences in micro structure. All these may lead to failures in service. Welding process parameters under consideration are friction force(4000 N), forge force (12000 N), friction time(5s) and forge time(5s).

4.3.1 Material properties

The welding of dissimilar metals is more complex than that of similar metals because of difference in the physical, mechanical and metallurgical properties of the metals to be joined. Solid state welding is a possible solution for these problems. The dissimilar parent metals used are AISI 304 austenitic stainless steel and AISI 430 ferritic stainless steel. The AISI 304 austenitic stainless steel has applications in the field of architectural panelling, tubing, chemical equipment, refrigeration equipments, food and pharmaceutical production equipment, pressure vessels, medical and surgical implants, springs, nuts, bolts and screws. The AISI 430 ferritic stainless steel have applications in the field of cabinet hardware, decorative appliance, automotive moulding, range hoods, stampings etc. Dissimilar metal combination between ferritic stainless steels and austenitic stainless steels is commonly employed in TiCl4 reduction retorts. The chemical composition of AISI304 austenitic stainless steel and AISI430 ferritic stainless steel is shown in Table4.9

Table 4.9: Chemical composition of AISI 304 and AISI 340

Name of steel	C	Mn	Si	P	S	Cr	Mo	Ni	N
AISI304 (%)	0.07	2.0	0.75	0.045	0.030	17.5-19.5	-	8-10.5	0.10
AISI430 (%)	0.1-2	1	0.75	0.04	0.30	16-18	-	-	-

4.3.2 Coupled Thermomechanical FE modelling

In the field of numerical simulation of the friction welding process, most of the models often have several limitations in either the representation of the geometries, or the material behaviour, or the boundary conditions. In the present research, a numerical procedure has been set up to

determine the residual stress field using the thermomechanically coupled FEM model in the ANSYS software. (i.e A non linear direct coupled-field transient analysis in which thermal and mechanical behaviours are mutually dependent and coupled together during the friction welding process). The FE model made in ANSYS possessed 1932 nodes and 600 elements. Following assumptions have been made for the analysis.

- The model is considered to be a two dimensional
- There is no heat transfer at the end face of the metals. As the radiation effect is very less heat loss by radiation may be neglected
- The temperature developed at the interface due to the heat flux is assumed as 1400 °C which is the liquidus temperature of the steel.
- The finite element modelling of rotary friction welding has been done using transient analysis by taking each cylindrical rods as 2D axisymmetric components.
- The materials of the model is assumed to be isotropic and homogeneous with temperature dependent material properties.

4.3.3 Elements

The element used for the dissimilar friction welding is Plane 223. This element can be used as as plane stress element, plane strain element and as an axi-symmetric element. It is a eight noded element with up to four degree of freedom per node. The element can incorporate plasticity, creep, swelling, stress stiffening, large deflection and large strain capabilities. It can also hold the conditions such as structural-thermal, piezo-resistive, electro-elastic piezo-electric, thermal-electric, structural-thermo electric, thermal piezo electric, structural diffussion, thermal-diffussion, structural thermal-diffussion etc. Structural capabilities include elasticity, plasticity, viscoelasticty, viscoplasticity, prestress effect etc. The thermoplastic effect is available for analyses with structural and thermal degrees of freedom. Figure 4.30 represents geometry, node locations and co-ordinate system for the PLANE 223 element. There are eight nodes L, P, I, M, J, N, K, O and the structural-thermal coupled-field have displacement degrees of freedom that are UX, UY, TEMP, force labels are FX, FY, HEAT. The element input data includes four nodes, a thickness (for the plane stress option only) and the material properties. Various combinations of nodal loading are available for this element. Nodal forces should be entered as input per unit of depth for a plane analysis and on a full 360 basis for an axisymmetric analysis.

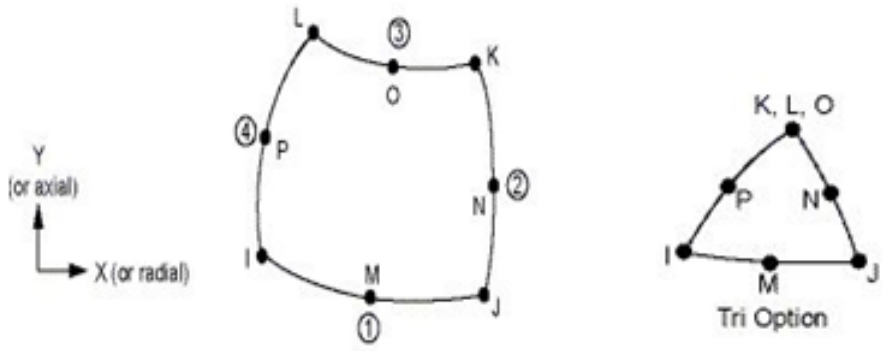

Figure 4.30: PLANE 223 element

Here also for contact pair modelling TARGET 169 and CONTACT 172 elements have been used. The coefficient of friction between the contact surfaces is taken as 0.35. The penetration tolerance factor is taken as 0.6. The TARGET 169 element is used to model the contact surface of the rotating work piece, and the element CONTACT 172 is used for the stationary work piece. Figure 4.13 shows the contact model of the welded joint.

4.3.4 Boundary conditions given

Displacement boundary conditions has been given as described in section 4.2.4. The rotating specimen is held in a chuck and is prevented from movement in the axial direction. The stationary specimen has given only axial motion. Force boundary conditions should be given to the model with the actual scenario of FW process. It is also noted that the material properties are temperature dependent. As per the FW process, the temperature developed is according to the axial loading as well as the speed of rotating specimen. Hence, time dependent step by step structural loading in the stationary specimen need to be given to simulate the FE results with the actual process. Considering these conditions, the force boundary conditions to the FE model has been given as three load steps. Prior to the first load step the model has been given a temperature loading of 20 °C. In the first load step (for 5s), rotating specimen has been given an angular velocity of 157 rad/S. The stationary specimen has been given an axial loading of 4000 N. A thermal loading of 1400 °C, which is near to the liqudus temperature of steel has been given at the welding interface.

In the second load step for 10s, angular velocity of the rotating work piece is removed and an additional forge force of 12000 N has been given to the stationary work piece. In the third load step, all the external load such as axial forces and thermal load has been removed, for 850s such that the temperature of the welded specimen to reach at 52 °C, to find the residual

stress (i.e the remaining stress existing in the specimen after removing these external loads is the residual stress). Figure 4.31 represents the overall procedure used for finding out the residual stress developed. The residual stress value obtained from the numerical analysis has

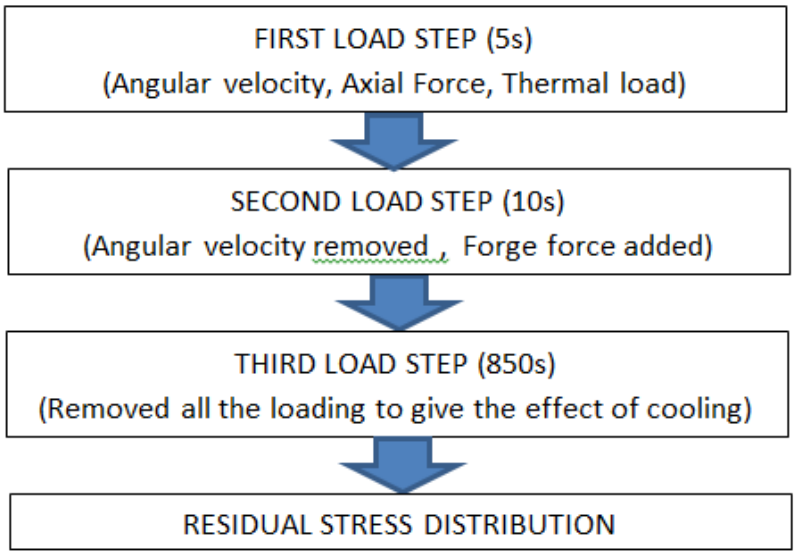

Figure 4.31: Flow chart - procedure to find out residual stress

been validated with the experimental residual stress value found by Reddy et al. (2005).

4.3.5 Results and Discussions

The results from the numerical studies to assess the residual stresses in friction welded joints are explained based on the contour plots and graphical plots. They are explained in the following paragraphs.

4.3.5.1 Temperature distributions in various loadsteps

The interface temperature is assumed as 1400 °C which is the approximate liquidus temperature of the steel. In the third load step, all the external load such as axial forces and thermal load have been removed, for 850s such that the temperature of the welded specimen to reach at 52°C, to find the residual stress. The remaining stress existing in the specimen after removing these external loads is the residual stress. Figure 4.32 shows the temperature distribution on the model at the first load step. Figure 4.33 represents the graphical representation of the temperature distribution.

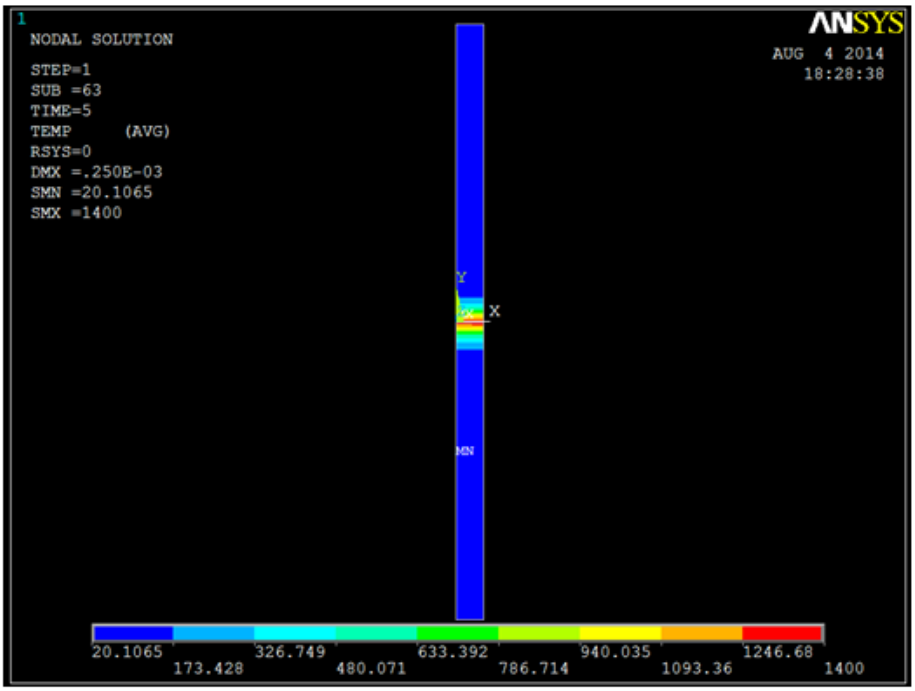

Figure 4.32: Contour plot-Temperature distribution

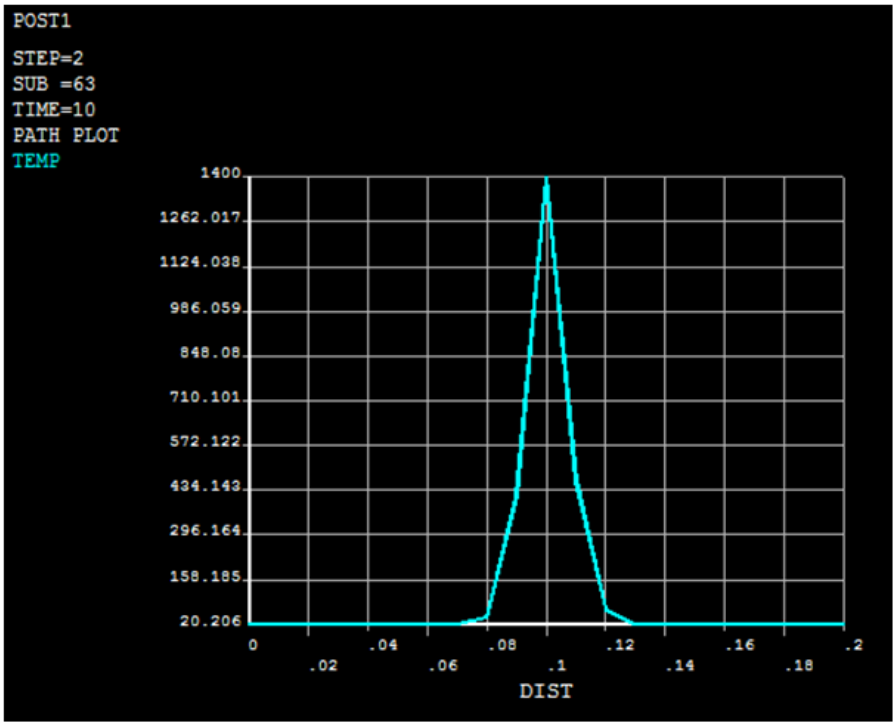

Figure 4.33: Graphical representation - temperature distribution

4.3.5.2 Displacement distributions

The maximum displacement value increases from $0.25 * 10^-3m$ to $0.354 * 10^-3m$ towards the end of the process which shows an increase in the displacement value at the constrained end of stationary specimen model from the initial stage to the final stage (at time=10s) of the process. Figure 4.34 and 4.35 show the displacement field distribution during initial (at time = 5s) and final stage (at time = 10s) respectively. The maximum value of displacement at the constrained

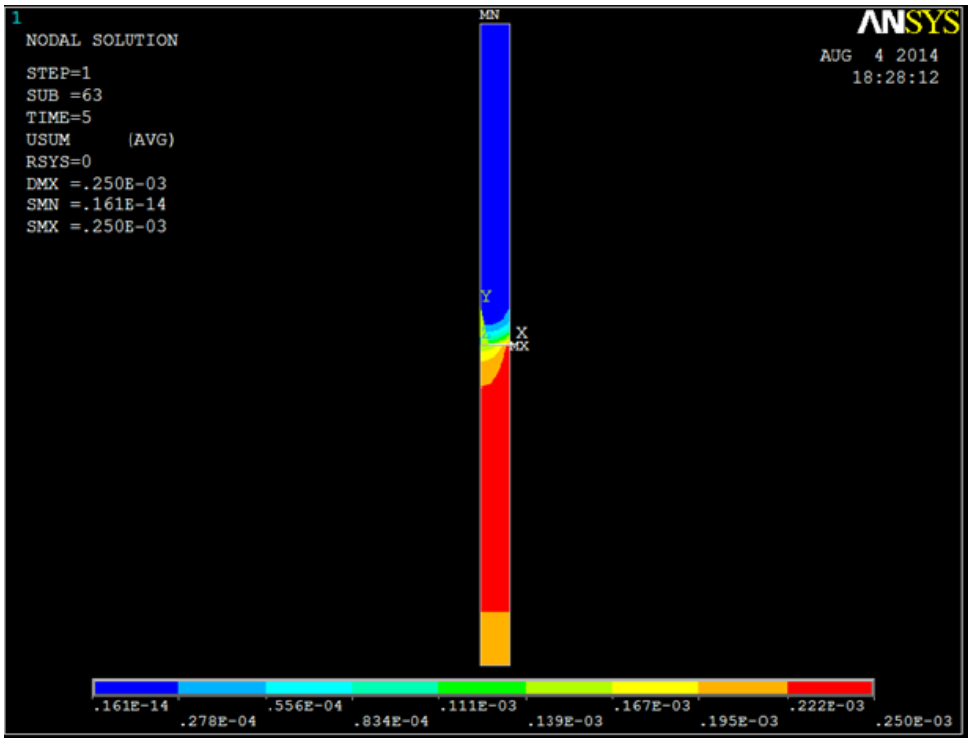

Figure 4.34: Displacement field distribution - initial stage

end of the stationary specimen caused by the application of forge force of 12000N at that end.

4.3.5.3 Von Mises stress distributions

The stress values at the initial stage are seen to be maximum on areas near the weld interface of austenitic 304 steel side with a value of $0.103 * 106^{10} N/m^2$. Towards the end of the process the stress has been found to be maximum on both sides of the contact region with a value of $0.255 * 10^{10} N/m^2$. At the initial stage as well as in the final stage, the minimum value of stress has been obtained away from the weld centre with a value of $0.251 * 10^7 N/m^2$ and $0.262 * 10^7 N/m^2$ respectively.(ref. Figure 4.36and 4.37). The relative motion caused by the rotation of the rotating specimen as well as the axial motion of the stationary specimen along

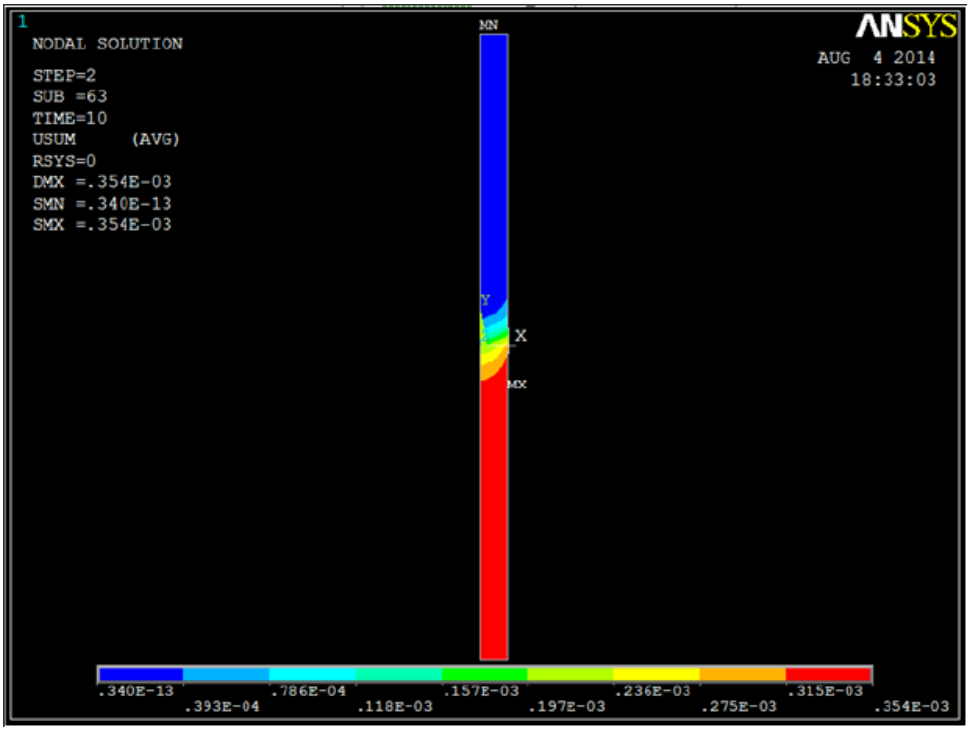

Figure 4.35: Displacement field distribution - final stage

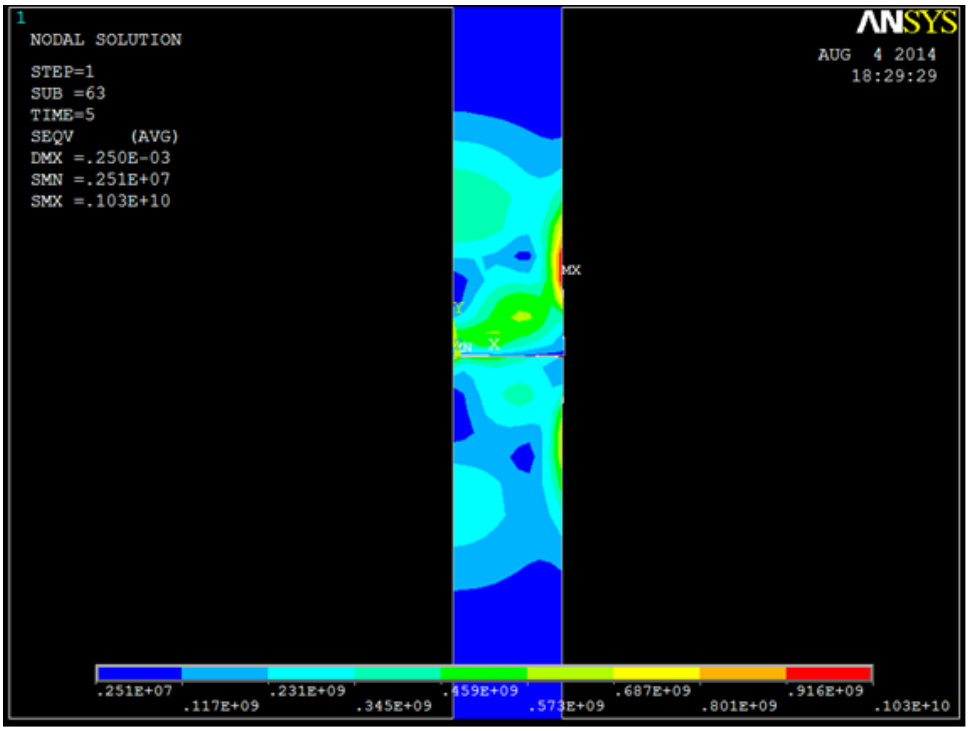

Figure 4.36: von Mises stress distribution - initial stages (at 5s)

with high temperature load at the contact interface resulted in stress concentrations on both sides of the contact interface towards the end of the process.

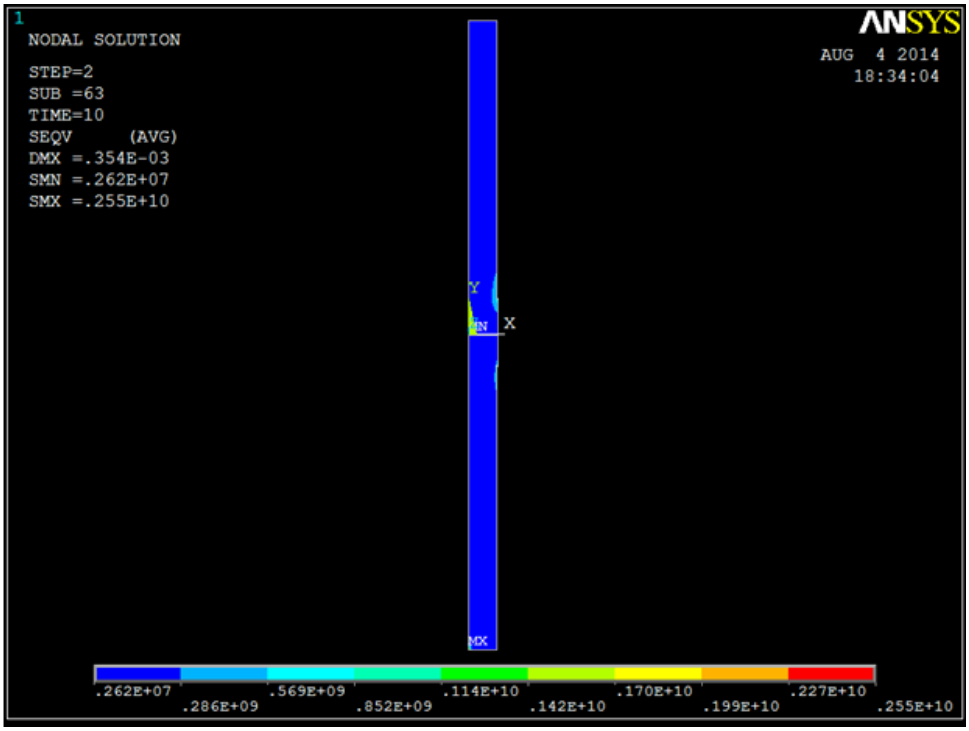

Figure 4.37: von Mises stress distribution-final stages (at 10s)

4.3.5.4 Strain distributions

At the initial stage as well as in the final stage, the minimum value of strain has been obtained with a value of $0.185 * 10^{-}4$ and $0.133 * 10^{-4}$ respectively.(ref Figure 4.38and 4.39). The relative motion caused by the rotation of the rotating specimen as well as axial movement of the stationary specimen along with plastic state of the material due to high temperature resulted in development of the high strain value at the initial stages. Upsetting action caused by the application of the high forge force also contributed to the development of high strain value at the outer surface of the contact region.

4.3.5.5 Residual (Von Mises) stress distributions

As already mentioned, residual stresses are the stresses that remain in a solid material after the original cause of the stresses has been removed. In the numerical modelling procedure, the external loads has been removed after the welding process and the temperature has been decreased near to the room temperature of 52^0C. Figure 4.40 represents the temperature distribution after third load step in the FE model. Figure 4.41 represents the temperature variation in the whole process. The displacement distributions of the welded specimen at third load steps are given in the Figure 4.42. From the figure, it is noticed that a shrinking effect is occurring

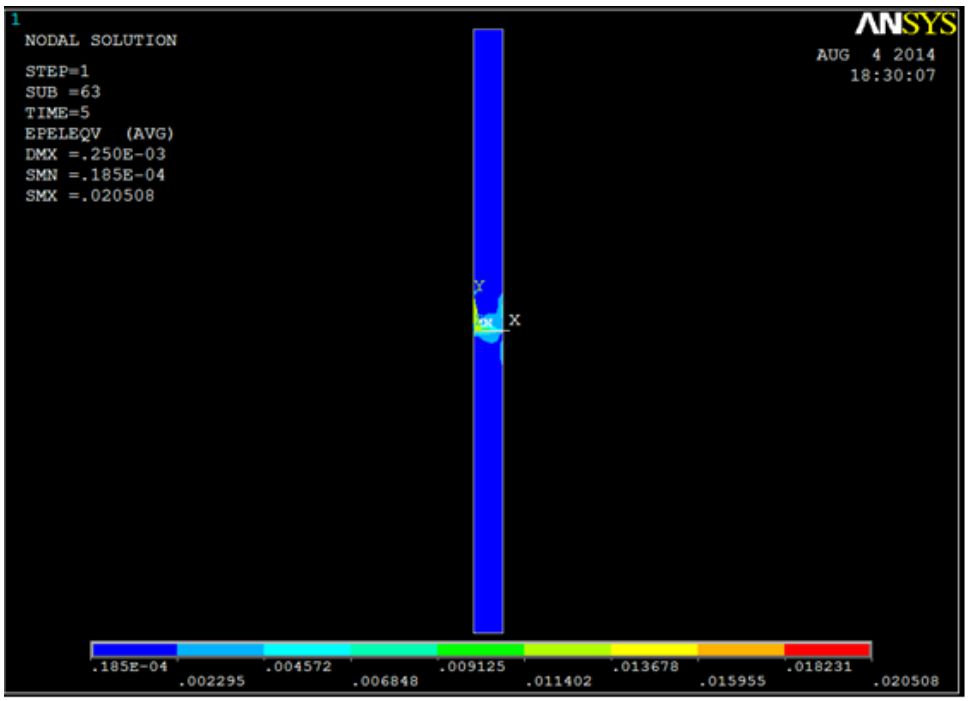

Figure 4.38: Strain distribution at initial stages (5s)

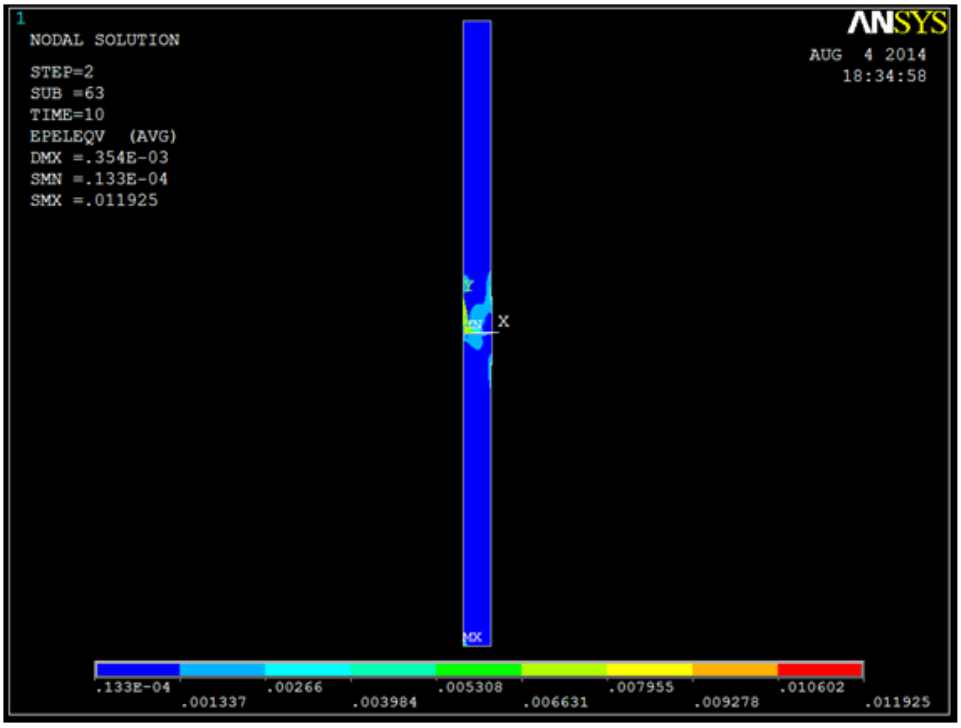

Figure 4.39: Strain distribution at final stages (10s)

towards the outer weld region during this load step. This is due to the cooling at this stage. The maximum stress value of 760 MPa has been seen during the first load step (at time = 5s). After the external load was removed such as axial forces, thermal loads for 850 s, the maxi-

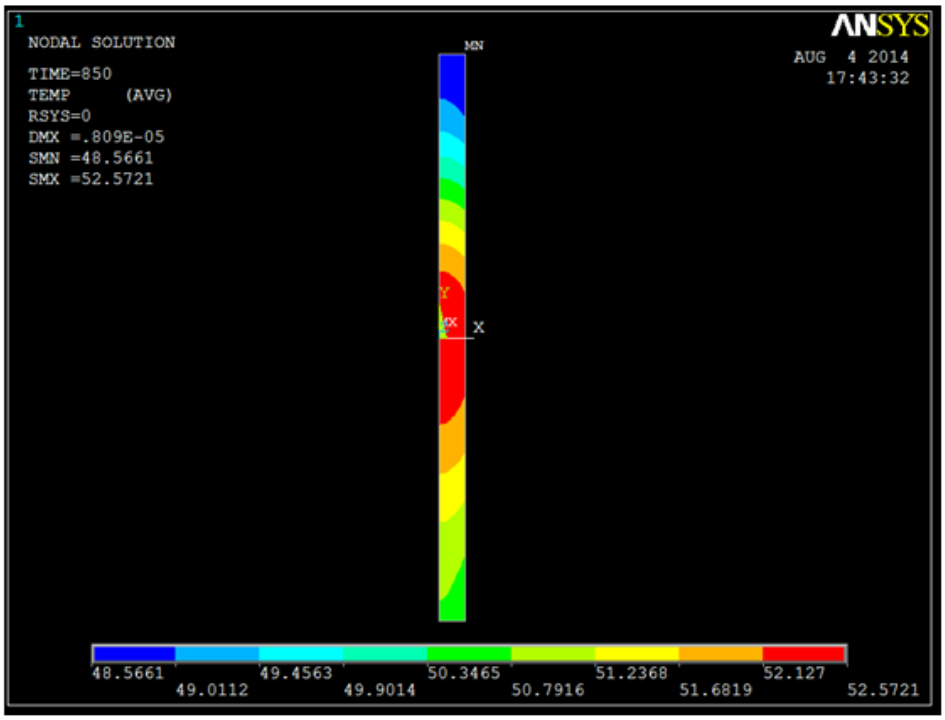

Figure 4.40: Temperature distribution after 3rd load step in the FE model

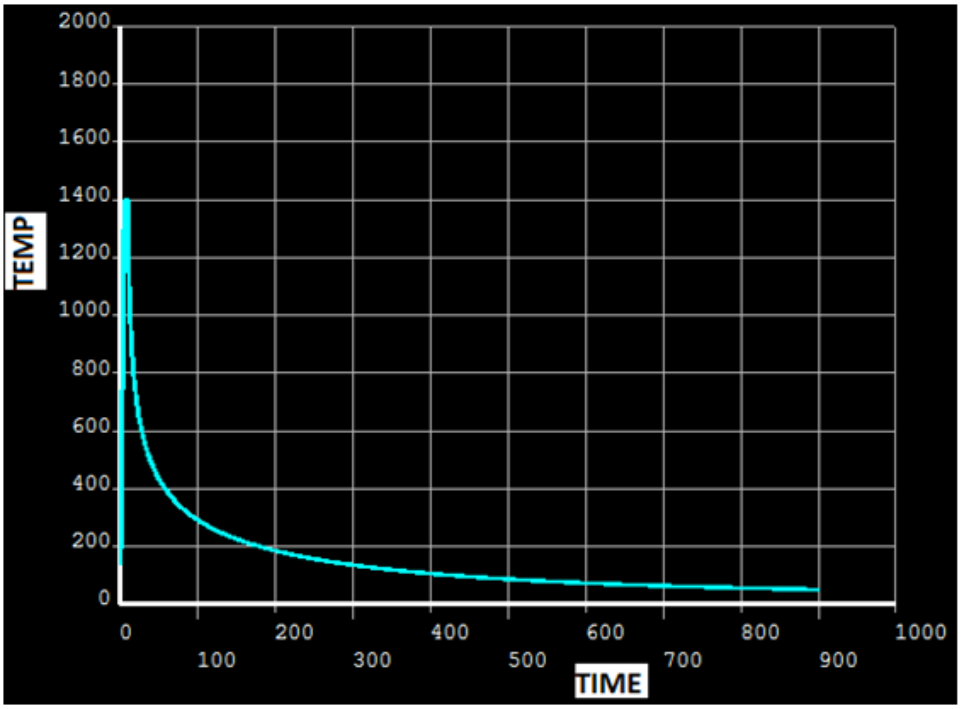

Figure 4.41: Temperature variation over the whole process

mum residual stress value of 192 MPa obtained at the AISI 304 austenitic stainless steel side compared to residual stress value of 225 MPa found in the reference journal paper. Figure 4.43 represents the residual stress distribution resulted in the FE model.

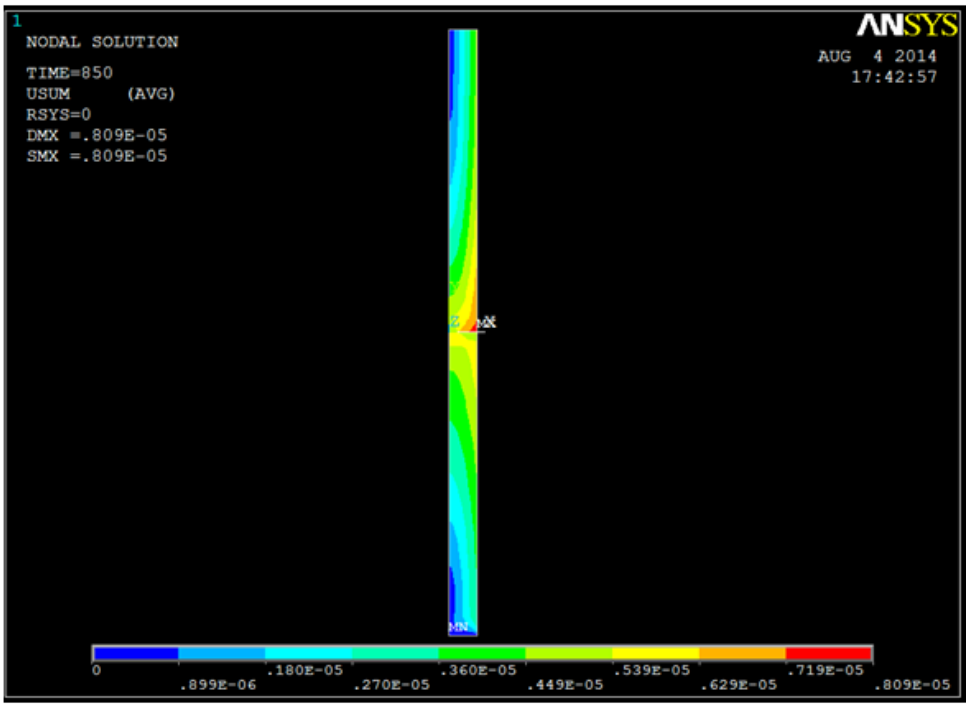

Figure 4.42: Displacement distribution at third loadstep

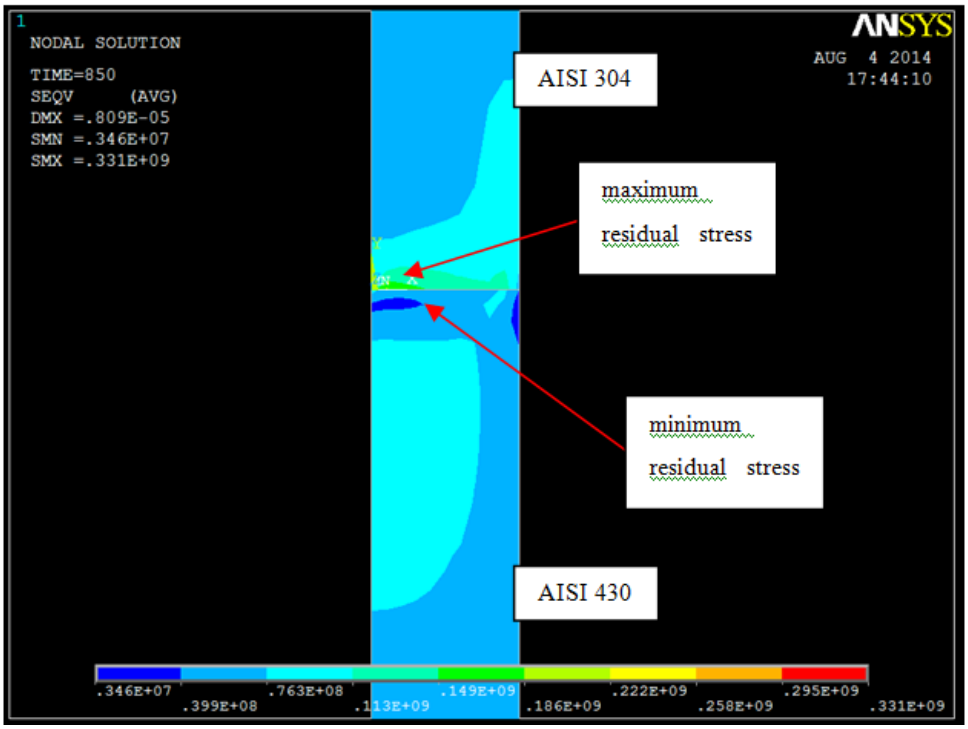

Figure 4.43: Residual stress distribution after the cooling process

4.3.5.6 Validation of results

The residual stress found has been validated with the experimentally found value by Reddy et al. (2005). Figure 4.44 is the graphical representation for the comparison of numerically obtained result and the experimentally found result. Figure 4.45 represents the residual stress distribution at the joint. The maximum residual stress value obtained through the numerical

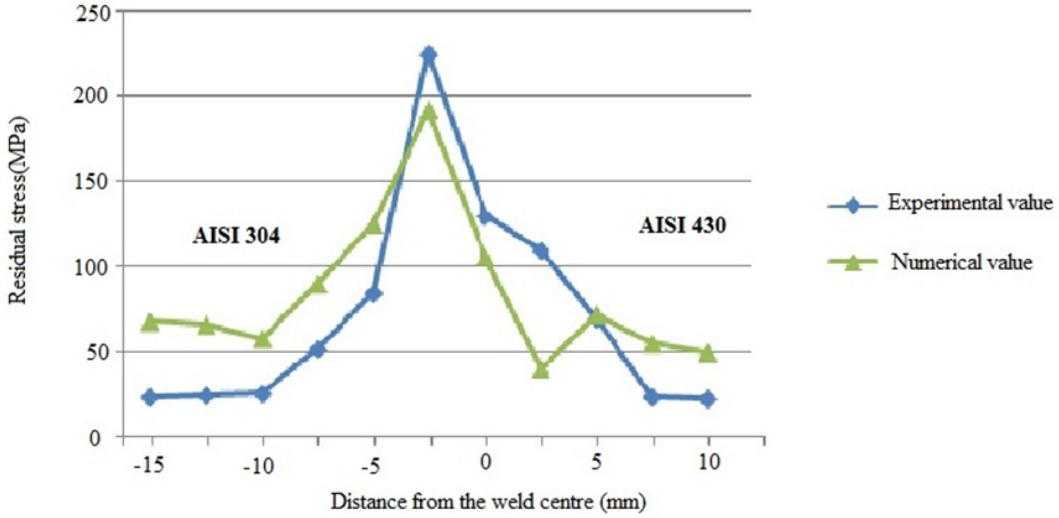

Figure 4.44: Validation of residual stress distribution

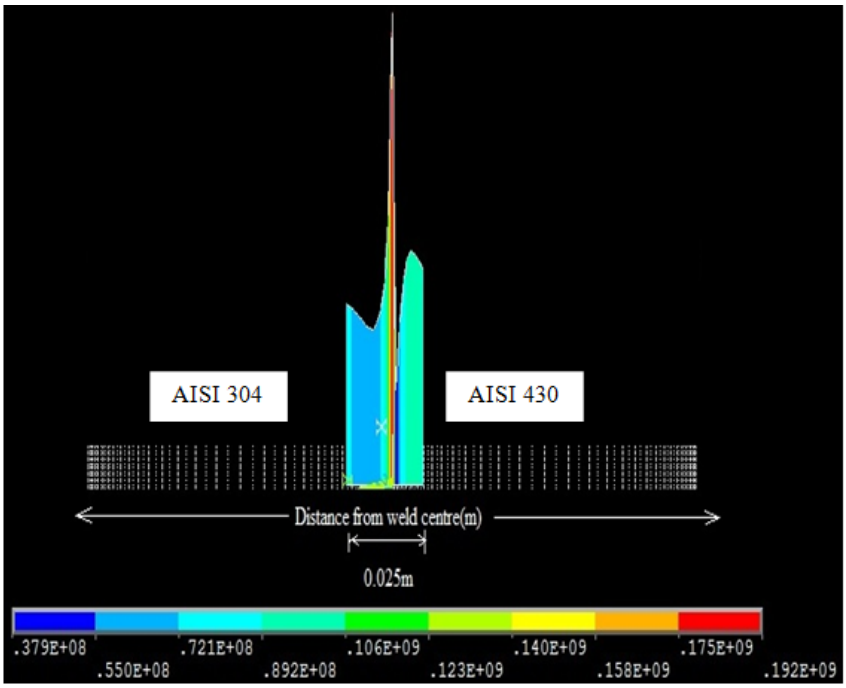

Figure 4.45: Residual stress distribution at the joint

modelling is 192 MPa (at the AISI 304 austenitic steel side of the interface) compared to the

experimentally found residual stress of 225 MPa from the same friction welding process parameters. Thus, an effective numerical modelling procedure has been implemented to assess the residual stress developed during friction welding process. If this modelling procedure has been incorporated with mathematical techniques to represent all type of heat transfer in all the load steps, it would have been more effective and more close to the experimentally found values. However to understand the basic ideas on the influence of process parameters on the temperature development, stress distribution, strain etc in a friction welded specimen during FW process, these procedures are found very effective.

A numerical procedure to determine temperature distribution, in specimen used for FSW has been realized through the numerical investigations on FSW. Foe the numerical modelling of FSW, the material considered was Al6061-T6 alloy, instead of the material used for the present experimental investigations. This is because another numerical model proposed byHamilton et al. (2008) was available in literature. Hence temperature dependent material properties was available for the numerical modelling. In addition, the present experimental studies on FSW was focussed on the comparative study on tensile characteristics of FSW joints with the CW joints. Hence attempt to measure temperature distribution during FSW process has not been carried out. Hence, materials used in the literature has been used for the numerical modelling of FSW.

In the case of numerical modelling on FW also, the material used for the experimental studies has not been used for the numerical modelling. This is because, the experimental investigations are mainly focussed on the influence of interface geometries in the strength characteristics of FW joints. Hence temperature measurements and stress measurement st ups has not been provided during the experimental studies. However temperature measurements at during weld formation, using IR thermometer has been utilized in the preliminary studies. But it was not much effective. Hence experimental studies from literature has been used for the validation of numerical studies on FW. Hence, material used in literature for experimental studies has to be considered for the numerical investigations.

From all these studies, effective procedures for the numerical modelling of FSW and FW has been realized.

Chapter 5

SUMMARY AND CONCLUSIONS

The experimental and numerical investigations carried out on FSW and FW in the present study have been summarized and given below along with the major conclusions drawn from that. The scope of the future investigations and significant contributions made through this research have also been given.

5.1 Summary

Experimental investigations on FSW have been initiated with the development of FSW setup, capable of providing maximum tool rotation of 2000 rpm and maximum tool traverse of 130 mm/minute, in a conventional vertical milling machine. Friction stir welded joints of AA2219 alloy have been produced using this setup. The experiments on FSW has been conducted as per Taguchi analysis and the optimum process parameters found are tool rotation of 1800 rpm and tool traverse of 100 mm/minute. The tensile and microstructure characteristics of friction stir welded joints have been compared with the joints produced with conventional welding techniques (ACSQW TIG and DCSP TIG welding techniques). Experimental investigations on FW have been initiated with the development of FW setup from a conventional medium duty lathe. Friction welded joints of Al 6061 Aluminium alloys have been made using the FW setup. Taguchi orthogonal arrays have been used to fix the number of experiment. Special attention has been made to find out the influence of various interface geometry in the mechanical characteristics of friction welded joints. Grey relational analysis has been used for the ranking of process parameter combinations and ANOVA has been used to find the percentage contribution of each process parameter in the response characteristics. It is found that Taper-Taper interface geometry has got significant influence on mechanical characteristics of friction welded joints.

Hence, experimental investigations have further extended to find out the most influencing taper angle in the mechanical and micro structure characteristics of friction welded joints.

Thermal modelling of FSW in Al6061- T6 Aluminium alloys has been carried out based on the FE procedures to find out the temperature distribution in weld specimen. The predicted temperature has been validated with those available in literature. Thermal modelling of FW process using AISI 316 Alloys has been carried out by FE procedures to find out the distribution of temperature, stress, strain in a weld specimen. The scope of the FE procedures has been extended to predict residual stress developed in dissimilar friction welded joints formed with AISI 304 and AISI 430 steel alloys. The residual stress predicted has been validated with the findings available in literature.

5.2 Conclusions

The major conclusions derived based on the experimental and numerical investigations in this research work on FSW and FW are as follows.

- A conventional vertical milling machine has been converted in to FSW setup and friction welded joints of AA2219 alloy have been produced. Based on the tensile characteristics studies, it is found that friction welded joints have possessed higher tensile strength than conventionally welded joints by ACSQW TIG and DCSP TIG welding techniques. From the microstructure studies, it is also found that friction welded joints have not exhibited clear distinct phase changes in WZ, HAZ and parent metal region compared to conventionally welded joints. This is a strong indication of effective joints with less stress concentration and comparatively similar microstructure with the parent metal. Hence from the experimental investigations on FSW it is concluded that FSW is an effective joining technique for low weight and high strength material like Aluminium alloys.
- A conventional medium duty lathe has been converted into FW setup and produced friction welded joints of Al6061 alloys. Based on the experimental investigations using Taguchi analysis, Grey relational analysis and ANOVA it is found that interface surface geometry is also influencing the strength characteristics of friction welded joints, almost similar to other process parameters like speed of rotating specimen and axial loading on stationary specimen. It is also found that, friction welded joints formed with suitable interface taper angle can achieve desired strength characteristics with respect to the required industrial application. The microstructure characteristic studies also support these findings. Hence from the experimental investigations on FW, it can be concluded that

high quality friction welded joint can be produced with medium speed for the rotating specimen and suitable modifications in the interface geometry.

- The finite element procedure formulated for the thermal modelling of FSW has been found effective by validating the results with that reported in literature. Based on these studies on FSW, it has been concluded that the same procedure can be extended to find out the temperature distribution in joints of other alloys subjected to FSW.
- The FE procedure for thermal modelling with the capability of estimating residual stress in dissimilar friction welded joint has been implemented. It has been concluded that, the numerical procedure developed for the present study can be used to evaluate residual stress in friction welded joint formed with other similar or dissimilar alloys.

5.3 Significant Contributions

The significant contributions made through this thesis are as follows

- A conventional vertical milling machine has been converted into a Friction Stir Welding setup. Welded joints of mechanical and microstructure characteristics comparable with that of the parent metal (AA2219) have been produced.
- A conventional medium duty lathe has been converted into a Friction Welding setup. Friction welded joints with optimized FW process parameters with special reference to the interface surface geometry have been produced. Friction welded joints produced with medium speed and Taper-Taper interface geometry have possessed better mechanical and microstructure characteristics. Besides, adequate taper angle can produce friction welded joint with desirable mechanical characteristics according to the industrial application.
- FE procedure for the thermal modelling of FSW has been validated with the the temperature distribution, reported using NX-5 software package in literature.
- The FE procedure used to evaluate the residual stress in dissimilar friction welded joint has been validated with the experimental results reported in literature.

5.4 Scope for Future Studies

FSW and FW setup with fully automatic process parameters monitoring system is a great challenge in the field of experimental studies. In addition to that, other statistical tool like Response Surface Methodology (RSM), Factorial designs etc. can also be utilized for optimizing process parameters. Software packages based on DOE procedures have much scope in optimising process parameters. The scope of optimizing major process parameters along with other interface geometry details can also be made for further investigations. In addition, the state of specimen (whether rotating or stationary) can also be considered for extended studies. In the case of numerical modelling, use of suitable governing equations representing actual heat flux in FW and FSW in consideration with actual boundary conditions give the scope for producing more accurate results.

Appendix A

Comparison of joints by FW and CW

Welding of high strength and low weight materials like aluminium alloys without any defects by conventional welding techniques is a major challenge in industries. Hence research on solid state welding techniques like FSW and FW have got much importance in joining of aluminium alloys. However most of the industries are not changing conventional techniques as skilled workers are available on that area. Most common conventional welding techniques used for the joining of aluminium alloys are Gas welding and Arc welding by giving too much care on controlling welding parameters. In this phase comparative study on tensile and micro structural characteristics of conventionally welded aluminium joints with FW joints has been carried out. The process parameters considered for these are presented in Table A.1. Microstructural studies were also carried out.

Table A.1: Process Parameters of various welding techniques considered

Arc Welding	Gas welding	Friction welding
Current Type : DC polarity :reverse polarity Temperature :3200C Amperage :50-70Amp Electrode :As4043	Gas type : Oxy acetylene Rod Diameter :2.3mm Type of flame :Neutral flame Filler rod diameter:3mm	Speed : 500rpm Forge Pressure : 3MPa Upset pressure : 5MPa Specimen diameter: 20mm

A.1 Tensile Characteristics Studies

For each welding processes (Arc welding, Gas welding and Friction welding) 6 joints have been taken, out of which best three have been selected for tensile characteristic studies. The values obtained are shown in Table A.2. It is seen that maximum load bearing capacity is found to be

Table A.2: Comparison of Tensile test results of FW joints

Type of joint	Maximum Load(kN)	Breaking Load (kN)	Percentage Elongation
Parent metal	27.849	25.14	22
Electric Arc welded	14.3	13.80	3.2
Gas welded	11.18	11.02	1.4
Friction welded	15.06	18.13	6.2

more in the case of friction welded joints compared to the parent metal. But breaking load was found higher for Arc welded joints. This may be due to the phase change occurred at the welded region of the Arc welded joint. Figure A.1 represents the comparison of percentage variation in maximum load for friction welded and conventional welded joints with the parent metal. Figure

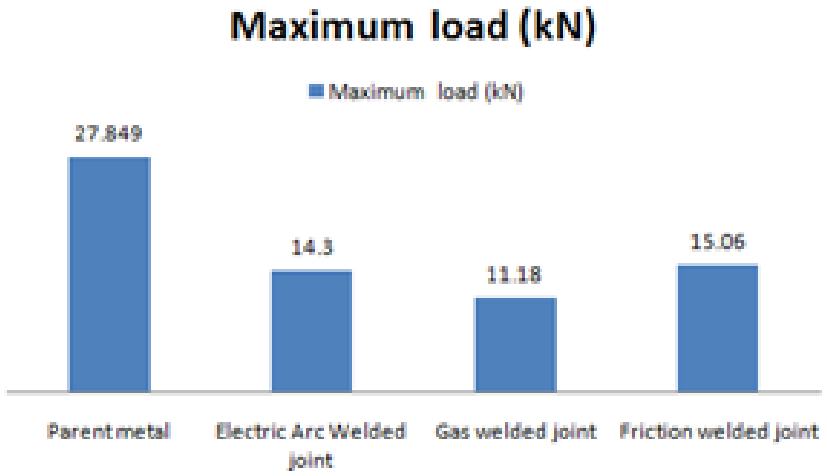

Figure A.1: Percentage variation in maximum load

A.2 represents the comparison of percentage variation in breaking load for friction welded and conventional welded joints with the parent metal. Comparison of percentage elongation for the friction welded and conventional welded joints with parent metal is shown in Figure A.3. It is seen that friction welded joints posses 3 times the percentage elongation compared with the parent metal. This may be due to the correct bonding between the material particles while friction welding, without disturbing the original properties of the parent metal.

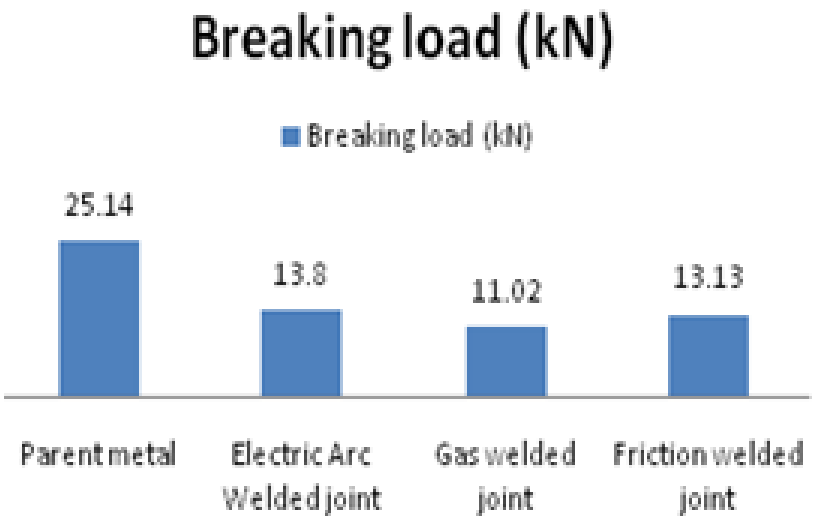

Figure A.2: Percentage variation in breaking load

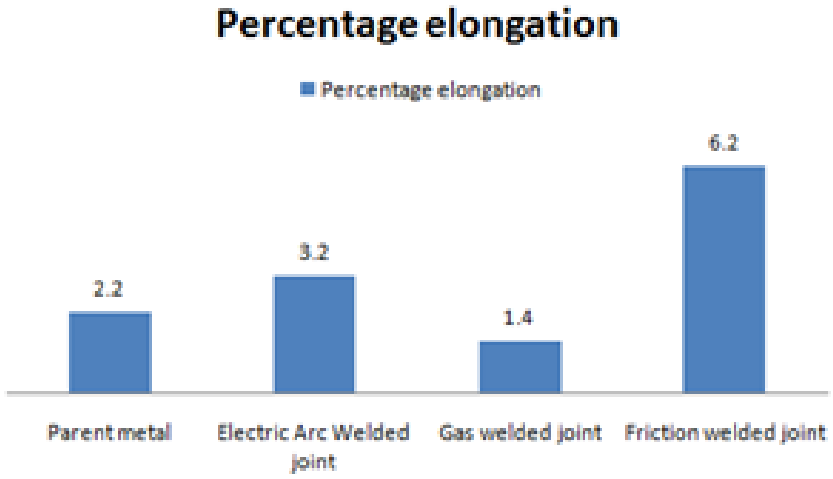

Figure A.3: Percentage elongation of friction welded and CW joints

A.2 Microstructure Studies

Figure A.4indicates the microstructure details at the weld zone of arc and gas welded joint. Figure A.5 indicates the micro-structure at weld zone of friction welded joint and microstructure of parent metal. Optical microscopic views of the parent metal shows dendritic structure with dispersion of SiC particle. In the case of conventionally welded joints, all the regions were clearly visualized, especially for arc welded joints. The fusion zone of arc welded joints can be clearly distinct from the parent metal. It may be due to the sudden heating and cooling of joining portion with the addition of filler material. It is also clear that this black eutectic region is filled with significant amount of Al and Si since the filler As4043 contained abundant

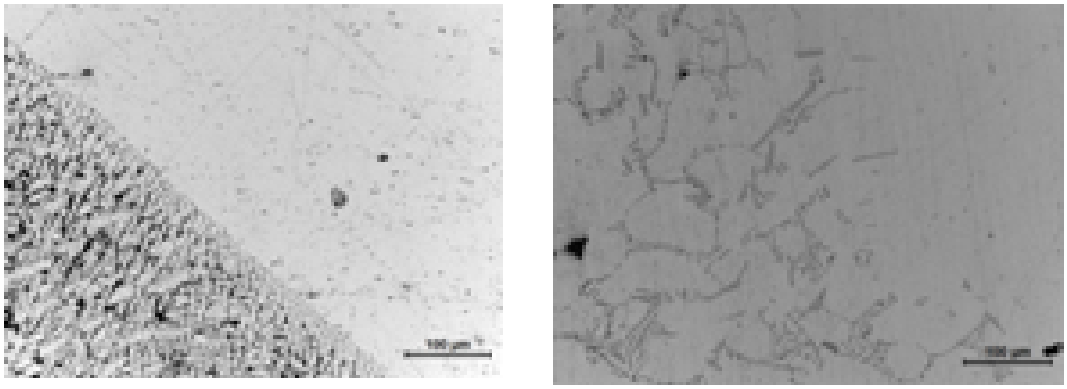

Figure A.4: Microstructure-WZ of arc and gas welded joints

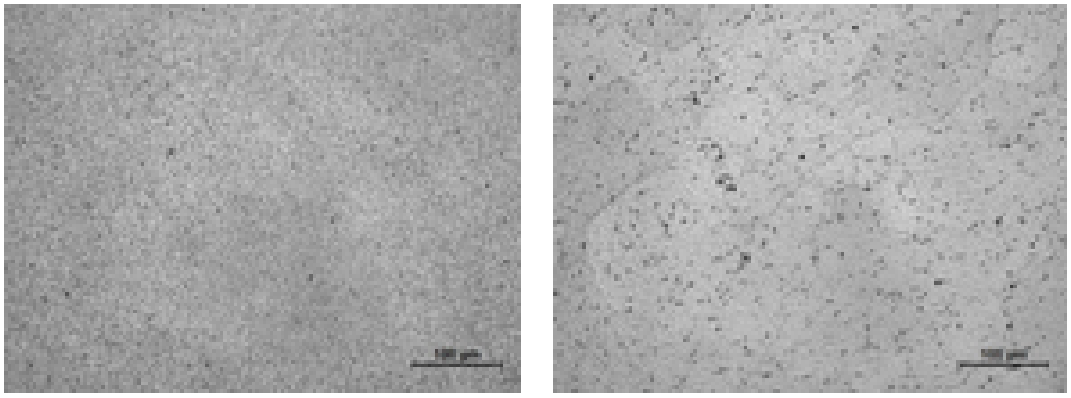

Figure A.5: Microstructure- WZ of FW joint and base metal

Si particles. In the case of Gas welded joint also, the heat affected zone and fusion zone are clearly visible. In the fusion zone dentritic structure seen as compressed and dispersed manner. Near to the thermo- mechanically affected zone and fusion zone, it is seen that large extension for dentritic structure has been occurred. In both cases, residual stresses may be presented at the weld region.

In the case of friction welded joints, it is found that both welded region as well as parent metal region are having almost similar grain structure. However weld region possessed with denser grain structure compared to parent metal. It is also seen that grains are equiaxed at the welded region. This may be due to the dynamic recrystallization occurred during friction welding process and that may be the main reason for keeping almost similar characteristics of friction welded joint with that of parent metal.

Thus from the micro-structure studies also, it is cleared that friction welding is more suitable for the joining of aluminium alloy rods as the microstructure of joints resembles almost like in the parent metal. Following points have been concluded from this studies.

- FW process has been found effective for the joining of Aluminium rods even though initial setting time is more compared to the conventional welding processes.
- Irregular surface has been observed in the conventionally welded joints. This may be due to the sudden heating and cooling occurred. In addition, as the material is aluminium alloy in order to with stand the high fusion temperature, intervals had to be given during welding process .In the case of friction welded joints, the weld region are seen uniform.
- FW has been occurred at plasticized stage followed with grain transfer instead of phase changes as in conventional welding processes.
- The friction weld region was found harder compared to the parent metal region, but lesser than conventional welded joints has.
- From tensile characteristic studies, it is seen that the friction welded joint are strong compared to the parent metal. Percentage variation of maximum load carrying capacity for Arc, Gas and FW joints were 48.7%, 60% and 45.9% respectively. But breaking load value has been found less for friction welded joints, may be due to the loosening of the grains when loading beyond the maximum load bearing capability of the joint.
- Micro structural photographs of conventionally welded joints exhibited clear distinct zones of various weld regions. In the case of friction welded joints, it showed comparable features both in parent metal and welded region. Geometry of particles are also seen almost same.

The aforementioned points revealed the suitability of FW techniques for the effective joining of aluminium alloys compared to the conventional welding techniques.

Appendix B

Steps in the Numerical Modelling

Various stages involved in the numerical modelling of FSW process using Comsol multiphysics software package and FW using ANSYS are as follows

B.1 Friction Stir Welding

1. specifying file name: Open Comsole -File - save as - (file name)
2. Specifying type of problem: Model wizard button- 3D-next-Add Physics-Heat transfer in solids- next- select study type-preset studies-stationary-finish
3. Define Global definitions: Global definitions-Right click-parameters - a table as shown in Table 4.1 will come - refer the table and input all the parameters
4. Specifying temperature dependent material properties: Global definitions-right click-Funtions-interpolation-Data source (Table)- Function name- Ybar-Fill the table by referring Table 4.3-click plot option (A graph will be generated)
5. Specifying range of steps: Global definitions - right click-step- smoothing-size transition zone-type 5
6. Modelling of FSW specimen, Tool shoulder and Tool pin: Model builder-Geometry 1-unit section-Length -mm -Geometry- right click-block-block 1-width = 320, depth = 102, height = 12.7- position-x= -160-build selected-geometry-right click-block-block2-size section-width =420, depth=102,height =12.7, x=-210-build selected Geometry-right

click-cylinder-cylinder 1-size and shape-radius=$r_{shoulder}$-height = 12.7 Geometry-rightclick-cylinder-cylinder2-radius=r_{pin}, height =12.7-buld selected Geometry-right click-block-block3-width = 2 * $r_{shoulder}$, depth = $r_{shoulder}$, height = 12.7, x= $-r_{shoulder}$, y=$-r_{shoulder}$ - build selected Geometry-right click-boolean operation-difference-select objects cyl1 and cyl 2-object to subtract-select block 3-form union-build selected- A 3D model as shown in Figure 4.1 will be created.

7. Definition of variables: Model builder definitions-right click-variables-variable 1-geometric entity level-boundary-select boundary 14 only- Model builder - definitions-right click-variables-variable 2-geometric entity level-boundary-select boundary 15 and 19 only-enter the data presented in Table 4.4

8. initial settings of Temperature for FSW process modelling: Heat Transfer in solids-Initial Values- T= T_0

9. initial settings for translation motion: Heat Transfer in solid1-right click-translation motion-specify u_trans vector as $-u_{weld}$,x, 0-y,0-z

10. specifying infinite element domain: Definitions-right click-infinite element domain-select 1 and 5 only

11. specifying surface to ambient radiation: Heat transfer in solids-right click-surface to ambient radiation-select
boundaries-3,4,8,9,13,25,26(i.e outside the tool shoulder)-surface to ambient radiation-user defined-type epsilon-Ambient temperature-T_0

12. specifying out flow: Heat transfer in solids-right click-out flow-outflow1-select boundary1 only-

13. specifying heat flux , boundary heat sources and Temperature: Heat transfer in solids-heatflux-heatflux1-select boundaries-3,8,13 and 25 only-heat transfer coefficient-$h_{downside}$-$T_exT = T_0$- Heat transfer in solids-heatflux-heatflux2-select boundaries-4,9,26-heat transfer coefficient-h_{upside}- $T_{ext} = T_0$- Heat transfer in solids-heatflux-heatflux3-select boundaries-14 only heat t transfer coefficient-h_{upside}- $T_exT = T_0$-in the q_0 edit field type $q_{shoulder}$ Heat transfer in solids- right click-boundary heat sources-select boundaries- 15 and 19 only-$q_b = Q_{pin}$ Heat transfer in solids-right click-temperature-select 28-$T = T_0$

14. specifying materials for specimen and FSW Tool: Material - right click-open material browser-builtin-Aluminium-right click-add material model -material -right click-open

material browser-built in -steel AISI 4340-right click-add material model-select domain 4 only-give the data to the table as shown in Table 4.2

15. specifying meshing: Model builder-MESH-mesh 1-right click-more option-Free Quad-select boundaries 4,9 and 26 only-size- predefined-extremely fine-click build all button-mesh1-right click-more option-free triangular-select boundaries-14 and 18 only -mesh 1-right click-swept 1-right click -distribution 1-number of element=2,click build all (1882 elements)

16. solution: study 1 - right click-solver configuration-solver 1-right click-stationary solver1-right click-enable-compute all

17. result: Temperature-Isothermal contours-isosurface 1-isosurface setting window-levels-entry method list-levels-type range-300 20 980 - coloring style section - clear color legend-model builder window-results-isothermal contours-arrow volume 1-disable-isothermal contours-slice-slice setting window-plain data-plane-xy plane-entry method list- co ordiantes-z- coordinate-coloring and style-color table-thermal light-3d plot group-plot

By executing these steps, the temperature distribution in the FSW specimen can be noted .

B.2 Friction Welding

1. specifying file name: File-change directory-select a folder (newely created one)-ok -file-change title-enter new title-"rfw"- ok

2. Specify problem type: Main menu-preference-structural-thermal-ok

3. Specifying element type: Main menu- preprocessor-element type-add-plane 42-(solid quad 4 node 42)-options-element behaviour k3-axisymmetric- ok

4. adding contact elements (target and contact): Add-contact-2D target 169 -options-element degree of freedom k4-select-UX,UY and ROTZ-ok-add-contact-2nd surf 171-options-element degree of freedom K1-select UX,UY,TEMP-OK

5. Specifying material properties: Main menu-preprocessor-material properties-material models-structural-linear elastic-isotropic-temperature dependent material properties (youngs modulus,poisson's ratio,density,friction coefficient) -use add temp to add more columns-graph-ok

6. specify thermal properties: thermal-conductivity-isotropic-specific heat-enthalpy-ok

7. Creation of 2D axi-symmetrical model: Main menu-preprocessor-modelling-create-areas-rectangle by two corners-WPX=0,WPY=0,width=0.015,height=.1 (upper rectangle)-WPX=0, WPY=0,width = .015,height- -0.1

8. To mesh the model: Main menu-preprocessor-meshing-mesh tool-element attribute-global-size controls-global-set-size element edge length = .002- ok-mesh-areas-mesh-select areas-apply-ok (see Figure 4.10)

9. Creation of contact pair: Contact Manager-contact wizard-target surface-nodes-pick target-box-select bottom nodes of top rectangle-ok-pick contact-box-select upper nodes of bottom rectangle-coefficient of friction=0.3-create contact pair(see4.13)

10. Application of boundary conditions-displacement: Main menu-solution-define loads-apply-structural-displacement-on nodes-box-select upper nodes of top rectangle-put UY= 0-apply-ok-similarly select bottom nodes of bottom rectangle-put-UY=0-apply-ok-select-entities-areas-by num/pick-from full-apply-select top area-apply-ok-plot-area (only top area come visible)

11. Application of boundary conditions-forces -angular velocity: Main menu-solution-define loads-apply-structural-inertia-angular velocity-global-OMEGY Global cartesian Y-comp = 125.66 (i.e 125.66rad/sec) -select every thing-plot-replot (both areas come visible)

12. Application of boundary conditions-forces - axial loading on stationary specimen: Main menu-solution-define loads-apply-structural-pressure-on lines-select bottom line of bottom area-apply-load PRES value = 100e6 (i.e 100MPa)-ok (see .Figure 4.14 and Figure4.15)

13. Defining analysis type: Main menu-solution-analysis type-solution controls-Basic analysis option-large displacement-static-automatic time stepping is on-number of sub step = 10- max no of substep = 1000 - min no of sub step = 1- frequency - write every sub step - solution options-write every nth substep-ok

14. Processing: Main menu- solution-solve-current ls

15. Post processing- to obtain contour plots on stress and strain: Main menu-general post processor-plot results-contour plots-nodal solution-stress-Von mises stress-ok-total mechanical strain-Vonmises total mechanical strain-ok (see Figure 4.17 to 4.23).

16. To plot responses at a point with respect to time through out the process (see Figure 4.24 to Figure 4.29): Main menu-time hist post pro-add data-add Vonmises stress-select outer most node on contact area-Graph (Can be obtained for strain,contact penetration,contact friction stress, X and Y component of displacement, contact sliding distance etc.)

The same procedure can be extended to model dissimilar friction welding and residual stress evaluation as per the procedure shown in the Figure 4.31

To validate the numerical model, the problem of FW process has been analysed in a manner similar to the case of a rotating shaft. The shaft is of 75 mm diameter, 0.5m span, rotating at 200 rpm and transmitting a power of 35 kW. It is subjected to an axial compressive end load of 80 kN. The shaft material possesses Youngs modulus of 210 GPa, Poisson's ratio of 0.3 and density of 7800 Kg/m^3.

This problem has been solved using FE procedure in Ansys by creating an axisymmetric model and meshed using PLANE 42 elements. The axisymmetric model constrained at one end by arresting all other degrees of freedom except rotation about its own axis. An angular velocity of 20.94 rad/s corresponding to 200 rpm has been given about the Y axis. At the other end, an axial load of 18.1 N/m^2 corresponding to 80 kN has been applied. The torque has been calculated from the equation, $P = 2\pi * N * T/60$ where P is the Power, N is the rotations per minute and T is the Torque. Shear stress is calculated using the equation $\tau = 16T/\pi d^3$ where d is the diameter of the shaft. The Von Mises stress (Equivalent stress) has been calculated using the equation $\sigma_e = (\sigma_x)^2 - \sigma_x\sigma_y + (\sigma y)^2 + 3\tau^2)1/2$. Thus a torque of 1671.13 Nm and shear stress of 20. 174 MPa are resulted respectively. It is also knew that $\sigma_x = (80*1000)/(\pi*(.075)2/4) = 8.1MPa$and $_y$ is equal to zero since there is no load in perpendicular direction. Thus, equation for von Mises stress (Equivalent stress) reduces to $((\sigma_x)^2 + 3\tau^2)1/2$. Then the von Mises stress (Equivalent stress) value became σ_e is 18108295.752 +3*20174173.452)1/2 = 39.36 MPa. It has been found out that the analytical and numerical results are almost similar. By analytical method, the value for the von Mises stress resulted is 39.36 MPa and by the numerical method, it is 34.50 MPa.

References

Al-Badour, Fadi, Nesar Merah, Abdelrahman shuaib, and Abdelaziz Bazoune (2013) "Coupled Eulerian Lagrangian finite element modeling of friction stir welding processes," *Journal of Materials Processing Technology*, Vol. 213, pp. 1433–1439.

Ambroziak, A., M. Korzeniowski, and P. Kustronb (2007) "Friction welding of dissimilar metal joints with intermediate layers," *Journal of Achievements in Materials and Manufacturing Engineering*, Vol. 21, pp. 37–40.

Assidi, Mohamed, Lionel Fourment, Simon Gurdoux, and Tracy Nelson (2010) "Friction Model for friction stir welding process simulation: Calibration from welding experiments," *International Journal of Machine Tools and Manufacture*, Vol. 50, pp. 143–155.

Barcellona, A., G. Buffa, and L.Fratini D. Palmeri (2006) "On micro structural phenomena occurring in friction stir welding of aluminium alloys," *Journal of Material Processing Technology*, Vol. 177, pp. 340–343.

Budau, Victor, Ion Mitelea, and Corneliu Craciunescu (2012) "Dissimilar friction welding of induction surface-hardened steels and thermochemically treated steels," *Journal of Materials Processing Technology*, Vol. 212, pp. 1892–1899.

Buffa.G, A.Ducato, and L.Fratini (2011) "Numerical procedure for residual stresses prediction in friction stir welding," *Finite Elements in Analysis and Design*, Vol. 47, pp. 470–476.

Cavaliere, P., A. De Santis, F. Panella, and Squillance P (2009) "Effect of anisotropy on fatigue properties of 2198 AI-Li plates joined by friction stir welding," *Engineering Failure Analysis*, Vol. 16, p. 1856 1865.

Cavaliere, P., A. Squillance, and F. Panella (2008) "Effect of welding parameters on mechanical and microstructural properties of AA6082 joints produced by friction stir welding," *Journal of Material Processing Technology*, Vol. 200, pp. 364–372.

Cavaliere, Pasquale (2013) "Friction stir welding of AI alloys: analysis of processing parameters affecting mechanical behavior," *Procedia CIRP*, Vol. 11, pp. 139–144.

Cavaliere.P, Squillance.A, Panella.F, and Campanile.G (2006a) "Effect of welding parameters on mechanical and microstructural properties of AA6056 joints produced by friction stir welding," *Journal of Material Processing Technology*, Vol. 180, pp. 263–270.

——— (2006b) "Mechanical and Microstructural behaviour of 2024-7075 aluminium alloy sheets joined by friction Stir Welding," *International journal of Machine Tools and Manufacture*, Vol. 45, pp. 588–594.

Ceretti.E, L. Fratini, C. Giardini, and D. La Spisa (2010) "Numerical modelling of the linear friction welding process," *International Journal of Metal Forming*, Vol. 3, pp. 1015–1018.

Ceschini, L., I Boromei, G. Minak, A.Morri, and F.Tarterini (2007) "Effect of friction stir welding on microstructure, tensile, fatigue properties of the AA7005/10 vol percentage Al2O3p Cotensite," *Composites Science and Technology*, Vol. 67, pp. 605–615.

Chen, C. M and R. Kovacevic (2013) "Finite element modelling of friction stir welding - thermal and thermomechanical analysis," *International Journal of Machine Tools and Manufacturing*, Vol. 43, pp. 1319–1326.

Deng, Xiaomin and Shaowen Xu (2004) "Two Dimensional Finite Element Simulation of Material Flow in the Friction Stir Welding Process of copper and steel bars," *Journal of Manufacturing Processes*, Vol. 6, pp. 125–133.

DUrso.G, C.Giardini, and T. Pastore S. Lorenzi (2014) "Fatigue crack growth in the welding nugget of FSW joints of a 6060 aluminium alloy," *Journal of Materials Processing Technology*.

Elangovan, K. and V. Balasubramanian (2008) "Influence of tool pin profile and welding speed on the formation of friction stir processing zone in AA2219 aluminium alloy," *Journal of Material Processing Technology*, Vol. 200, pp. 163–175.

Elatharasan, G. and V.S Senthil Kumar (2012) "Modelling and Optimization of friction stir welding parameters for dissimilar aluminium alloys using RSM," *Procedia Engineering*, Vol. 38, p. 3477 3481.

E.Massoni, S.J. Wall, and L. DAlvise (2002) "Finite element modelling of the inertia friction welding process between dissimilar materials," *Journal of Materials Processing Technology*, Vol. 125, pp. 387–391.

Ericsson.M and Sandstorm.R (2003) "Influence of welding speed on the fatigue of friction stir welds and comparison with MIG and TIG," *International Journal of Fatigue*, Vol. 25, pp. 1379–1387.

Galvao, I., D Verdera, D. Gesto, A. Loureiro, and D. M. Rodrigues (2013) "Influence of aluminium alloy type on dissimilar friction stir lap welding of aluminium to copper," *Journal of Materials Processing Technology*, Vol. 213, pp. 1920–1928.

GohariKia, M. and S.A Akbarimousavi (2011) "Investigations on the mechanical properties and microstructure of dissimilar cp-titanium and AISI 316L austentic stainless steel continuous friction welds," *Materials and Design*, Vol. 32, pp. 3066–3075.

Hamilton, C., A. Sommers, and S. Dymek (2008) "A Thermal Model of Friction stir welding in aluminum alloys," *International Journal of Machine Tools and Manufacture*, Vol. 48, pp. 1120–1130.

——— (2009) "A Thermal Model of Friction stir welding applied to Sc-modified Al-Zn-Mg-Cu alloy extrusions," *International Journal of Machine Tools and Manufacture*, Vol. 49, pp. 230–238.

Heurtier, P., M. J. Jones, C. Desrayaud, J. H. Driver, F. Montheillet, and D. Allehaux (2006) "Mechanical and thermal modeling of Friction Stir Welding," *Journal of Material Processing Technology*, Vol. 171, pp. 348–357.

Hwang, Y. M., P. L. Fan, and CH Lin (2010) "Experimental study on friction stir welding of copper metals," *Journal of Materials Processing Technology*, Vol. 210, pp. 1667–1672.

Hwang, Yeong-Maw, Zong-Wei Kang, and Yuang Cherng Chiou nd Hung-Hsiou Hsu (2008) "Experimental study on temperature distributions within the workpiece during friction stir welding of aluminium alloys," *International Journal of Machine Tools and Manufacture*, Vol. 48, pp. 778–787.

H.W.Zhang, Z. Zhang, and J.T. Chen (2007) "3D modeling of material flow in friction stir welding under different process parameters," *Journal of Material Processing Technology*, Vol. 183, pp. 62–70.

Inc, SPINWELD (2016) , URL: `http://www.spinweld.com/friction-welding/`.

Izani, Ahmad, Md. Ismail, Endri Rachman, and Hazman Seli Zainal Arifin (2010) "Mechanical evaluation and thermal modelling of friction welding of mild steel and aluminium," *Journal of Materials Processing Technology*, Vol. 210, pp. 1209–1216.

Jackuin, D., B.de Meester, A.Simar, D.Deloison, F.Montheillet, and C.Desrayaud (2011) "A simple Eulerian thermo-mechanical modelling of friction stir welding," *Journal of Materials Processing Technology*, Vol. 211, pp. 57–65.

Jau-WenLin, His-Cherng Chang, and Ming-Hsiu Wu (2013) "Comparison of mechanical properties of pure copper welded using friction stir welding and tungsten inert gas welding," *Journal of Manufacturing Processes*.

Kim, Dongun, Harsha Badarinarayan, Ji Hoon Kim, Chongmin Kim, Kazutaka Okamoto, R.H. Wagoner, and Kwansoo Chung (2010) "Numerical simulation of friction stir butt welding process for AA5083-H18 sheets," *European Journal of Mechanics A/Solids*, Vol. 29, pp. 204–215.

Kubiszyn, I. and A. Pietras (2003) "Numerical modelling of the friction-welding process," *Welding International*, Vol. 17, p. 425 430.

Lee, B Y, Y H Moon, J R Cho, and C J Van Tyne (2004) "Investigation of residual stress and post weld heat treatment of multipass welds by finite element method and experiments," *Journals of material processing technology*, Vol. 3, pp. 1690–1695.

Madhusudhan.G and Venkata Ramana.P (2012) "Role of nickel as an interlayer in dissimilar metal friction welding of maraging steel to low alloy steel," *Journal of Mater*, Vol. 212, pp. 66–77.

Mandal, S. and K. Williamson (2006) "A thermomechanical hot channel approach for friction stir welding," *Journal of Material Processing Technology*, Vol. 174, pp. 190–194.

Marzoli, L. M., A.V.Strombeck, J.F.Dos-Santos, C. Gambaro, and L.M. Volpone (2006) "Friction stir welding of an AA6061/ Al2O3 /20p reinforced alloy," *Composites Science and Technology*, Vol. 66, pp. 363– 371.

Minton.T and Mynors.D.J (2006) "Utilisation of engineering workshop equipment for friction stir welding," *Journal of Material Processing Technology*, Vol. 177, pp. 336–339.

Mohandas.T, G. Madhusudhan Reddy, and S.D. Meshram (2007) "Friction welding of dissimilar pure metals," *Journal of Materials Processing Technology*, Vol. 184, pp. 330–337.

Mumin-Sahin (2005) "Joining with friction welding of high-speed steel and medium-carbon steel," *Journal of Materials Processing Technology*, Vol. 168, p. 202210.

Paulo.R.M.F, P.Carlone, R.A.F.Valente, F.Teixceira-Dias, and G.S.Palazzo (2014) "Influence of Friction Stir Welding Residual Stresses on the Compressive Strength of Aluminium Alloy plates," *Thin - Walled Structures*, Vol. 74, pp. 184–190.

Prater, Tracie (2014) "Friction Stir Welding of Metal Matrix Composites for use in Aerospace structures," *Acta Astronautica*.

Radoslaw-Winiczenko and Mieczyslaw-kaczorowski (2013) “Friction welding of ductile iron with stainless steel,” *Journal of Materials Processing Technology*, Vol. 213, p. 453 462.

Reddy, G.Madhusudhan, T.Mohandas, and V.V. Satyanarayana (2005) “Dissimilar metal friction welding of austeniticferritic stainless steels,” *Journal of Materials Processing Technology*, Vol. 160, p. 128 137.

Sahin, Mumin (2004) “Simulation of friction welding using a developed computer program,” *Journal of Materials Processing Technology*, Vol. 153, pp. 1011–1018.

Shanjeevi.C, Satish Kumar S, and Sathiya.P (2013) “Evaluation of Mechanical and Metallurgical properties of dissimilar materials by friction welding,” *Procedia Engineering*, Vol. 64, pp. 1514– 1523.

Skalski, K., W. Wlosinski, Z. Lindemann, and J. Zimmerman (2006) “Thermo-mechanical phenomena in the process of friction welding of corundum, ceramics and aluminium,” *Bulletin of the Polish Academy of Sciences Technical Sciences*, Vol. 54, pp. 1–8.

Song, M. and R. Kovacevic (2003) “Thermal modelling of friction stir welding in a moving coordinate system and its validation,” *International Journal of Machine Tools and Manufacture*, Vol. 43, pp. 605–615.

Soundararajan, Vijay, Srdja Zekovic, and Radovan Kovacevic (2005) “Thermo-mechanical model with adaptive boundary conditions for friction stir welding of Al 6061,” *International Journal of Machine Tools and Manufacture*, pp. 1577–1587.

Stephan Kallee, Cambridge UK, TWI (2000) , URL: `http://www.twi-global.com/technical-knowledge/published-papers/application-of-friction-stir-welding-in-the-shipbuilding-industry/`.

Su.H, C S Wu, A. Pittner, and M . Rethmeier (2013) “Simultaneous measurement of tool torque, traverse force and axial force in friction stir welding,” *Journal of Manufacturing Processes*, Vol. 15, pp. 495–500.

tpub (2016) “DCSP and DCRP TIG welding,” URL: `http://constructionmanuals.tpub.com/14250/css/Figure-8-4-Effects-of-polarity-on-the-weld-179.htm`.

Trimble.D, J Monaghan, and G E ODonnell (2012) “Force generation during friction stir welding of AA2024-T3 CIRP Annals,” *Manufacturing Technology*, Vol. 61, pp. 9–12.

Udayakumar, T., K. Raja, A. Tanksale Abhijit, and Sathiya P (2013) "Experimental investigation on mechanical and metallurgical properties of super duplex stainless steel joints using friction welding process," *Journal of Manufacturing Processes*, Vol. 15, pp. 558–571.

Watanabe, Takehiko, Hirofumi Takayama, and Atsushi Yanagisawa (2006) "Joining of aluminum alloy to steel by friction stir welding," *Journal of Material Processing Technology*, Vol. 178, pp. 342–249.

Williamson, Keith M and Tarek Abdel-Salam (2006) "A moving boundary formulation for recursive plastic heat release during friction stir welding," *Journal of Mate*, Vol. 180, pp. 49–52.

Wladyslaw-Wlosinski, Zdzislaw, R. Lindemann, and Jolanta-Zimmerman (2009) "Thermomechanical and diffusion modelling in the process of ceramicmetal friction welding," *Journal of materials processing technology*, Vol. 209, p. 16441653.

Yu-E-Ma, Z.C. Xia, R.R. Jiang, and Wen-Ya-Li (2013) "Effect of Welding parameters on mechanical and fatigue properties of friction stir welded 2198 T8 aluminium lithium alloy joints," *Engineering Fracture Machines*, Vol. 114, pp. 1–11.

Zhang, Z. and H. W. Zhang (2009) "Numerical Studies on controlling of process parameters in friction stir welding," *Journal of Materials Processing Technology*, Vol. 209, pp. 241– 270.

LIST OF PUBLICATION

- Baiju Sasidharan, Narayanan.K.P, Prakash.R.S.Tensile and Microstructural Characteristics of DCSP TIG welded and Friction Stir Welded AA2219 Aluminium Alloys, Proc. of International Conference on Emerging Trends in Engineering and Management (ICETEM 2014, 30-31 Dec.2014), International Journal of Design and Manufacturing (IJDMT) vol.5, Issue 3, 2014, pp.121-129.

- Baiju Sasidharan, Narayanan.K.P, Thanoj Surendran. Comparative Study on Hardness,Torsion and Microstructural Characteristics of Friction Welded Joints of Al 6061 rod formed with various interface geometry, Proc. of International Conference on Emerging Trends in Engineering and Management (ICETEM 2014, 30-31 Dec.2014), International Journal of Design and Manufacturing (IJDMT) vol.5, Issue 3, 2014, pp.115-120.

- Baiju Sasidharan, Narayanan.K.P, Prakash.R.S. Tensile and Microstructural Characteristics of AC Square wave welded and DCSP welded AA2219 Aluminium Alloys, IMMM 2014, Proc.of 2^{nd} International Conference on Materials Mechanics Management,pp. 722-728, International Journal of Scientific and Engineering Research, Volume 5, Issue 7, July-2014 ISSN 2229-5518, pp 711-717.

- Baiju Sasidharan, Narayanan.K.P, Sreejith.S Mechanical and Physical Characteristics of Friction Welded AL6161 rod with various tapered interface geometry, IMMM 2014, Proc.of 2^{nd} International Conference on Materials Mechanics Management, pp.783-788, International Journal of Scientific and Engineering Research, Volume 5, Issue 7, July-2014, ISSN 2229-5518, pp.772-777.

- Baiju Sasidharan, Narayanan.K.P, R.Arivazhakan, Influence of Interface surface Geometries in the Tensile Characteristics of Friction Welded Joints from Aluminium Alloys, International Journal of Innovative Research in Science, Engineering and technology, vol.2, spl. Issue 1, Dec. 2013(ICEE 2013), pp. 786-793.

- Baiju Sasidharan, Narayanan.K.P,Aneesh.K.N. A comparative Study of Tensile and Microstructural Charactetristics of Friction Welded Joints and Conventionally Welded Joints of Aluminium Alloy 6061, International Journal of Innovative Research in Science, Engineering and technology, vol.2, spl. Issue 1, Dec. 2013(ICEE 2013), pp. 557-564.

- Baiju Sasidharan, Narayanan.K.P, Darwin.K. A Rotary Friction Welding Setup from a Conventional Lathe, Proc. of the National Conference and Workshop on Advances in Materials and Advances in Bioprocess Engineering, TECHYNOD'14, 10-12 Dec. 2014, pp.152-163.

BIODATA

Name and Address:	BAIJU SASIDHARAN Aswathy Gardens, RRA 9, Sreekariyam, Sreekariyam PO, Thiruvananthapuram 17 Phone No:9495627920, email id: bsdharan@cet.ac.in
Academic Details:	M Tech - CASAD at Dept. of Ship Technology, CUSAT B Tech at College of Engineering Trivandrum, University of Kerala
Present status:	Associate Professor in Dept. of Mechanical Engineering College of Engineering Trivandrum (CET), Thiruvananthapuram 16
Achievements in Carrier:	Guided 13 B Tech project and 7 M Tech thesis, evaluated 26 Nos. of M Tech thesis at MG and Kerala University, Participated and presented 6 papers in International Conferences. Performed duty as traffic management controller during the visit of Hon.The President of India, Sri. Pranab Mukhargi at CET. Participated the interactive session of Dr. APJ Abdul Kalam at CET First person in CET, doing PhD in FSW and FW. Completed my PhD programme at Dept. of Ship Technology under the supervision of Dr. K.P Narayanan in CUSAT.
Service to the society:	Due to my dedicated efforts and by the guidance of higher officials I could organize and conduct more than 10 Nos. of orientation programs for the Engineering students belong socially, economically and educationally backward classes under the sponsorship of TEQIP. Almost all the participants got placements and admission to IIMs, IITs and NITs for higher studies. Based on this result Govt. of Kerala has implemented projects in all Govt. Engineering colleges by accepting the orientation programs in CET as a model, by naming the program OPES under STEP4U. An amount of Rs 2.5 Crore has been sanctioned in this regard. In that Rs 1.25 Crores has been spent in CET. I could make a difference in reducing the failure rate of students from weaker sections through this programs in all the Govt. Engineering Colleges in Kerala.